A thesis submitted to the University of Cape Town in partial fulfilment of the requirement for the degree of Master of Science in Engineering

THE EFFECT OF WELD-INDUCED IMPERFECTIONS ON THE BUCKLING BEHAVIOUR OF SPHERICAL AND CONICAL SHELLS

by

B.K. STEYN

Department of Civil Engineering
University of Cape Town
March 2005

DECLARATION

I, Brett Kenneth Steyn, herby declare that this thesis is my own work and all contributions have been referenced accordingly. This thesis has not been submitted in full or part to any other university.

Brett Kenneth Steyn
March 2005

AKNOWLDGEMENTS

I would like to thank the following people for their contributions throughout the course of my postgraduate studies.

Professor A. Zingoni for all his encouragement, support and guidance during the duration of my studies.

Mr V. Balden for all his help in understanding finite element analysis

The National Research Foundation for their funding of my research.

This institution for granting me to the opportunity of pursuing my master's degree.

Alex Capostagno for her love and patience and my family and friends for all their support.

ABSTRACT

The effect of imperfections on the buckling of thin walled structures has been a dominant area of research since the early 1930's. This was initiated due to discrepancy between c lassical theory and e xperimentally observed results. In most cases it was found that cylinders under axial compression failed at loads that were far below the predicted classical buckling load. The cause was found to be the presence of imperfections due to fabrication techniques, while the classical theory was derived on the basis of a perfect shell surface. This lead to a stream of research focused on understanding the effect of imperfections on buckling behavior, specifically for cylindrical shells.

The early research was on general imperfections most commonly in the form of the lowest buckling modes. The use of steel pates to fabricate silos in a regular pattern led to the civil engineering interest in the weld-induced imperfection. This imperfection was found to be in the circumferential direction and the dominant cause for the reduction of the classical buckling load. As previous research was conducted on cylindrical shells the current thesis focused on studying two different shell geometries.

The study involved a determination of analytical weld-induced imperfection shapes due to the lack of sufficient measured data. Once the weld imperfection shape had been derived it was used to perform a numerical analysis on an axially loaded conical shell and a spherical shell under uniform external pressure. The analysis was conducted using the finite element software ABAQUS. The analysis indicates that a single circumferential weld can result in a definite reduction of the classical buckling loads for the given shells. Specifically the reduction can be as much as 70% for the conical shell and 50% for the spherical shell.

The results of the numerical analysis can be used to support designers in their understanding of shell behavior, indicates that the presence of welds although necessary for construction, does contribute to a loss of load carrying capacity.

TABLE OF CONTENTS

TABLE OF FIGURES

NOMENCLATURE

All symbols are to be taken as indicated here, unless otherwise indicated in the text.

E - Young's Modulus

v - Poison's Ratio

t - Thickness

R - Radius of Latitude; Circumferential Radius

ϕ - Meridional Angle

θ - Circumferential/Hoop Angle

N_θ - Hoop/Circumferential Force per meter

N_ϕ - Meridional Force per meter

x - Axial Coordinate for Axis of Revolution Cylindrical Shell

N_x - Meridional Force for Cylindrical Shell

w - Radial Displacement

u - Circumferential Displacement

v - Axial Displacement

ΔV - Strain Energy

ΔT - Work Done

σ_{cl} - Classical Buckling Stress

P_{cl} - Classical Axial Buckling Load, Cylindrical and Conical Shells

q - Uniform Pressure Load

q_{cl} - Classical Buckling Load; Spherical Shell under Uniform External Pressure

a - Radius of Curvature Spherical Shell

H - Rise of Shallow Spherical Shell, Height of Conical Shell

λ_{ss} - Geometric Factor Shallow Spherical Shell

λ - Geometric Factor Spherical Shells

λ^* - Factor of Actual Buckling Load over Classical Buckling Load

s - Coordinate for Conical Generator

β - Apex Angle Conical Shell

α - Angle of Generator Conical Shell

N_s - Meridional Force Conical Shell

w_0 - Imperfection Amplitude

D - Flexural Rigidity of Shell of Revolution

λ_0 - Bending Half Wave Length Cylindrical Shell

σ_y - Yield Stress

N - Shape Functions

$\overline{U}$ - Trial Solution

$[K]$ - Stiffness Matrix

$\{a\}$ - Displacement Matrix

$[F]$ - Force Matrix

$\{\varepsilon\}$ - Strain Matrix

$\{\sigma\}$ - Stress Matrix

$[C]$ - Constitutive Stress Strain Relationship

$[K_G]$ - Initial Stress Matrix / Geometric Stiffness Matrix

$\{D\}$ - Pre-Buckling Displacements

$\{\delta D\}$ - Buckling Mode

$[M]$ - Stress Matrix due to Loading

$[S]$ - Tensor Stress Matrix

$[K_T]$ - Tangent Matrix

$[K_L]$ - Stiffness Matrix due to Large Deflections

P^N - Loading Pattern ABAQUS

I^N - Internal Force Matrix, ABAQUS

R^N - Residual Force, ABAQUS

Q_ϕ - Transverse Shear Force per Unit Length

V - Meridional Rotation at a Point

V^b - Meridional Rotation due to Bending

δ - Lateral Displacement

δ_e^b - Lateral Displacement at Shell Edge due to Bending

δ_M - Lateral Displacement due to M_e

δ_H - Lateral Displacement due to H_e

ϕ_e - Meridional Angle at Shell Edge

l - Location of Conical Shell Edge along Generator

H_e - Lateral Force at Shell Edge

M_e - Moment at Shell Edge

ϕ_w - Meridional Location of Circumferential Weld, Spherical Shell

l_w - Meridional Location of Circumferential Weld, Conical Shell

ϕ_s - Meridional Location of Supports, Spherical Shell

1 LITERATURE REVIEW

Shell structures have been used in Civil and Mechanical engineering applications for a number of years. In particular thin steel shells have been used to create the fuselage of aircrafts in the aeronautical industry, silos and other containment structures in civil engineering, and pressure vessels in mechanical engineering. It is clear that thin shells provide and fulfil everyday industrial and structural requirements. Zingoni (1997) gives a concise summary of the applications of thin shells in civil and mechanical engineering.

The last 100 years has seen an increase in the research on thin shells and their applications. This is brought about through the need to correlate theoretical understanding with the practical reality of actual observed behaviour. This is most important when confronted with the detrimental effect of failure of the structure and it requires an ability to accurately predict both the failure load as well as the mode of failure. It was determined early on that the actual buckling behaviour was a result of loads occurring below the predicted theoretical loads for a perfect shell. This was a consequence of inherent imperfections within the actual structure. The imperfections are introduced through the construction process due to the difficulty in recreating the form of the perfect theoretical shell. Thus the issue of imperfections became a vital area of research.

The early research was focused predominantly on cylindrical shells due to their use in the aeronautical industry. The research work was conducted by Von Karman, Tsien, Donnell and Koiter. This was later followed by an increased amount of research in the 1950's and 1960's by the likes of Abrocz, Babcock and Hutchinson. Calladine (2000) presents a historical overview of this research.

More recently the use of thin steel shells in civil engineering structures has bought about research focused on specific imperfections: weld-induced imperfections. This area has focused on the use of welding to create the whole from parts. The result is localised imperfections in both the meridional and circumferential directions. The

study of imperfections in recent years has also been aided by the introduction of the finite element method along with improved computational facilities. This chapter will focus on the literature on all these studies.

The initial focus will be on the derivation of the classical buckling strengths. This will be done for three shell forms, namely the cylindrical, conical and spherical shells. This will provide an understanding of the theoretical background to the behaviour of the perfect shell. It will provide a benchmark by which to measure the relative effects of imperfections later on.

The research on imperfections affecting the buckling behaviour of the three shell structures will then be reviewed. The focus is on the effect of general imperfections, mostly in the form of the lowest buckling mode for the perfect shell. The bulk of material in this area is on the cylindrical shell, although there has also been significant work on both the spherical and conical shells.

The final sections will focus particularly on the effect of weld imperfections. Again the bulk of the research has covered the cylindrical shell. However there has also been a small number of papers concerning both the spherical and conical shells.

Taking the findings of the literature review into account, the final section of this chapter will focus on the research aims and methodology adopted in this thesis. This will cover the approach to be adopted for the spherical and conical shell to determine the effect of weld imperfections on their buckling behaviour.

1.1 CLASSICAL BUCKLING THEORY

To develop an understanding of shell behaviour with initial imperfections, the classical buckling loads are needed as a benchmark with which we can evaluate the respective loss of strength due to initial imperfections. This chapter focuses on the derivation of the classical buckling strengths for geometrically perfect shells subject to axisymmetric loading conditions.

The classical buckling load will be investigated for three shell types; the cylindrical shell, the spherical shell and the truncated conical shell.

1.1.1 Buckling of Cylindrical Shells under Axial Compression

This section focuses on the buckling formula for a cylindrical shell under axial compression. This is a rather typical situation in applications such as grain silos, for which weld imperfections have been investigated. The derivation of the basic formula for the classical buckling of cylindrical shells is given by Timoshenko (1939) and Flugge (1973).

The classical buckling formula of a cylindrical shell is based on the assumption of perfect geometry. The Pre-buckling deformation and stress state is adequately represented by the membrane forces. Flugge (1973) took this into account when he determined three differential equation's governing the buckling condition. Figure 1.1 gives a diagrammatic representation of the cylindrical shell with the membrane forces acting on it.

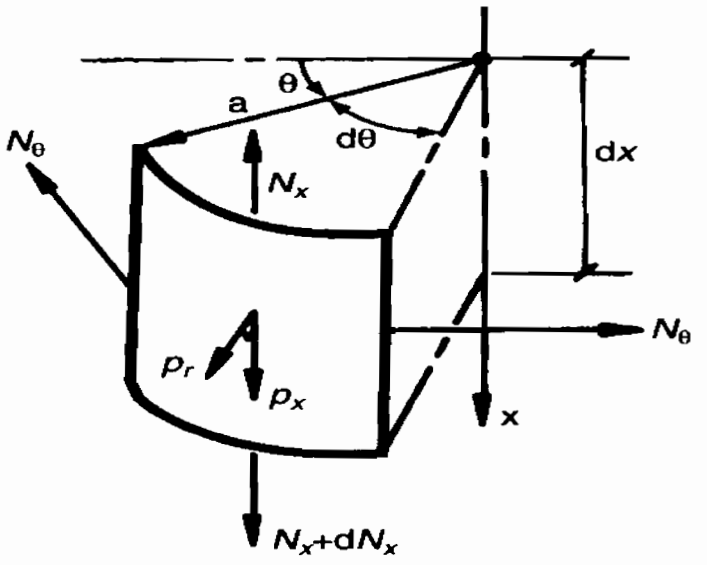

Figure 1.1: Membrane Forces in Circular Cylindrical Shell

For the purpose of the analysis Flugge (1973) calculated the final meridian and circumferential forces by imposing additional deformations on to the membrane solution. This resulted in the condition:

$$\overline{N}_x = N_{xI} + N_x \qquad [1.1]$$

where:

N_x is due to the small deflections at the onset of bending.

N_{xI} is the membrane force

Thus all axial and circumferential forces consisted of the membrane solution superimposed with the forces due to bending. The deformations in the radial, circumferential and axial directions are *w, u* and *v* respectively.

Timoshenko (1939) made use of the energy method to calculate the critical buckling load. The bifurcation point is determined by equating the strain energy (ΔV) and the work done by the applied load (ΔT).

$$\Delta V = \Delta T \qquad [1.2]$$

The strain energy for a cylindrical shell is a function of bending, as the transverse shear forces are assumed to be negligible. The strain energy of a shell comprises of two components:

- The strain energy due to the elongation of the middle surface
- The strain energy due to bending deformation

Timoshenko (1939) assumed that the buckling mode could be represented by a sine curve.

$$w = -A\sin\left(\frac{m\pi x}{L}\right) \qquad [1.3]$$

where m represents the number of axial half waves. This represents the basic axisymmetric buckling mode with no circumferential waves.

The strain energy and work done for a cylindrical shell under axial compression is given as: (Timoshenko, 1939)

$$\Delta V = -2\pi t E \nu \varepsilon_0 \int A\sin\left(\frac{m\pi x}{L}\right) + \frac{\pi A^2 EtL}{2R} + A^2 \frac{\pi^4 m^4}{2L^4}\pi RLD \qquad [1.4]$$

$$\Delta T = 2\pi N_{cr}\left(\nu \int_0^L A\sin\left(\frac{m\pi x}{L}\right)\right)dx + \frac{R}{4}A^2\frac{\pi^2 m^2}{L} \qquad [1.5]$$

Equating Equations 1.4 and 1.5 results in the determination of the classical buckling stress which is given as:

$$\sigma_{cl} = \frac{Et}{R\sqrt{3\left(1-\nu^2\right)}} \qquad [1.6]$$

The actual buckling load P_{cl} can be written as:

$$P_{cl} = \frac{2\pi E t^2}{\sqrt{3(1-\nu^2)}} \qquad [1.7]$$

1.1.2 Buckling of Spherical Caps

The classical buckling load of a spherical shell has been determined by a number of authors. The most common case is for a spherical shell under uniform external pressure, the derivation of which may be seen in Timoshenko (1935) and Almroth (1975).

Figure 1.2 gives the membrane forces for a segment of a shell of revolution. This is to have a mental picture of the terminology used in the derivation.

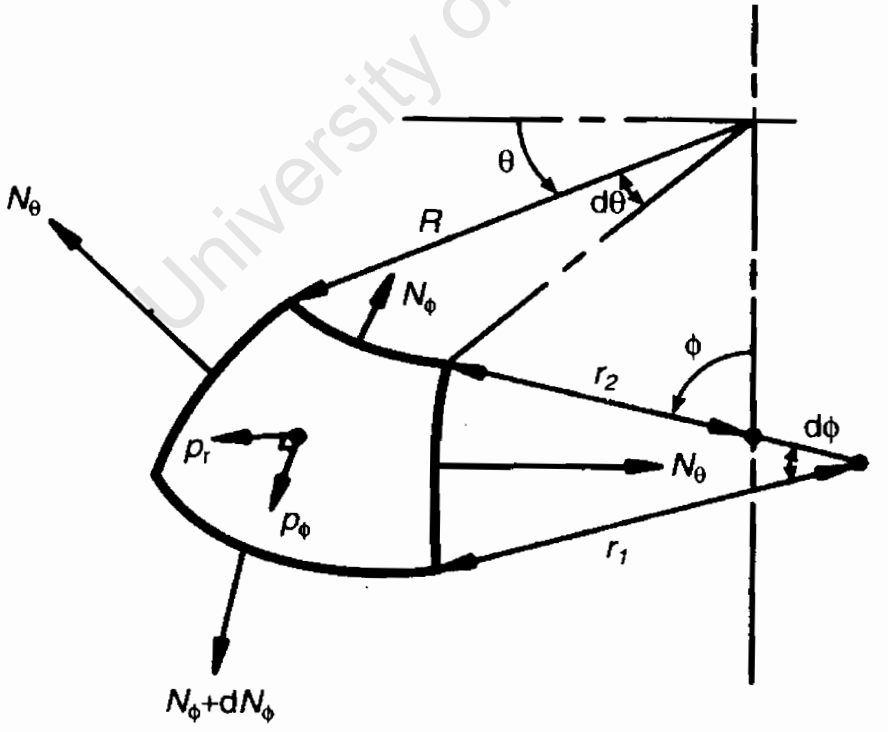

Figure 1.2: Membrane Forces in Shell of Revolution

From Figure 1.2 the following terms can be defined for a spherical shell:

N_θ - Circumferential/Hoop force per unit length

N_ϕ - Meridional Force per unit length

$r_1 = r_2 = a$ - Radius of Curvature of shell surface equals radius of sphere

R - The Radius of the Hoop Circle (Circumferential Circle of latitude)

ϕ - Meridional angle measured from the vertical axis

θ - Circumferential angle

Timoshenko (1935) used a small displacement theory to derive the buckling strength of a spherical shell. He assumed a symmetrical buckling pattern and made use of the equilibrium equations defining the bending deformation of a spherical shell. Timoshenko (1935) defined the following parameters:

$$N_\phi = -\frac{qa}{2} + N'_\phi \qquad [1.8]$$

$$N_\theta = -\frac{qa}{2} + N'_\theta \qquad [1.9]$$

Here the value $\frac{-qa}{2}$ is the membrane force per unit length.

N'_ϕ and N'_θ are the forces resulting from bending associated with the small displacements due to the external pressure loading on the shell. The equation representing the meridional and circumferential forces was substituted into the equilibrium equations for a shell of revolution undergoing bending deformations. Timoshenko (1935) manipulated these equilibrium equations and made use of spherical functions to develop two homogenous equations to describe the stability problem. A non-zero solution of the homogenous equations is required for the buckling load; correspondingly the determinant of the equations was set to zero. This resulted in the development of the following equation given by Timoshenko (1935):

$$\left(1-\nu^2\right)+\alpha\left(\lambda_n{}^2+2\lambda_n+\left(1+\nu\right)^2\right)-\varpi\lambda_n\left(\lambda_n+\left(1+3\nu\right)\right)=0 \qquad [1.10]$$

where:

$$\alpha=\frac{D\left(1-\nu^2\right)}{a^2Et} \qquad [1.11]$$

$$\varpi=\frac{qa\left(1-\nu^2\right)}{2Et} \qquad [1.12]$$

This equation has the trivial solution $\lambda_n=0$ and a non trivial solution $\lambda_n\neq 0$. Rearranging the equation and setting its derivative with respect to λ_n equal to zero we obtain a minimum:

$$\varpi=\frac{\left(\left(1-\nu^2\right)+\alpha\left(\lambda_n{}^2+2\lambda_n+\left(1+\nu\right)^2\right)\right)}{\lambda_n+\left(1+3\nu\right)} \qquad [1.13]$$

Setting $\frac{d\varpi}{d\lambda_n}=0$, we obtain

$$\lambda_n=-\left(1+3\nu\right)+\sqrt{\frac{\left(1-\nu^2\right)}{\alpha}} \qquad [1.14]$$

The above solution can be rearranged to give the buckling pressure for a spherical shell of:

$$q_{cl}=\frac{2E}{\sqrt{3\left(1-\nu^2\right)}}\left(\frac{t}{a}\right)^2 \qquad [1.15]$$

Timoshenko (1935) indicates the buckling load can change and obtain a lower value with the introduction of non-symmetrical buckling patterns.

The value is similar to the classical buckling strength for a cylindrical shell. However Almroth (1975) states that the solution does not satisfy the edge conditions of the spherical cap and thus the above equation is limited to the case where buckled wave patterns are small in comparison with the radius of the shell. The problem arises as to how to quantify the buckling characteristic of a spherical shell with edge conditions that are not applicable to the membrane solution.

The pinned and fixed boundary conditions create incompatibilities with the membrane theory. These result in the introduction of bending moments into the shell adjacent to the boundary. The bending moments increases the stress state of the shell. The stresses in the meridional and hoop directions are now a function of the membrane stress superimposed with the bending stresses. This increased stress state could lead to a lowering of the load at the point of bifurcation. In the case of a shallow spherical shell this reduction can be as much as 50% and the buckling mode is predominated by a snap through of the upper portion of the shell. This issue will be examined in the next section.

1.1.3 Non-linear theory for the buckling of spherical shells

As indicated in the previous section the discontinuities introduced by the boundary conditions should be solved making use of nonlinear techniques. The previous classical buckling solutions were obtained on the assumption of infinitesimal deflections and rotations. In effect the introduction of bending moments due to the discontinuity leads to large displacements and rotations within the shell. The nonlinear technique accounts for the presence of large deflections and rotations hereby giving a more accurate representation of the buckling problem.

The nonlinearity investigated in this section is purely in relation to the geometric nonlinearity. The spherical shell is assumed to behave elastically under the uniform external pressure. Figure 1.2 is a summary of the geometry of an arbitrary shell of revolution.

Research into nonlinear buckling of shallow spherical shells has been conducted by a number of researchers. Budiansky (1959) investigated the axisymmetric buckling of clamped shallow spherical shells. Tillman (1970) and Huang (1963) both investigated the effect of asymmetric buckling patterns. Experimental work was conducted by Kiernan and Krenzke (1963) as well as some work done by Tillman (1970). The results of these investigations will be discussed in the following section.

Budiansky (1959) investigated the effect of non-linear buckling of shallow spherical shells. This involved the analysis of axisymmetric buckling as well as the effect of initial axisymmetric imperfections on the buckling strength. The geometry of the spherical shell is given as:

$$Z_0 = H\left(1-\left(\frac{R}{b}\right)^2\right) \qquad [1.16]$$

where:

H – is the vertical rise of the shallow spherical shell

Here R is the circumferential radius and b is the value of R at the base of the shell. All authors make use of a geometric factor:

$$\lambda_{ss}^{\ 4} = 48\left(1-\nu^2\right)\left(\frac{H}{t}\right)^2 \qquad [1.17]$$

Budiansky developed non-dimensional, non-linear stability equations.

$$\frac{\partial\left(x\dfrac{\partial\gamma}{\partial x}\right)}{\partial x} - \frac{\gamma}{x} + x\psi = -2px^2 + \gamma\psi \qquad [1.18]$$

$$\frac{\partial\left(x\dfrac{\partial\psi}{\partial x}\right)}{\partial x} - \frac{\psi}{x} - x\gamma = -\frac{1}{2}\gamma^2 \qquad [1.19]$$

where the non dimensional variables are defined as:

$$x = \frac{\lambda_{ss}R}{a} \quad ; \quad \gamma = \left(\frac{b\lambda}{2H}\right)\beta \quad ; \psi = \left(\frac{12\left(1-\nu^2\right)b}{Et^3\lambda_{ss}}\right)\varphi$$

Here β and φ are the rotation of a shell element and a stress function respectively and q_{cl} is the classical buckling strength of a spherical shell. The clamped boundary conditions are also converted to account for the non dimensional parameters. These become: (Budiansky 1959:69)

$$\gamma\left(\lambda_{ss}\right) = 0$$
$$\lambda_{ss}\frac{\partial\psi\left(\lambda_{ss}\right)}{\partial x} - \nu\psi\left(\lambda_{ss}\right) = 0 \qquad [1.20]$$

Huang (1963) focused on asymmetrical buckling of shallow spherical shells. The shell was under external uniform pressure. Huang (1963) illustrated the derivation of Marguerre's nonlinear differential equations for the stability of shallow spherical shells. Huang (1963) also introduces non dimensional parameters to simplify the governing differential equations and solves these numerically using the method of finite differences. The non dimensional parameters used by Huang (1963) which differ to those proposed by Budiansky are given below, all others are taken equal.

$$w = \frac{\lambda^2}{2H} W \qquad [1.21]$$

$$\psi = \frac{\lambda_{ss}^{\ 4}}{4EH^2 t} F \qquad [1.22]$$

F represents a stress function and W is the vertical displacement. Huang (1963) used these non dimensional parameters to simplify Marguerre's differential equations. The solution was made by assuming the non dimensional parameters to be a function of both axisymmetric and asymmetric components in the prebuckled state. This is illustrated as:

$$w = \omega^*(x) + \omega(\theta, x) \qquad [1.23]$$

$$\psi = \tau^*(x) + \tau(x, \theta) \qquad [1.24]$$

Huang (1963) describes the variables $\omega^*(x)$ and $\tau^*(x)$ as the non dimensional deflection and stress function respectively representing the axisymmetric state before buckling. The factors $\tau(x,\theta)$ and $\omega(\theta,x)$ are due to unsymmetrical buckling. Huang (1963) considered the unsymmetrical components to be infinitesimally small at the onset of buckling. After rearrangement the differential equations take on the same form as those derived by Budiansky (1959) for the symmetrical buckling. The results for Huang's numerical calculations are compared graphically with those of Budiansky. Huang solution of the stability problem was essentially reduced to the solution of an eigenvalue problem. The graphical results represent the lowest eigenvalue. Figure 1.4 plots the buckling load as a fraction of the classical buckling load (λ^*) against the geometrical parameter λ.

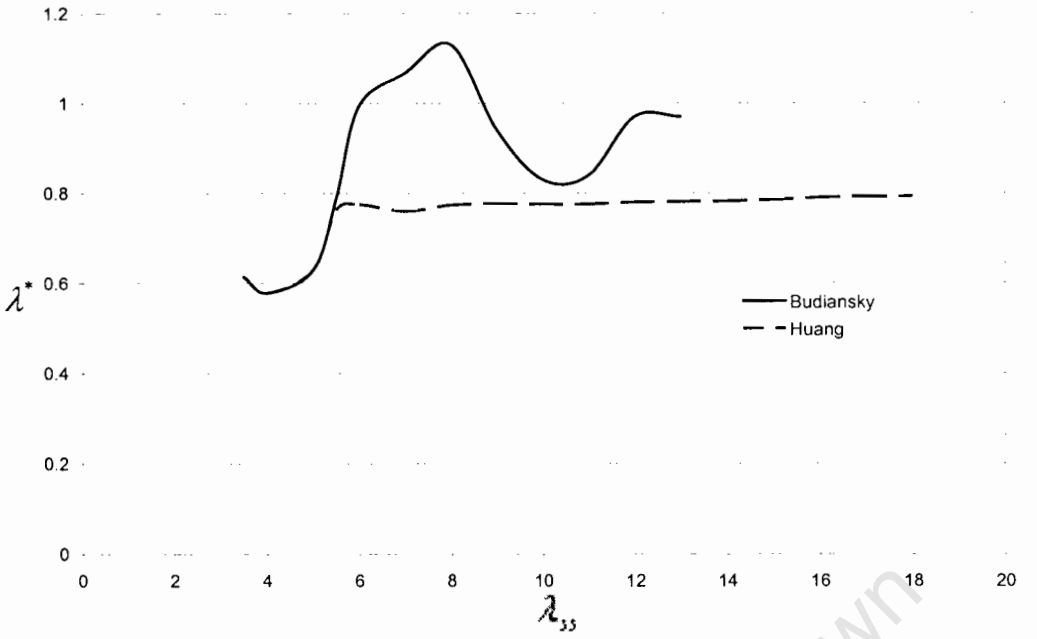

Figure 1.3: Shallow Spherical Shell Buckling Capacity

It is clear from Figure 1.3 that for low values of λ_{ss} the results of Huang and Budiansky show good agreement. However for values of λ_{ss} greater than 5 the asymmetrical buckling model of Huang provides the lower bound solution, this also appears to become asymptotic with a value of $\lambda^* = 0.8$, indicating a loss of 20% of the classical buckling strength.

Tillman (1970) also investigated the effect of asymmetric buckling of shallow spherical shells. The analysis was conducted numerically and experimentally. The numerical solution was based on Marguerre's shallow shell differential equations. Tillman (1970) solved the differential equations using the Ritz-Galerkin method.

Krenzke & Kiernan (1963) conducted experimental work on seventeen machined shallow spherical shells. The shells were subjected to an external hydrostatic pressure. The shells had clamped edge conditions, and were machined from aluminium bar stock. The measured variations of radius and the shell thickness were kept to less than 1%, to ensure a near perfect shell. It is evident that machining the shell bypasses the normal method of assembling plates with curvatures to form the whole. This reduces the possibility of imperfections.

The test results will be illustrated in the diagram below. The vertical axis gives the ratio of actual buckling load to the classical buckling load for a spherical shell. The horizontal axis is a non dimensional parameter Φ.

$$\Phi = \left(\frac{3}{4}\left(1-\nu^2\right)\right)^{\frac{1}{4}} \frac{C}{\sqrt{Rt}} \qquad [1.25]$$

C – is the unsupported chord length

The results indicated in the curve bellow show a distinct pattern and thus reproducibility.

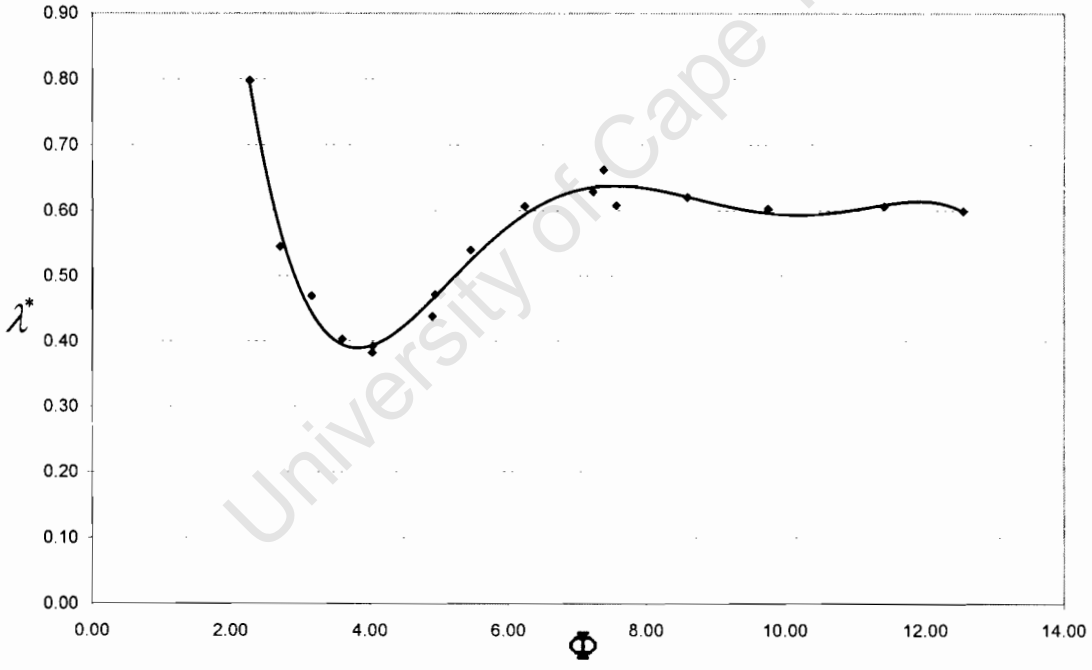

Figure 1.4: Experimental Results (Krenzke & Kiernan, 1963)

Krenzke and Kiernan (1963) point out that the buckling mode was predominantly axisymmetric below $\Phi < 5.5$ while the predominant buckling mode above a value of 5.5 was non-symmetric and there was good agreement with results obtained by Huang (1964). There was also some agreement with Budiansky (1960) results for low values of Φ.

1.1.4 Buckling of Truncated Conical Shells

The truncated conical shell will form the third shell type for which the classical buckling strength is derived; however it differs from other shell types in that the solution needs to be found using numerical methods.

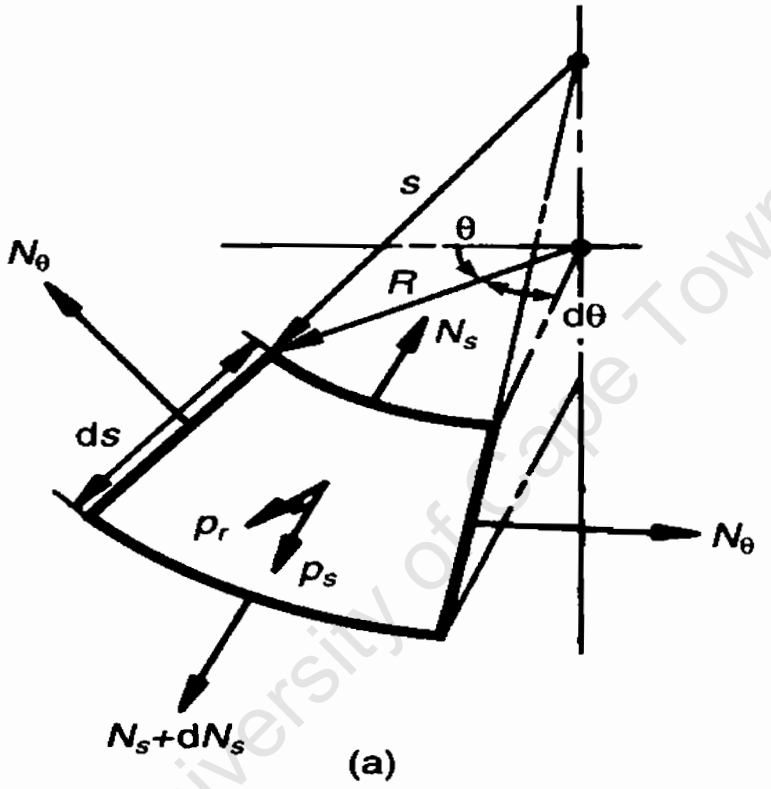

Figure 1.5: Geometry of a Conical Shell (Zingoni, 1997)

Figure 1.5 gives the notation used for the conical shell. All notations are consistent with those of a general shell of revolution except in the case of the meridional force and the generator parameter:

N_s - Meridional force pre unit length

s - measure of distance form the shell apex along the generator

β - Apex angle of the conical shell (Not indicated in the diagram)

A concise background to the stability of conical shells is summarized by Brush and Almroth (1975). The stability equations are illustrated for the case of a truncated conical shell.

Due to the nature of the experimental work conducted for this dissertation, the classical buckling load for an axially compressed conical shell is of interest. The solution given by Seide (1956) was based on Timoshenko's (1935) approach for cylindrical shells.

Seide (1956) determined that the classical buckling strength of an axially loaded truncated conical shell as:

$$P_{cl} = P_{cylinder}\left(\cos^2 \beta\right) \qquad [1.26]$$

where:

$$P_{cylinder} = \frac{2Et^2}{\sqrt{3\left(1-\nu^2\right)}} \qquad [1.27]$$

1.2 Review of Imperfections in Shells

This chapter focuses on the effect of imperfections on the buckling of shells of revolution. Much of the work on imperfections has been done on cylindrical shells, due to their applicability in the aeronautical industry and common use in civil engineering. The review will cover work done on cylindrical, spherical and conical shells.

Calladine (1995) gave a description of three issues that give an overview of imperfection sensitivity, these are:

- Buckling loads falling short of classical theory predictions
- Unpredictability of loads, given a wide scatter of experimental results
- Unstable dynamic behaviour of the shell after the maximum load has been reached

1.2.1 Imperfections in Cylindrical Shells

This section covers the development of ideas relating the effect of imperfections on the buckling behaviour of cylindrical shells. The focus will be on the development in this field covering both axisymmetric and local imperfections.

An initial study into the effect of imperfection sensitivity in the buckling of cylindrical shells was conducted by Donnell (1934) and Donnell & Wan (1950). Donnell (1935) sought to use a large deflection non-linear theory. He sought to explain the discrepancies between the observed buckling strengths and wave patterns to those predicted by the classical buckling methods. Donnell made no measurements of the initial imperfections but merely sought to make use of a double harmonic to describe the imperfection. Donnell (1935) made the main assumption that the initial imperfection shape and the final buckled shape would be the same, thus the amplitude of the imperfection would grow at the onset of loading, till the point of failure. Donnell and Wan (1950) sought to build on the larger deflection theory that had been developed by Donnell (1935). However Koiter (1963) raises some concerns regarding the assumption that the form of the initial imperfection and the final buckled shape were made the same. The imperfection would merely grow till the point of failure, and would not bring about the rapid failure as indicated by experiments, but rather a gradual failure. Von Kármán and Tsien (1940) indicate that to achieve the required loss of load the imperfection amplitude assumed by Donnell (1935) would have to be of an order greater than the shell thickness, which would be clearly visible as an imperfection prior to testing and as such is not practical.

Von Kármán and Tsien (1940) investigated the buckling of thin cylinders under axial compression to explain for the discrepancies in both the experimental buckling load

and the predicted wave pattern. They sought to explain this discrepancy by means of a non-linear large deflection theory. The paper indicates that the sustained load drops with increasing deflection. Von Kármán and Tsien also indicated that there was a drop in the buckling load due to the presence of imperfections.

Von Kármán and Tsien (1940) made use of an approximate method for the calculation of the buckling behavior of thin cylindrical shells. The use of the energy method was based on the initial assumption of the radial deformation of the cylinder. The calculation then involved determining the:

- The extensional element energy
- The bending energy
- The Virtual work of the applied force

The buckling pattern was taken to be diamond shaped. The radial deflection w was estimated using a cosine function that would satisfy the boundary conditions.

$$\frac{w}{R} = \left(f_0 + \frac{f_1}{4}\right) + \frac{f_1}{2}\left(\cos\left(\frac{mx}{R}\right)\cos\left(\frac{ny}{R}\right) + \frac{1}{4}\cos\left(\frac{2mx}{R}\right) + \frac{1}{4}\cos\left(\frac{2ny}{R}\right)\right) + \frac{f_2}{4}\left(\cos\left(\frac{2mx}{R}\right) + \cos\left(\frac{2ny}{R}\right)\right) \quad [1.28]$$

where:

f_0, f_1 & f_2 are unknowns to be determined from the minimum energy condition.

While Von Kármán and Tsien (1940) realized that the deflection did not allow for edge effects, work by Nojima and Kanemitzu as cited by Von Kármán and Tsien (1941) indicated that when the length is greater than 1.5 times the radius the edge effects could be ignored.

Formulating the equations and minimizing the energy (bending energy + extensional energy – virtual work) the minimum buckling parameter was found.

$$\min\left(\frac{\sigma R}{Et}\right)_{\varepsilon\to 0} = \frac{1}{\sqrt{3(1-\nu^2)}} \qquad [1.29]$$

where: ε is the wave amplitude and a reflection of the imperfection of the shell thus as ε tends to zero the initial shape of the cylinders tends to perfection and thus Equation 1.29 above represents the classical buckling strength.

Koiter examined the effect of an axisymmetric imperfection in two instances, Koiter's (1945) general theory and Koiter's (1963) submission of his special theory. He based his analysis on the nonlinear equations of shallow shell theory. Koiter (1963) restricted the numerical evaluation to axisymmetric imperfections in the shape of the axisymmetric buckling mode of a perfect cylindrical shell.

The equations of both the special and general theory are detailed below:

$$2(1-\lambda^*)^2 - c\mu(\lambda^* + 2) = 0 \text{ (Special theory)} \qquad [1.30]$$

$$2\left(1-\lambda^*\right)^2 - 3c\mu\lambda^* = 0 \text{ (General Theory)} \qquad [1.31]$$

where:
μ is the amplitude of the imperfection as a fraction of the shell thickness t
λ* is the critical buckling stress as a fraction of the classical buckling stress

Koiter (1963) created a middle surface for the cylinder by deflecting all points on the cylindrical surface by the value $w_0(x)$. In this case he chose the arbitrary axisymmetric deviation to be a simple harmonic function given by:

$$w_0(x) = -\mu t \cos\left(\frac{2px}{R}\right) \qquad [1.32]$$

where $2p$ represents the wave number and the minus facilitates an inward deflection at $x = 0$. The boundary conditions were applied at the points $x = +/- L/2$. Koiter (1963) chose Equation 1.33 to represent the buckled pattern of the cylinder:

$$w(x,y) = t\sum C_j \cos[(2j-1)\frac{px}{R}]\cos(\frac{ny}{R}) \qquad [1.33]$$

Solving out for the critical load, Koiter (1963) came up with the basic equation governing the effect of the imperfection w_0(x) as seen in the equation:

$$\begin{aligned}&(1-\lambda^*)^2\left[\left(\frac{1}{2}+\tau^2\right)^2+\left(\frac{1}{2}+\tau^2\right)^{-2}-2\lambda^*\right]\\&-2c\mu(1-\lambda^*)\tau^2\left[\lambda^*+2\left(\frac{1}{3}+\tau^2\right)^{-2}\right]\\&+4(c\mu)^3\tau^4\left[\left(\frac{1}{2}+\tau^2\right)^{-2}+\left(\frac{9}{2}+\tau^2\right)^{-2}\right]=0\end{aligned} \qquad [1.34]$$

Equation 1.34 applies for the special case where τ^2=0.5, where τ is the reduced circumferential wave number.

Tennyson & Muggeridge (1969) sought to do an experimental validation of Koiter's (1963) special theory. They manufactured photoelastic plastic circular cylindrical shells with the axisymmetric imperfection using the spin-casting technique. The cylindrical shells had clamped edge constraints. Previous work by Tennyson (1964) had shown that edge constraints only result in a 10% loss in the critical buckling load.

The experimental work involved varying the imperfection wavelength and the imperfection amplitude. Koiter (1963) made use of the wavelength parameter $\tau^2 = 0.5$. Tennyson and Muggeridge used the following definitions to define their wavelength parameter K:

$$2p = \sqrt{\left(\frac{R}{t}\right)}\left(12\left(1-\nu^2\right)\right)^{\frac{1}{4}} \qquad [1.35]$$

$$\rho^2 = 2K^2 \qquad [1.36]$$

Thus by varying the values of K and μ in the equations and the experimental fabrication Tennyson and Muggeridge (1969) were able to come up with a correlation between Koiter's special extended theory and the experimental results. The axisymmetric imperfection of Equation 1.32 was machined into the inner wall of the photo elastic cylinders using a template. Thus the thickness of the shell varied according to the imperfection. The poisons ratio for the elastic material was given as 0.4.

Figure 1.6 below is a graphical representation of Koiter's axisymmetric imperfection given in Equation 1.32.

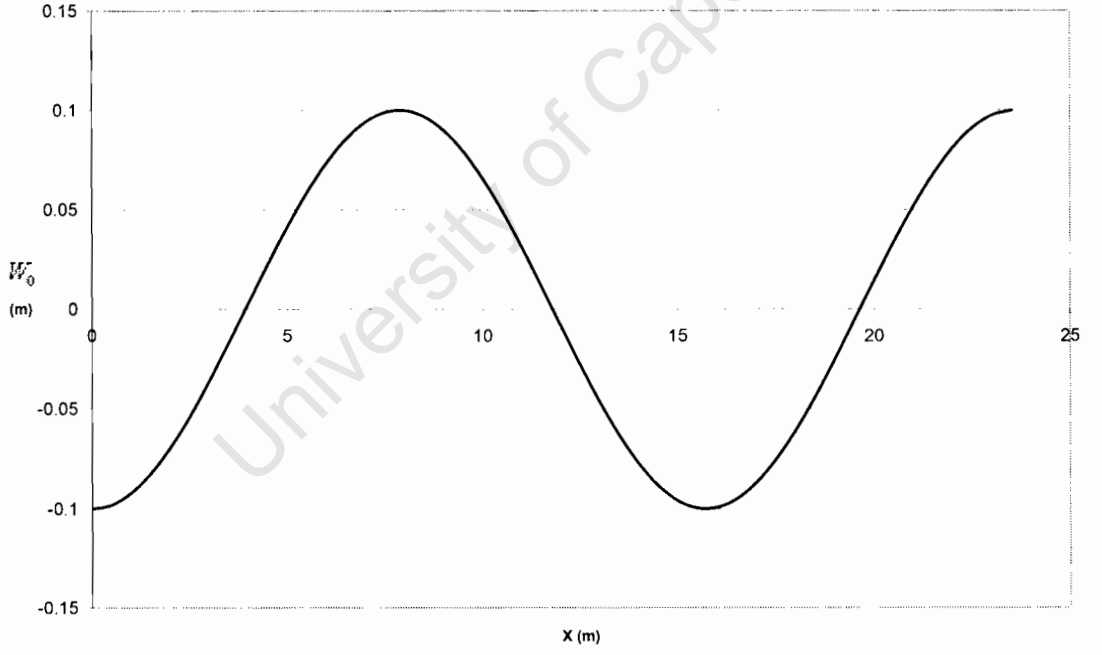

Figure 1.6: Koiter's Axisymmetric Imperfection

To determine the effect of imperfection amplitude on the critical buckling load, three shells were tested having nominally the same axial wave number parameter (K_{avg} = 0.592) and varying values of imperfection amplitude (Tennyson & Muggeridge, 1969). The results compared favourably with Koiter's theory and the critical buckling

load was shown to decrease with increasing imperfection amplitude. Tennyson and Muggeridge (1969) further sought to determine whether there was a minim value of K that would determine the lowest buckling value. This was evaluated by keeping the imperfection amplitude constant and altering the axial wavelength parameter. Once again the results compared favourably with Koiter's theory.

Amazigo and Budiansky (1969) developed an asymptotic formula for the buckling of imperfect cylindrical shells. They developed the formulae for the case of an axisymmetric imperfection; the development of interest here is their solution for a cylinder containing a local axisymmetric imperfection. The asymptotic formula is given as:

$$\left(1-\lambda^*\right)^{\frac{3}{2}} = \left(\frac{3c}{2^{\frac{3}{2}}}\right)\left|\Delta\right|\left(\lambda^*\right) \qquad [1.37]$$

where

$$\Delta = \int_{-\infty}^{\infty} \frac{w_0}{t} e^{i\bar{x}} d\bar{x} \qquad [1.38]$$

is the local axisymmetric imperfection and

$$c = \sqrt{3\left(1-\nu^2\right)} \qquad [1.39]$$

Hutchinson (1970) sought to investigate the above asymptotic formula, to validate it by comparing numerical results and experimental results. The shells used by Hutchinson (1970) were made using the spin-casting technique and a photoeleastic liquid epoxy. The local imperfections were machined into the wall, an inward and outward facing. The researchers investigated the effect of a cosine dimple with the equation:

$$w_0 = \frac{-\delta}{2}\left(1+\cos\left(\frac{\pi x}{l_x}\right)\right) \qquad [1.40]$$
$$|x| \le l_x$$

where l_x is the dimple half length.

Thus using the cosine dimple Equation 1.38 yields:

$$\Delta = \left(\frac{\sin(\pi\beta)}{\beta^2} - 1\right)\left(\frac{\delta}{t}\right) \qquad [1.41]$$

Hutchinson investigated the solutions for different values of β, where β is defined as the dimple half-length divided by the half wave of the classic axisymmetric buckling mode. Hutchinson found that the maximum reduction in buckling strength for any value of imperfection amplitude corresponds to a value of β=0.8.

For the comparison of Amazigo and Budiansky (1966) asymptotic formula Hutchinson (1970) choose β=1. The following graphs indicate Hutchinson (1970) machined local imperfection as well as the results obtained from his experimental work. It can be seen that there is good agreement between the numerical, experimental and asymptotic results for varying values of imperfection amplitude.

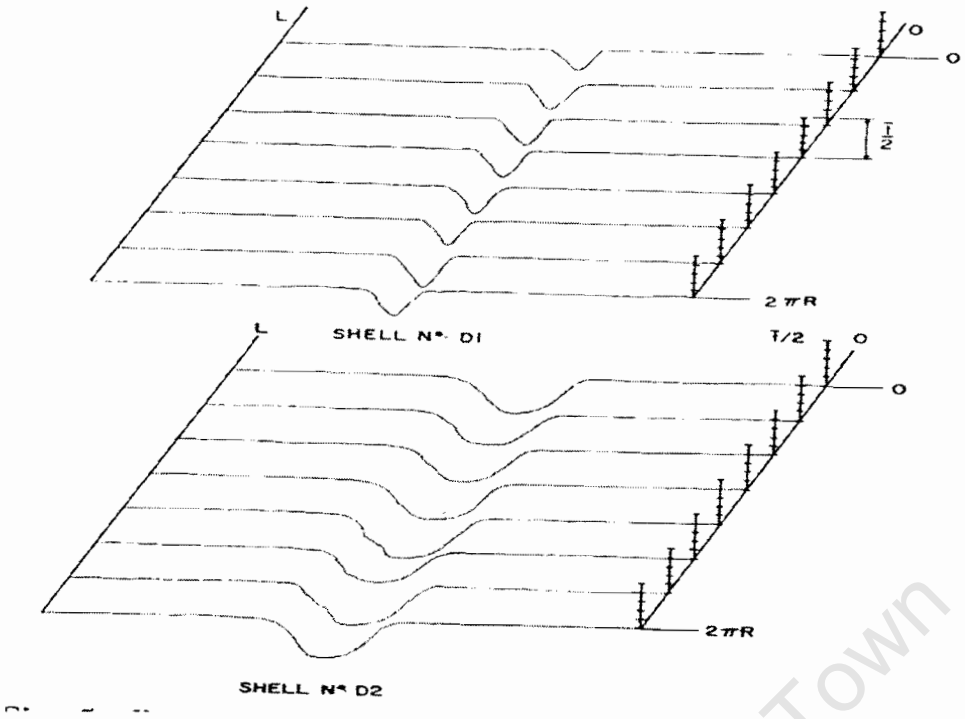

Figure 1.7: Local Axisymmetric Imperfection (Hutchinson, 1970)

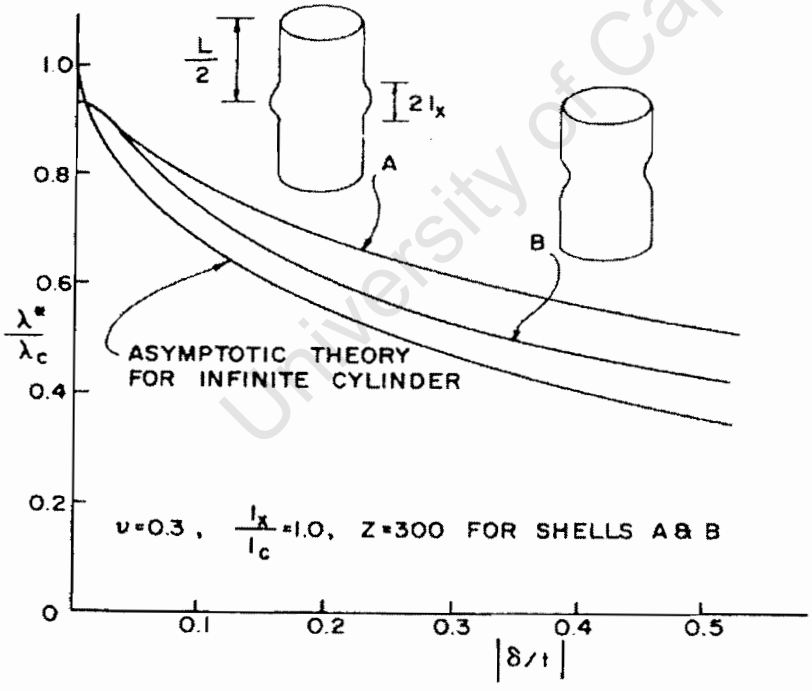

Figure 1.8: Results of Local Axisymmetric Imperfection (Hutchinson, 1970)

The experimental value for the test specimens yielded a buckling strength which was a good comparison with Hutchinson's numerical results and the asymptotic formulae.

The researchers above investigated the effects of predominantly axisymmetric imperfections. Koiter (1963) however hypothesized that the effect of asymmetric imperfections could have a resulting larger reduction in the load capacity. This was investigated by Arbocz and Babcock (1969) who measured the actual imperfections of their test specimens. A thorough account of the development of imperfection studies is given by Arbocz (1974).

Arbocz and Babcock (1969) highlighted three factors that could account for the reduction in strength of cylindrical shells. These are

- Influence of boundary conditions
- The effect of prebuckling deformations caused by edge constraints
- Effect of initial imperfections

In this work they sought to make precise measurements of the imperfections present in the cylindrical shell. Arbocz and Babcock (1969) made use of electroformed copper shells taking surface measurements before and at loading intervals, this included measuring the post buckled state.

"The harmonic components of the measured initial imperfection were used in the theoretical analysis and the analytical predictions were compared." (Arbocz & Babcock, 1969:29)

The end result of the scanning was contained in the development of three Fourier representations, whose coefficients were determined by a double harmonic analysis. The three Fourier representations were (Arbocz & Babcock, 1969:31):

- Full-wave representation in the axial direction
- Half-wave cosine representation in the axial direction
- Half-wave sine representation in the axial direction

Along with the experimental work a theoretical analysis was conducted. Arbocz and Babcock (1969) made use of the nonlinear Donnell-type shell equations. "The initial

imperfection being represented by only three terms of the general double Fourier series, one axisymmetric and two asymmetric" (Arbocz & Babcock, 1969:35)

$$\frac{1}{Et}\nabla^4 F - \frac{1}{R}\frac{\partial^2 W}{\partial x^2} + \frac{1}{2}L\left(W, W + 2\overline{W}\right) \qquad [1.42]$$

$$\frac{Et^3}{12\left(1-\nu^2\right)}\nabla^4 W + \frac{1}{R}\frac{\partial^2 F}{\partial x^2} - L\left(F, W + \overline{W}\right) \qquad [1.43]$$

where:

W is the deflection of the mid-surface

$\overline{W}$ is the imperfection

where L is the nonlinear operator given as:

$$L(s,t) = \frac{\partial^2 s}{\partial x^2}\frac{\partial^2 t}{\partial y^2} - 2\frac{\partial^2 s}{\partial x \partial y}\frac{\partial^2 t}{\partial x \partial y} + \frac{\partial^2 s}{\partial y^2}\frac{\partial^2 t}{\partial x^2} \qquad [1.44]$$

and the term F is an Airy stress function such that

$$N_x = \frac{\partial^2 F}{\partial y^2} \qquad N_y = \frac{\partial^2 F}{\partial x^2} \qquad N_{xy} = \frac{\partial^2 F}{\partial y \partial x}$$

Abrocz and Babcock (1969) reached the following conclusions:

- The comparison of analytical and experimental results showed good agreement for the case of global buckling.
- The shape of the asymmetric imperfection that was the most influential in reducing the buckling load was determined by two criteria:
    - The axisymmetric mode to which it was coupled has a significant value
    - The asymmetric mode corresponded to a buckling mode with the buckling load close to the classical value.

- There existed several "critical modal components" instead of an isolated one.

1.2.2 Imperfections in Spherical Shells

The effect of imperfections in spherical shells has been studied by Budiansky (1959), Tillman (1970) and Hutchinson (1967) among others. Budiansky investigated the effect of imperfections numerically in shallow spherical shells, whilst Tillman did experimental work on shallow spherical shells. Hutchinson adopted the numerical approach to a shallow section of a full sphere.

Budiansky (1959) focused on the effect of an axisymmetric imperfection. The shell geometry was defined with an imperfection. This is given as:

$$Z_0 = H\left(1-\left(\frac{R}{b}\right)^2 - \varepsilon e(R)\right) \qquad [1.45]$$

Here the shape of the imperfection is given by the function *e(R)* and the factor ε is the amplitude of the imperfection. Thus the Budiansky (1959) nonlinear governing equations can be rewritten as:

$$\frac{\partial\left(x\frac{\partial\gamma}{\partial x}\right)}{\partial x} - \frac{\gamma}{x} + x\psi = -2px^2 + \gamma\psi + \varepsilon h\psi \qquad [1.46]$$

$$\frac{\partial\left(x\frac{\partial\psi}{\partial x}\right)}{\partial x} - \frac{\psi}{x} - x\gamma = -\frac{1}{2}\gamma^2 - \varepsilon h\gamma \qquad [1.47]$$

Budiansky (1959) chose the shape of the imperfection to be of the form:

$$e(R) = \left(1-\left(\frac{R}{b}\right)^2\right)^2$$

Budiansky (1959) noted that the parabolic shape did not constitute a deviation from sphericity, and as such the membrane solutions to the differential nonlinear equations could still be applied.

"This state does not however satisfy the fixity conditions, and so bending of the clamped shell must occur all *p*"(Budiansky 1959). Budiansky (1959) results are represented in the graphics below as a comparison with his nonlinear behaviour of the perfect spherical cap. The imperfect curve follows the same pattern; however there is a reduction in the capacity of the shell. The graph plots the normalised capacity (i.e. actual applied load over classical buckling load of a sphere) against the geometric parameter λ_{ss}.

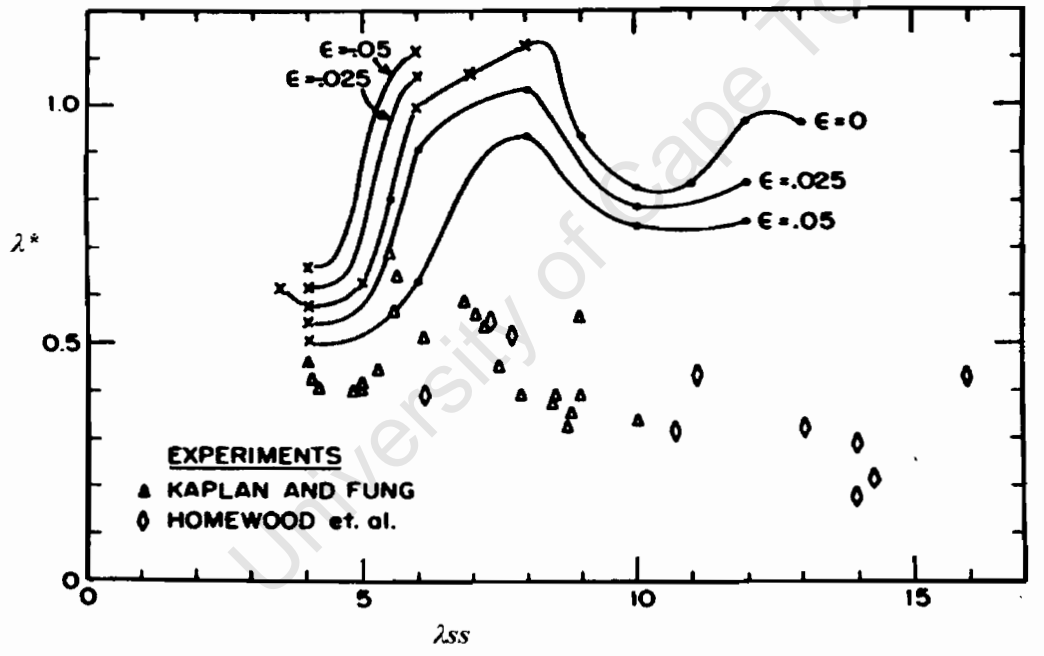

Figure 1.9: Budiansky (1959) Imperfections in Spherical Caps

Tillman (1970) conducted experimental work on shallow spherical shells with a geometrical parameter of λ_{ss} = 5.0. The imperfections consisted of axisymmetrical circular flats of varying diameter. Tillman (1970) represented his results graphically (Figure 1.10) and it indicated that the buckling strength decreased with a corresponding increase in the diameter of the flat section. Figure 1.10 is a measure of

the reduction of the classical buckling strength versus the vertical deflection of the spherical cap V_d.

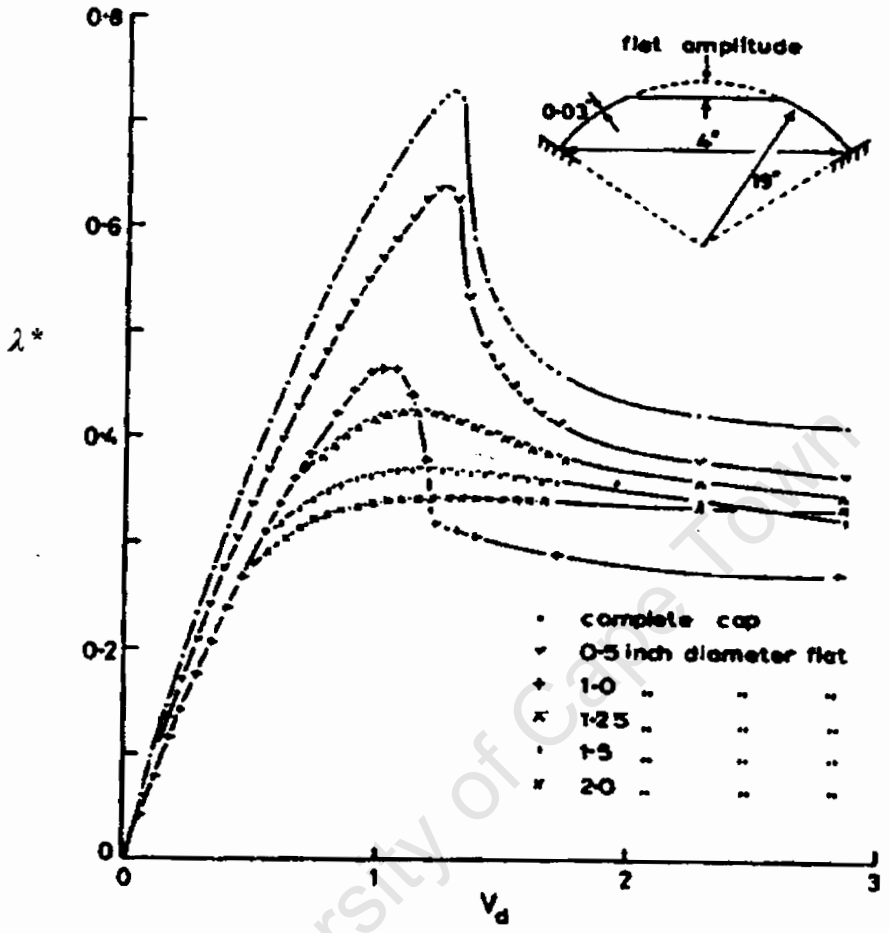

Figure 1.10: Experimental Results from Tillman (1970)

Hutchinson (1967) investigated the initial post buckling behaviour of spherical shells. Hutchinson (1967) made us of Koiter's post buckling theory. The post buckling theory essentially describes the behaviour of the shell after the point of bifurcation. The classical linear theory discussed in the previous sections can only describe the bifurcation point, as the post buckling range is characterised by geometrically nonlinear behaviour. The focus was on multimode buckling, thus the buckling modes from the classical buckling load combine to result in a large decrease in the initial post buckling range.

Hutchinson (1967) illustrated Koiter's use of the variational principle of potential energy to determine equations governing both the prebuckling and post buckling regions. The potential energy of a structure can be written as:

$$PE = \frac{1}{2}\{\sigma, \in\} - \chi B_1(u) \qquad [1.48]$$

where:

χ - the intensity of the applied load

$\chi B_1(u)$ = the work done by the applied load.

u - the displacement filed

The displacement of the structure is a function of the prebuckling displacement as well as the displacements associated with the classical buckling modes. The assumption is that there are several linearly independent buckling modes ($u_c^{(1)}$, $u_c^{(2)}$) at the critical load (χ_c). The total displacement can be written as:

$$u = \chi u_0 + \sum_n \zeta_n u_c^{(n)} + \bar{u} \qquad [1.49]$$

where:

χu_0 - the prebuckling displacements

$\sum_n \zeta_n u_c^{(n)}$ - the buckling modes; these are orthogonal to each other

$\bar{u}$ - the initial imperfection

Hutchinson (1967) included the presence of initial imperfections by making them equal to a form of the classical buckling mode. This can be represented by:

$$\bar{u} = \sum_n \bar{\zeta} u_c^{(n)} \qquad [1.50]$$

Here:

$\bar{u}$ - the imperfection

$\bar{\zeta}$ - the amplitude relative to the wall thickness

$u_c^{(n)}$ - the classical buckling mode

Hutchinson (1967) solved the governing equations for the post buckling region for the case of an imperfection consisting of two and three operative buckling modes. The results of an analysis with a spherical shell containing two operative buckling modes can be seen below.

$$\left(1-\lambda^*\right)^2 = \frac{9C}{8}\left|\bar{\zeta}_1\right|\lambda^* \qquad [1.51]$$

where:

$\bar{\zeta}_2 = 0$ (placing the imperfection in the orthogonal direction equal to zero)

and

$$\left(1-\lambda^*\right)^2 = \frac{27\sqrt{3}C}{32}\left|\bar{\zeta}_2\right|\lambda^* \qquad [1.52]$$

where:

$\bar{\zeta}_1 = 0$

Thus the imperfection was taken to be equivalent to a single mode. Hutchinson performed a further analysis on a spherical with three operative buckling modes at the critical uniform external pressure. The result of an imperfection can be seen as:

$$\left(1-\lambda^*\right)^2 = \frac{9C}{16}\left|\overline{\zeta_3}\right|\lambda^* \qquad [1.53]$$

where:

$$\overline{\zeta}_2 = \overline{\zeta}_1 = 0$$

For all of the above equations:

$$\lambda^* = \frac{q}{q_{cl}} \text{ - Actual Buckling Load / Classical Buckling Load} \qquad [1.54]$$

Thus the effect of the imperfections can be seen in the figure below. The plot represents the actual buckling strength as a factor of the classical buckling strength versus the imperfection amplitude.

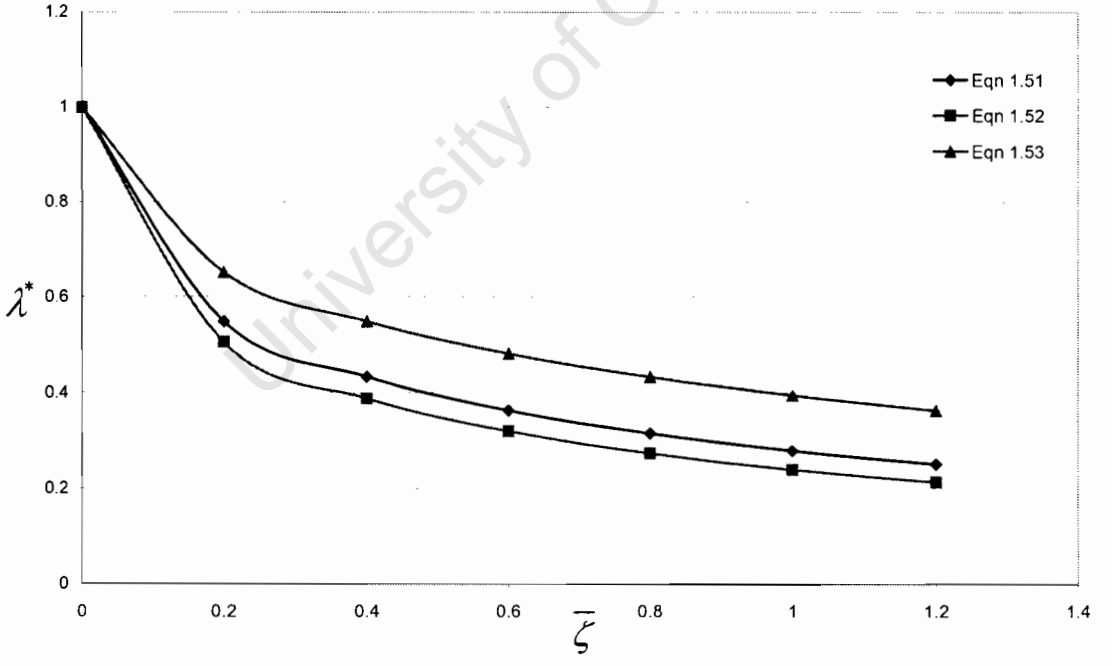

Figure 1.11: Hutchinson Imperfection Equations

Figure 1.11 indicates that there is a loss of buckling capacity with the inclusion of initial imperfections. The solution indicates that having three orthogonal buckling

modes occurring at the critical load with an imperfection in the form of one of the buckling modes leads to the largest loss of capacity for the spherical shell under uniform external pressure.

1.2.3 Imperfections in Conical Shells

The work on imperfections in conical shells is rather limited. Of interest though is work done by El Damatty et al (1997 &1998). The investigation focused on the collapse of a water retaining structure.

The imperfections investigated by El Damatty et al (1997) included an axisymmetric imperfection and a nonaxisymmetric imperfection. These are given below:

$$w = w_0 \sin\left(\frac{2\pi S}{l_r}\right) \qquad [1.55]$$

$$w = w_0 \sin\left(\frac{2\pi S}{l_r}\right)\cos(n\theta) \qquad [1.56]$$

The effect of residual stresses due to welding was also considered, this is however discussed in Chapter 4. The actual geometric effect of a weld imperfection was not considered as the above imperfections were determined as the lowest eigenmodes/buckling modes for the conical shell.

The study conducted by El Damatty et al (1997) involved the use of finite elements. The cone was an inverted truncated and fixed by means of a plate at the lower end and free at the upper end. The support condition was taken as pinned, which can be considered conservative as it does not offer as much restraint as a fully fixed condition. The layout is given in Figure 1.12 below. The load was applied incrementally and the Newton Raphson method used to determine the load path. The load was applied by factoring the hydrostatic load by p, at the bifurcation point $p = p_{cr}$. Thus p_{cr} is a reflection of the factor of safety as a factor of 1.0 indicates that the shell can handle the full application of the hydrostatic load.

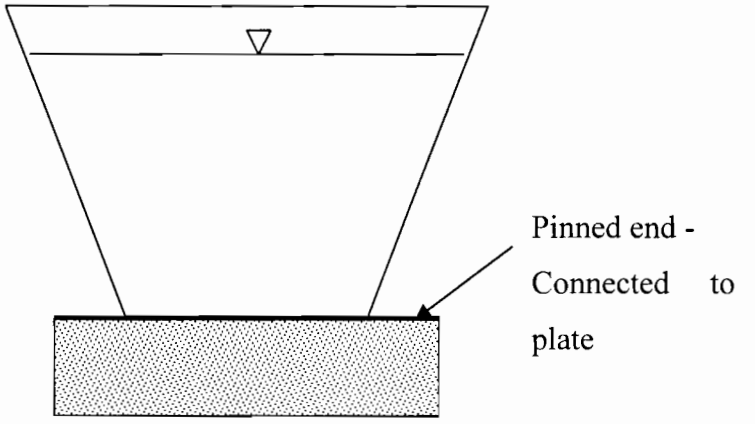

Figure 1.12: Basic Layout of Conical Shell under Hydrostatic Pressure

The investigation was done using a non linear elastic analysis and a nonlinear inelastic analysis. The results were determined for two types of shells a broad shell and a tall shell the vertex angle's are 60 and 45 degrees respectively.

The comparison of axisymmetric and nonaxisymmetric imperfection shapes indicated that the axisymmetric imperfection resulted in the lowest buckling load. The imperfection amplitude was taken as $0.01lr$, where lr is the wavelength of the lowest buckling mode.

The shells were then analysed for inelastic response using purely the axisymmetric imperfections. The imperfection amplitude was taken equal to the shell thickness. El Damatty et al (1997) found that yielding of the material preceded elastic buckling. The failure of the cone was thus an inelastic buckling response. This is specifically viewed in the contrasting results for a tall tank given in the table below.

Table 1.1: Comparison of Elastic and Inelastic Analysis (El Damatty et al 1997:709)

Tank	p_{cr} Elastic Analysis	p_{cr} Inelastic Analysis
T1	1.3	0.7

The buckling mode is illustrated by the diagram below. The buckling is due to the formation of compressive meridional stresses. The hydrostatic pressure does induce internal pressure resulting in tensile hoop stresses which tend to add stability; as such this tends to stiffen the shell, and is the most likely cause that the axisymmetric buckling mode results in the lowest strength. Figure 1.13 shows the transverse displacement (δ) for the non linear elastic analysis and is taken from Damatty et al (1997)

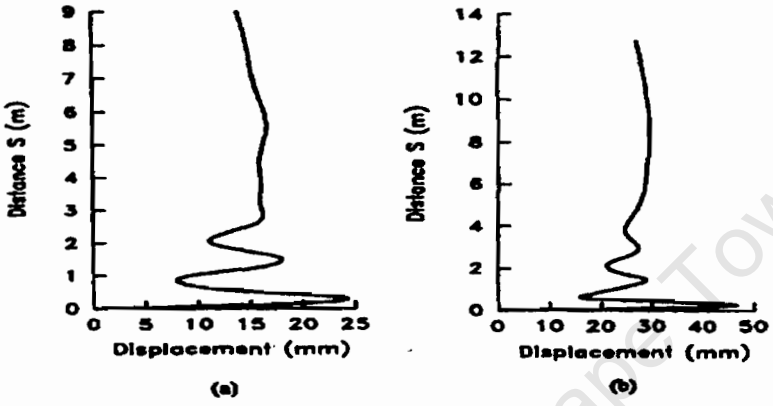

Figure 1.13: Buckling Modes Conical Shell (El Damatty, 1997)

Further research of unstiffened conical shells was conducted by Chryssanthopoulos et al (1998). The research involved the numerical modelling of the buckling behaviour of conical shells. The finite element modelling will be discussed in Chapter 2 along with the assumptions used in this analysis.

Chryssanthopoulos et al (1998) indicates that under the ECCS (1988) recommendations conical shell buckling was treated as an equivalent cylinder problem. The effect of imperfections as per the ECCS was indicated by the use of a knock down factor: α_0. These knock down factors are:

$$\alpha_0 = \frac{0.83}{\sqrt{1+0.01(R_{1e}/t)}} \quad \text{for } R_{1e}/t \le 212 \qquad [1.57]$$

$$\alpha_0 = \frac{0.7}{\sqrt{0.1+0.01(R_{1e}/t)}} \quad \text{for } R_{1e}/t \ge 212 \qquad [1.58]$$

where:

$$R_{1e} = \frac{R_1}{\cos r} \qquad [1.59]$$

Chrysanthopoulos et al (1998) did a comparison of the actual shell behaviour as predicted by finite elements to the ECCS recommendations. The finite element models were validated through matching experimental data with the finite element predictions.

The finite element study involved the use of three models under axial compression. These are:

A) Axisymmetric conical model containing an axisymmetric imperfection
B) A full sector model containing an asymmetric imperfection
C) A full sector model containing an axisymmetric imperfection

The imperfection used for this study was chosen to correspond to the first eigenmode of the linear finite element buckling analysis. The imperfection amplitude w_0 was taken between 0.1 – 1.0 times the wall thickness. The results of the analysis are compared with the ECCS knockdown factors in Figure 1.14 below.

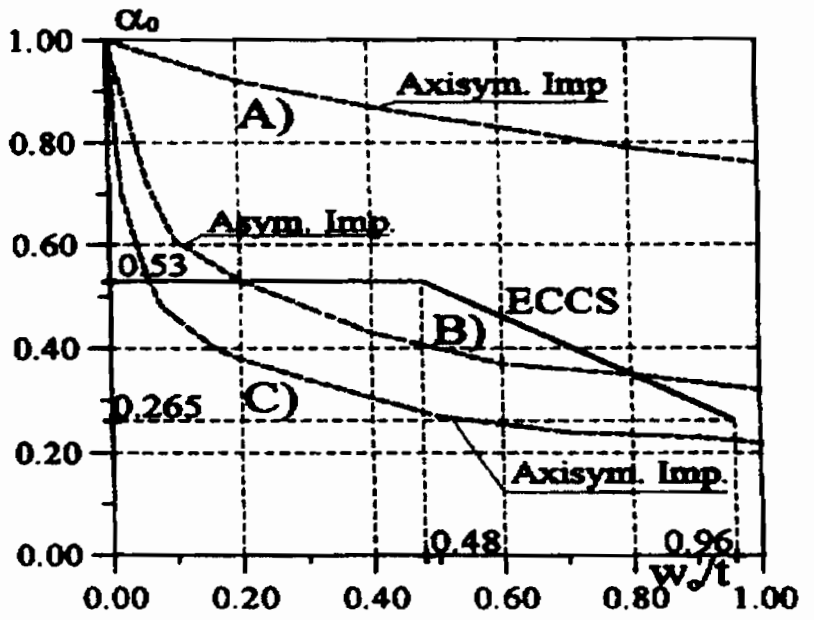

Figure 1.14: Effect of Imperfection on a Conical Shell (Chryssanthopoulos et al, 1998)

From Figure 1.14 it is clear that the use of a full model to study the effect of the imperfection results in a greater reduction in the buckling capacity. This is attributed to the fact that the full finite element model allows the development of asymmetric buckling patterns. The further observation to b made is the axisymmetric imperfection of model *C)* results in the lowest load for the conical shell. .

Chrysannthopoulos et al (1998) did more work on the equivalent cylinder assumption, to determine the effect of the apex angle. This was achieved by altering the conical apex angle and conducting on nonlinear analysis on the axially loaded conical shell. The results are represented in Figure 1.15.

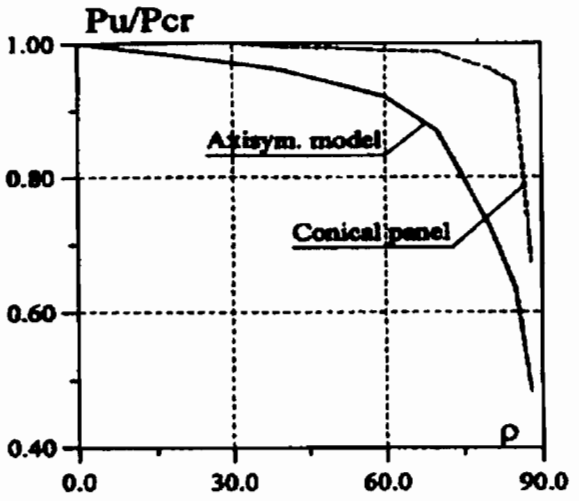

Figure 1.15: Buckling Load of Cone with Differing Apex Angles (Chryssanthopoulos et al, 1998)

From Figure 1.15 it should be noted that in terms of the notation adopted for this dissertation the apex angle:

$$\beta = \rho$$

The results indicate that there is a loss of the buckling capacity with the increase of the apex angle in comparison to the classical axial compression load of an equivalent cylinder.

1.3 Weld-Induced Imperfections

The effect of weld imperfections on the buckling behaviour of shells is receiving increasing attention from researchers worldwide. This chapter aims to give a concise report of these findings.

The weld imperfections occur in structures such as steel silos. The cylindrical silo is fabricated from components (strakes), which are welded in the meridian and the circumferential directions. The circumferential weld is shown by research to be the most detrimental to the stability of steel shells. The circumferential welds are classified as an axisymmetric imperfection, which was shown by a number of researchers to have a reducing effect on the buckling strength.

Pircher and Bridge (2001) highlight four key factors that have an influence on the buckling strength for a welded cylindrical shell:

- The geometric shape of the weld imperfection
- The amplitude of the weld
- The interaction between neighbouring welds
- The effect of residual stresses

The shape and the amplitude of the imperfection will be discussed together, followed by a review of the interaction and residual stresses.

1.3.1 Shape and Amplitude of Weld Imperfection

The effect of an axisymmetric imperfection can significantly reduce the buckling capacity of a cylindrical shell. This section will focus on research regarding the geometric shape of the imperfection; it will include the effect of amplitude on the buckling strength.

The geometric weld imperfection is a combination of weld shrinkage and the rolling process of the steel plates, leaving the plate edges at a slightly different curvature to the rest of the plate. The imperfection can thus be recognized as a geometric shape, which can be described as a function of the axial coordinate x. Picher and Berry (2001) presented a graphical summary of all shape functions derived by previous researchers. These are visible in Figure 1.16 below along with the original researcher's name.

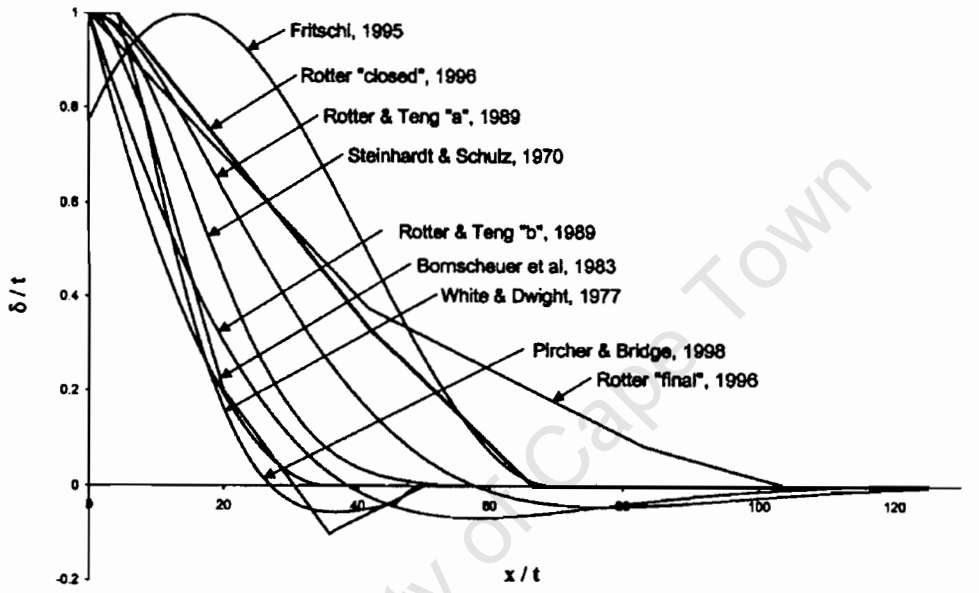

Figure 1.16: Shape functions of Weld Imperfections (Pircher & Bridge, 2001)

The graph illustrates the different shapes by representing the deflection normalised with respect to the thickness and its corresponding location x also normalised with respect to the thickness of the shell. The position $x\backslash t = 0$ thus corresponds to the maximum amplitude of the weld imperfection. The image is thus half of the imperfection as it is mirrored about the vertical axis for the full shape.

The shape functions were later analysed by Bridge and Pircher (2001) who calculated the effect of each imperfection on the buckling of a single strake. The buckling parameters were influenced by the interaction between two adjacent strakes; i.e. whether or not the boundary conditions reflect symmetry or asymmetry.

Picher (2001) developed a basic shape function using an analytical approach. This shape function was later corrected with measurements taken from the port Kembla silo-Australia. Picher (2001) made use of Rotter and Teng's (1989) estimation of the shape functions. Rotter & Teng (1989) had developed their shape functions based on the following premise: "The cooling weld imposes a radial inward force on the shell, which is assumed to remain predominantly elastic. The final shape of the shell is then dependant on the extent to which bending yielding takes place in the weld during cooling. Uncertainty on this question leads to two limiting shapes for the cylinder near the weld". Their Case A represented a weld resisting flexural yielding, while their Case B represented one that was completely flexible. Thus,

TYPE A :

$$w(x) = w_0 e^{\frac{-\pi x}{\lambda}} (\cos\frac{\pi x}{\lambda} + \sin\frac{\pi x}{\lambda}) \qquad [1.60]$$

Applying the boundary condition $\beta_0 = 0$

TYPE B :

$$w(x) = w_0 e^{\frac{-\pi x}{\lambda}} \cos\frac{\pi x}{\lambda} \qquad [1.61]$$

Applying the boundary condition $M_0 = 0$

where:

$$\beta_0 = \frac{dw}{dx} \text{ - the slope of the shell at the weld centre} \qquad [1.62]$$

$$\lambda = \pi \sqrt{\frac{Rt}{\sqrt{3(1-\nu^2)}}} \qquad [1.63]$$

The two shapes are illustrated in Figure 1.17.

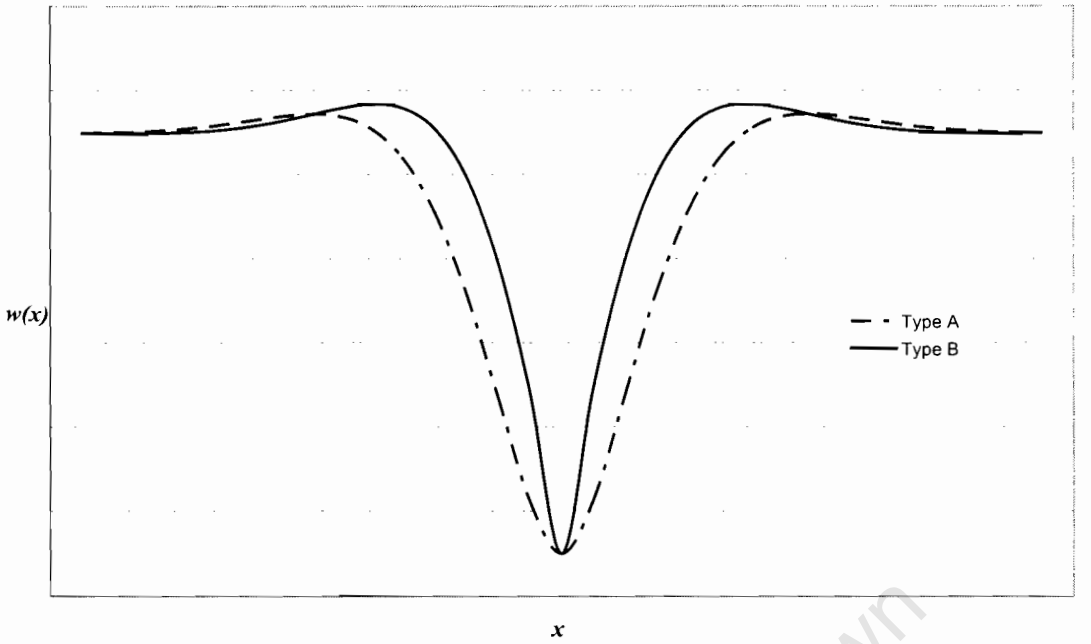

Figure 1.17: Type A and B Geometric Shapes (Rotter and Teng, 1989)

Pircher (2001) developed a shape function that lay in between the envelope shape functions Rotter & Teng A & B. They assumed that the weld offered some flexural resistance to bending; it would have some stiffness *k* and behave like a spring.

Making use of the governing equation for the bending of an axisymmetrically loaded cylindrical shell, Pircher (2001) determined the equation for the shape function. The basic equations are set out below:

The governing equation for axisymmetric bending of a cylindrical shell is given as:

$$D\frac{d^4w}{dx^4}+\frac{Etw}{R^2}=0 \qquad [1.64]$$

Thus assuming the weld to provide an amount of bending stiffness the moment can be written as:

$$M_0=\alpha k\beta_0 \qquad [1.65]$$

where:

α - is the measure of stiffness between 0 – 1.0 [1.66]

$$k = 2\pi \frac{D}{\lambda_0} \quad [1.67]$$

$$\lambda_0 = \pi \sqrt{\frac{Rt}{\sqrt{12(1-\nu^2)}}} \quad [1.68]$$

thus:

$$w(x) = w_0 e^{\frac{-\pi x}{\lambda_0}} (\cos\frac{\pi x}{\lambda_0} + \varsigma \sin\frac{\pi x}{\lambda_0}) \quad [1.69]$$

where:

$$\varsigma = \left(\frac{\alpha}{\alpha+1}\right) \quad [1.70]$$

This represented the basic analytical equation describing the axisymmetric weld imperfection. This equation was later adjusted for the actual measured data of the Port Kembla silo.

What was the effect of the weld imperfection on the buckling strength of a cylindrical shell under axial compression? Pircher & Bridge (2001) used the shape functions in Figure 1.16 to do a buckling analysis on a single strake. The buckling was done using the finite element package ABAQUS. The pattern was set to an asymmetric one and by manipulation of the boundary conditions it was found that this produced the lowest buckling load due to interaction of weld imperfections, this is illustrated in Figure 1.19 below. The results are represented in Figure 1.19, as a ratio of actual buckling stress (σ) vs. classical buckling stress (σ_{cl}).

The equation for the imperfection gained analytically as an intermediate of Rotter and Teng's extreme was investigated separately. The investigation focused on the

influence of half-length and amplitude of the imperfection. The results are correspondingly listed in Figure 1.19.

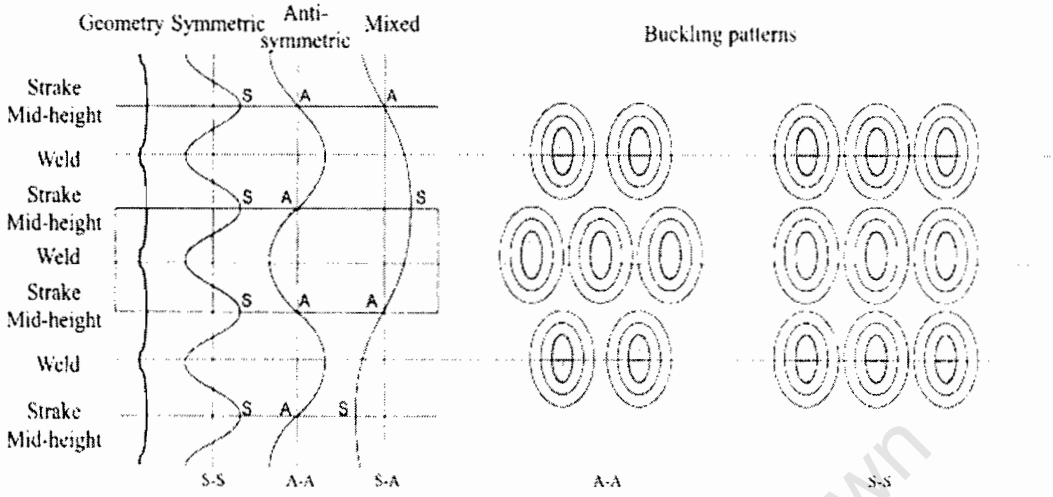

Figure 1.18: Buckling Modes (Pircher & Bridge, 2001:572)

Figure 1.18 is an illustration of the boundary conditions adopted by Pircher & Bridge (2001) for the finite element study. They did not study a full model, but only a single strake thus the boundary conditions needed to be applied in such a way as to mimic the desired behaviour. Thus the boundary conditions were dictated in the finite element model by the above scenarios of symmetrical or asymmetrical behaviour.

The boundary conditions were utilized in an analysis of the shape functions illustrated in Figure 1.16. The results are represented graphically below in Figure 1.20. It can be seen that overall the effect of an axisymmetric weld is deleterious to the buckling strength of a cylinder. Figure 1.19 shows that the single circumferential weld in a cylinder under axial compression can account for a loss of 78 – 74% of the classical buckling strength derived in section 1.2.1. Figure 1.19 also illustrated the individual effect of the shape functions summarised in Figure 1.16. It can also be seen that the inclusion of residual stresses leads to a strengthening effect on the buckling strength this will be discussed in a later section.

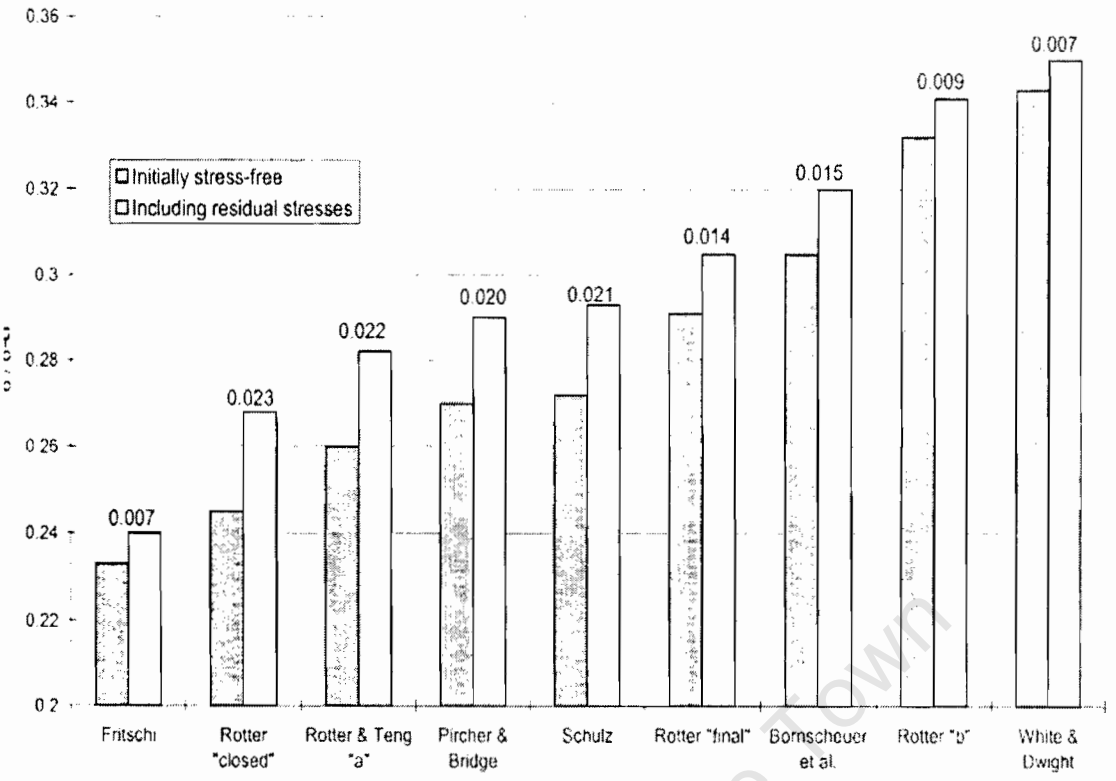

Figure 1.19: Buckling Stresses for corresponding shape functions (Pircher & Bridge, 2001)

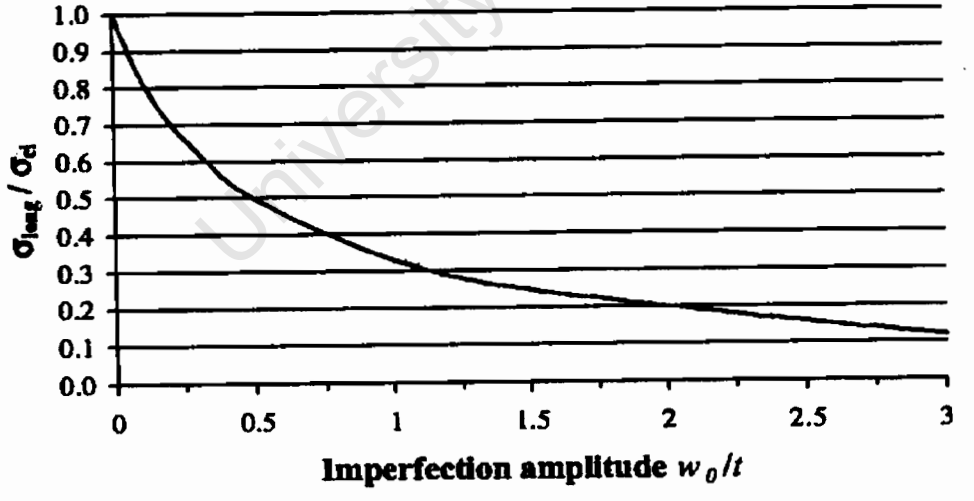

Figure 1.20: Buckling for a variation of imperfection amplitudes (Pircher & Bridge, pg.56)

Figure 1.20 focuses on the effect of varying the imperfection amplitude of the weld imperfection. The graphical results show the actual buckling stress as a fraction of the

classical strength versus the imperfection amplitude as a fraction of the thickness. It is clear that an increase in imperfection amplitude has a resulting decrease in the bucking load.

Rotter and Teng (1989) investigated the effects of their two shape functions A and B. They used a shell of constant thickness with a radius to thickness ratio of 1000, and the shell was under an axially compressive force. The study made use of the following parameters:

$$\frac{L}{R} = 3 \qquad [1.71]$$

$$w_0 = 1.0t \qquad [1.72]$$

The finite element mesh was refined in the region of the weld imperfection to account for the increased bending stresses. The mesh size used was given as a function of:

$$0.25\sqrt{(Rt)} \qquad [1.73]$$

The results for the two shape functions are:

Type A: $\lambda^* = 0.306$

Type B: $\lambda^* = 0.363$

The buckling occurred in the circumferential direction with the number of waves being 18 for both weld types. Rotter and Teng (1989) indicated that the buckling mode is strongly located in the region of the weld imperfection. The meridional form of the buckle coincides with the assumed shape functions. This is better illustrated in the figure below which plots the meridional buckle for the respective geometric weld imperfections.

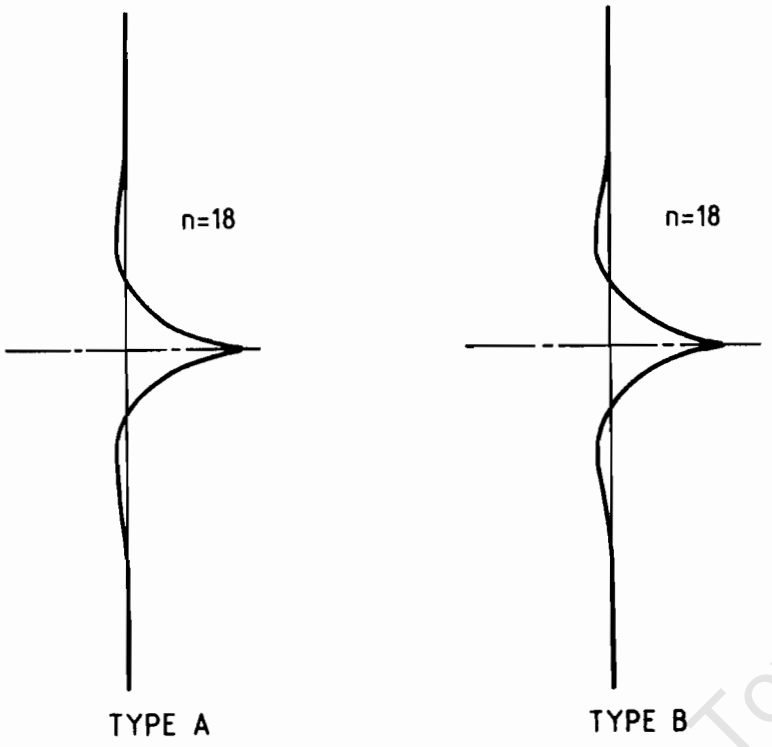

Figure 1.21: Buckled Shape of Axially Loaded Cylinder (Rotter & Teng, 1989)

Berry and Rotter (2000) sought to conduct experimental work that was representative of the civil engineering structure. This was done by constructing cylindrical test specimens that contained a circumferential weld imperfection. The cylinders also contained longitude imperfections but as shown this are not as detrimental to the buckling strength. Berry and Rotter (2000) layout the fabrication procedure for the test samples, they used a pulsed tungsten inert gas machine with an automatically regulated torch. The test cylinders were measured both initially and at loading intervals by means of a laser displacement meter.

The axisymmetric imperfection was measured and Berry and Rotter (2000) made use of finite elements to model the shell geometry. They were able to model the experimental results fairly accurately. The following figure represents the finite element model used.

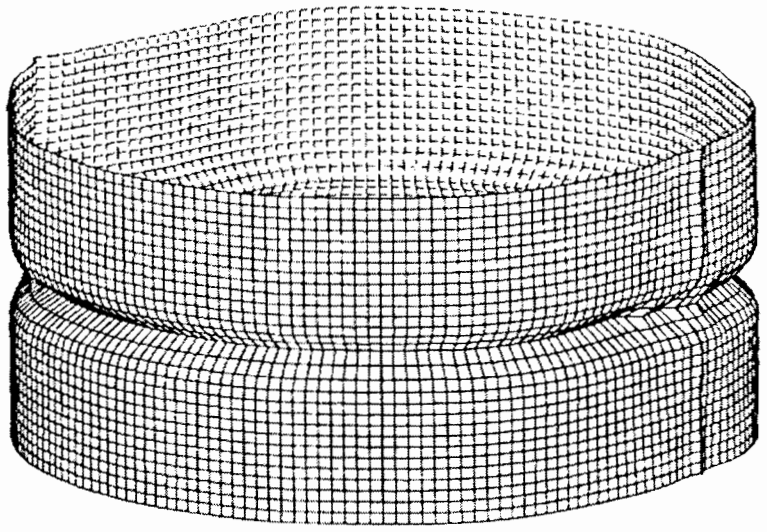

Figure 1.22: Finite Element Model of Cylindrical shell Containing and Axisymmetric Weld Imperfection (Berry & Rotter, 2000:407)

Berry and Rotter (2000) also made a comparison of the earlier shape functions Rotter & Teng A & B with the actual measured weld imperfection. The measured weld imperfection was found to lie between the two shape function which was to be expected as the weld will offer some bending resistance as previously stated by Pircher (2001). Figure 1.23 indicates the shape of the weld imperfections.

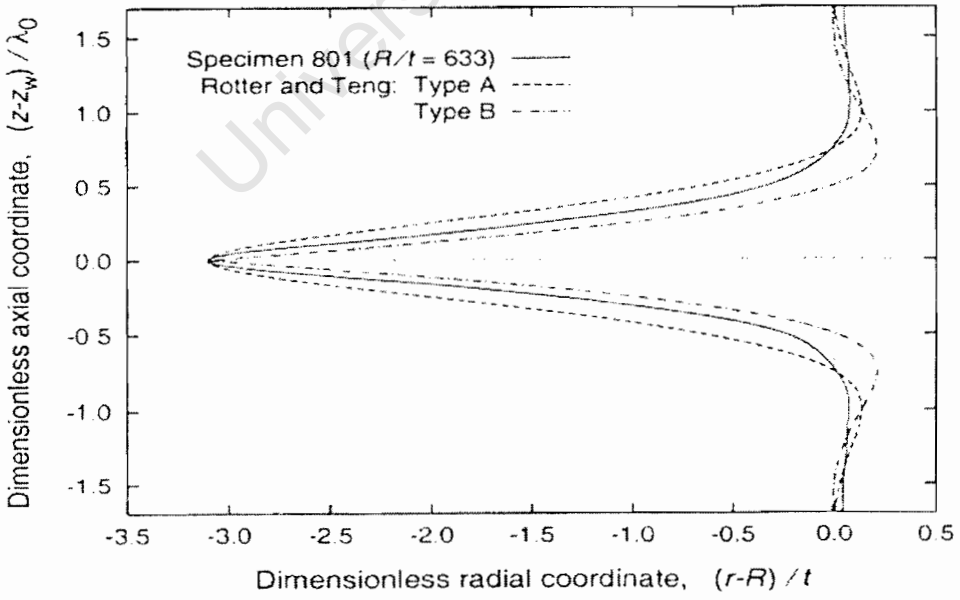

Figure 1.23: Comparison of Rotter & Teng shape functions with the actual measured shape. (Berry & Rotter, 2000:408)

The following represents the important findings in the experimental work by Rotter and Berry (2000); imperfection amplitude of 1.8-3.4 times the thickness can result in buckling loads of between 17-21% of the classical value. It was further found that the closer the half wavelength of the imperfection was to the linear meridional bending wave length the more critical the imperfection. This is observed more in the measured geometric weld imperfections as the analytical approach limited the extent of the imperfection to decay as a function of the shell bending. Finally Berry and Rotter (2000) indicate the for high imperfection levels failures tend towards plastic collapse rather than a typical bifurcation failure.

1.3.2 Residual Stresses

Welding induces residual stresses due to the cooling process. The shrinkage in the vicinity of the weld also results in the formation of residual stresses as the shell deforms trying to relieve the stress build up. There have currently been few papers focusing on the effect of residual stresses in Cylindrical shells. These consist of Rotter (1996), Bornscheuer (1983) and Holst et al (1999 & 2000). The last two papers of Holst were mostly concerned with the lack of misfit due to curvature changes, but they do give a coherent technique for the inclusion of residual stresses.

Bornscheuer & Hafner (1983) made use of three idealised residual stress fields. The shapes were taken as:

- Parabolic
- Rectangular
- Decreasing

The parabolic stress field is illustrated in the diagram below.

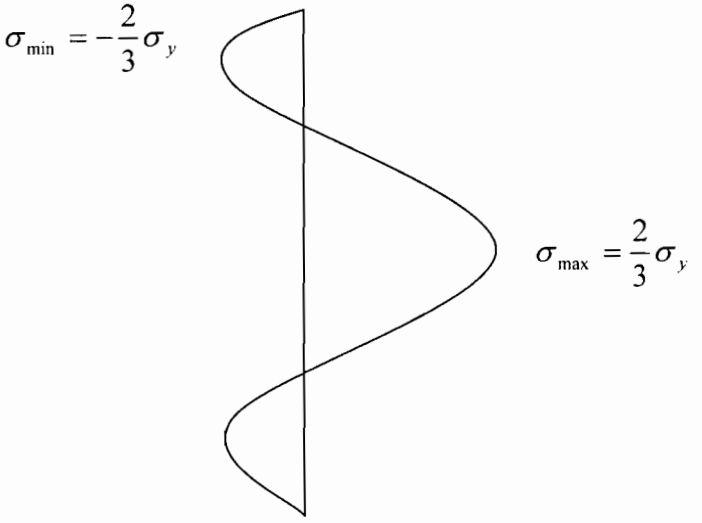

Figure 1.24: Bornscheuer & Hafner Parabolic Residual Stress Field

The max and minimum residual stresses are a function of the yield stress of the material. The numerical analysis was conducted using the parabolic residual stress function along with the imperfection shape defined earlier in Figure 1.16 by Pircher and Bridge (2001). Bornscheuer & Hafner (1983) found that there was a further loss of 5 -10% in strength with the inclusion of residual stresses.

Rotter (1996) found contradicting results to those proposed by Bornscheuer and Hafner (1983). His analysis was based on the assumption that the residual stresses could be induced into the structure through the application of a residual strain as a load to the shell. This allowed the shell to develop the corresponding stresses and deformations to gain equilibrium. This is different from the above approach which applied the stress pattern; Pircher and Bridge (2001b) indicate that this does not fully allow the shell to reach equilibrium under loading.

Rotter (1996) sought to analyse the effect of imperfections whose amplitude was the same as the shell thickness. He assumed an initial geometric imperfection of amplitude 9.4mm, the application of the residual shrinkage would result in total amplitude of 12mm that corresponded to the thickness. Rotter (1996) applied a residual strain equivalent to the yield strain for mild steel of $\varepsilon = 0.00125$. The

resulting stress pattern is visible in Figure 1.25 below. Rotter assumed a large residual strain to provide a clear indication of its effects on strength. This doe not necessarily correspond to real residual strains but provides a coherent reference with which to understand their likely effects.

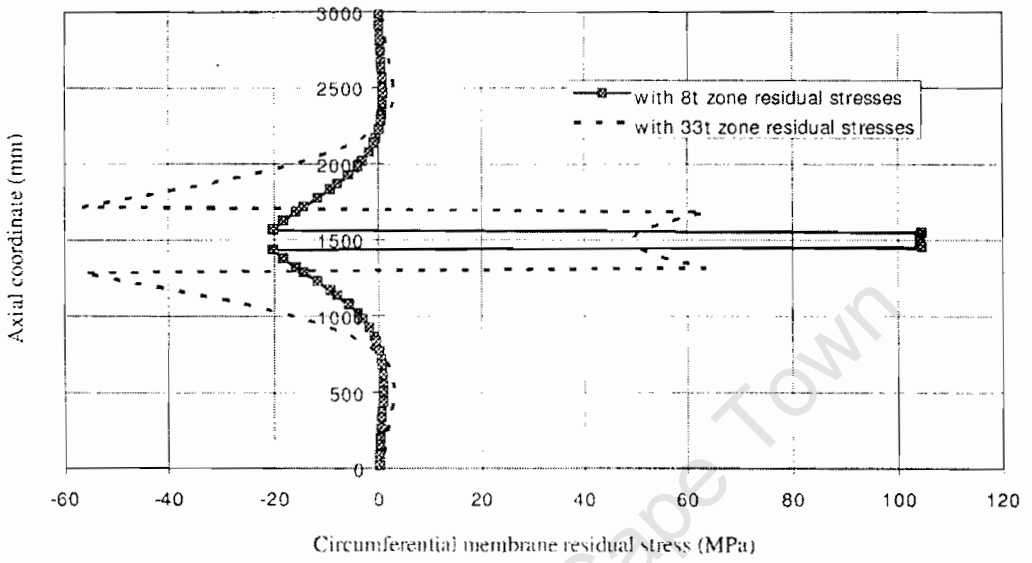

Figure 1.25: Rotter (1996) Residual Stresses

The residual strain was applied over a length of 50mm above and below the weld centre. This corresponds to the distance of 8t in Figure 1.25. The numerical results indicate that the residual stresses actually increase the buckling load. The residual stresses lead to the development of tensile circumferential stresses which results in the increase. "The imperfection sensitivity of the depression arises principally from the development of compressive circumferential stresses in the middle of the depression. Thus the depression with out residual stresses leads to lower buckling strength because there are both meridian and circumferential compressive stresses" (Rotter 1996:133)

Pircher and Bridge (2000) did further work on residual stresses that confirmed the approach adopted by Rotter (1996). They correspondingly found that the presence of residual stresses increases the buckling strength of the imperfection sensitive shell.

Holst et al (1999) and Holst et al (2000) give a further illustration of the technique for the use of residual strains as a loading pattern. The research was primarily focused on the lack of fit in the uniaxial and biaxial directions. The lack of fit thus became the residual strain through forcing the closure. Of primary interest is the uni-axial shrinkage.

Residual stress calculations in conical shells were conducted by El Damatty et al (1997). This included both the weld in the circumferential and longitudinal directions. The residual stress pattern was based on that derived by Bornscheuer & Hafner (1983) in which the stress distribution was parabolic and described by:

$$\sigma_b = \sigma_y \left[2\left(\frac{Y}{L}\right)^2 - \frac{4}{3}\left(\frac{Y}{L}\right) \right] \qquad [1.74]$$

$$L = 60t$$

El Damatty et al (1997) indicated that for the residual stresses to be self equilibrating an adjustment for the change of surface area in the cone had to be considered. Thus the residual stress was determined as:

$$\sigma_{res} = \sigma_b \left(\frac{r}{r_u} \right) \qquad [1.75]$$

The analysis found that the effect of the residual stresses was only a reduction of 5-10% in the load carrying capacity. In the subsequent inelastic analysis conducted by El Damatty et al (1998) the effect of residual stresses was ignored. The diagrams below give a graphic representation of the residual stresses resulting from a) two longitudinal welds and b) from two circumferential welds. The investigation did not involve any assumed weld imperfection shape for the conical shell.

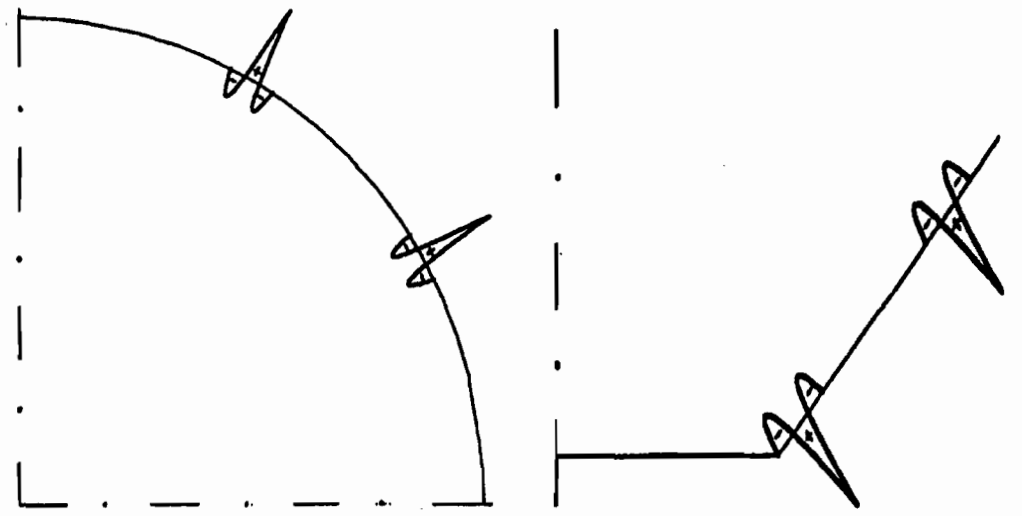

Figure 1.26: Residual Stress Patterns; a) Longitudinal b) Circumferential (Damatty et al 1997:709)

1.3.3 Effect of Adjacent Weld Imperfections

Civil engineering structures such as silos are fabricated out of components (strakes) that are welded in the circumferential and longitudinal directions at regular intervals. Hence the actual structure's behaviour will be influenced by the interaction of the weld depressions. Investigations into this have been conducted by Rotter (1996) and Pircher & Bridge (2001a,b,c).

Rotter (1996) took as a reference state the presence of a single weld in a long cylinder (Isolating the effect of the boundary conditions). The analysis was then performed on a shell containing identical weld imperfections at equal spacing. Rotter (1996) assumed that each weld was equally detrimental to the buckling strength, Pircher and Bridge (2001) point out that this is a conservative approach but entirely valid.

For the purposes of the numerical analysis Rotter (1996) and Pircher & Bridge (2001) had to assume an interaction between the adjacent welds which were placed the height of a single strake apart. This is represented in Figure 1.17 as the symmetric interaction, asymmetric and mixed. Thus threes conditions would be enforced in the finite element analysis through the manipulation of the boundary conditions. (it must

be indicated that to analyse a full shell is computationally expensive, thus the shell was most likely modelled using the boundary's to enforce conditions of symmetry or asymmetry). Rotter (1996) results can be seen in Table 1.2 below.

Table 1.2: Axial Compression Buckling Strength Predictions (Rotter 1996)

Shape	Amazigo & Budiansky (1972)	Rotter & Teng Type A (1989)	Rotter & Teng Type B	Single Weld In Long Shell	Adjacent Welds S/S	Adjacent Welds S/A	Adjacent Welds A/A
λ^*	0.320	0.305	0.363	0.301	0.429	0.260	0.250

Thus it is visible that the assumption of asymmetric interaction between the adjacent welds results in the largest loss of buckling strength to a value of 0.25 compared with a single weld of 0.301.

Pircher and Bridge (2001) indicate that the buckling strength is further influenced by the strake height. They found that when imposing the A/A condition that buckling strength varied with the change in strake height, reaching a minimum of roughly 0.25 for a strake height in the vicinity of 2.5-5m.

Thus we can conclude that the interaction between adjacent welds does tend to reduce the buckling strength. However this is dependant on the type of interaction that occurs or is allowable by the structure.

1.3.4 Measurement of Imperfections

The measurement of imperfections has been done by a number of researchers. Rotter (1996), Pircher & Wheeler (2003) made some measurements of imperfections in cylindrical shells. The two approaches differed and each will be discussed below.

Rotter (1996) wished to ascertain information regarding the weld imperfection. The approach adopted was that outlined in the ECCS code for the measurement of imperfections in large structures. Rotter (1996) describes the stipulated method; one has to use a rod. The rod length is given by the condition:

$$L_{rod} = 4\sqrt{Rt} \qquad [1.76]$$

Rotter (1996) indicates that an exception in the ECCS code exists in the case of circumferential welds where the length of the rod should be *25t*. In the investigation Rotter (1996) relied purely on a rod length of 1500mm or 3000mm to determine the shape of the weld imperfections. The following figure indicates the outline of the measurement techniques described by Rotter (1996).

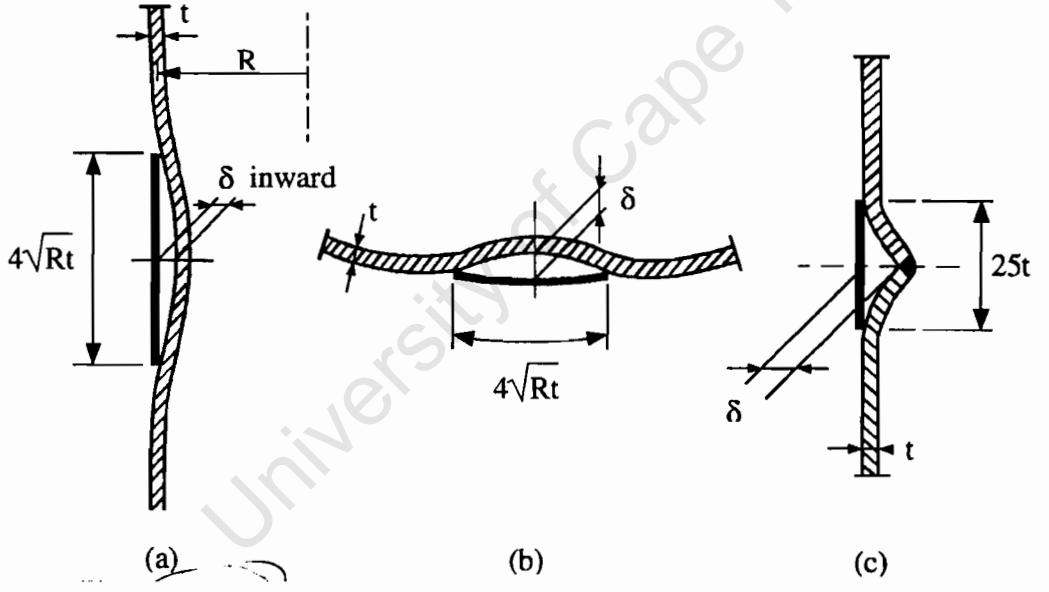

Figure 1.27: ECCS Measurement Guidelines (Rotter 1996:123)

Rotter (1996) found that the circumferential weld was the dominant source of imperfections after collecting data from a number of steel silos. The measurements were taken vertically across the weld imperfection and away from the weld to get a representative nature of the imperfections. The rod was then used as a reference to determine the amplitude of the imperfections. Further detailed measurements were made in the vicinity of the weld by Rotter (1996) to get a complete representative shape of the weld imperfection. Numerous readings were taken around the

circumference of the cylinder and statistical data was constructed from the measured values. Rotter (1996) found that the characteristic value provided a reasonable representation of the weld, if not slightly higher than that of the mean value for a single circumferential weld.

Pircher & Wheeler (2003) conducted imperfection measurements on cylindrical shells in a laboratory environment. They made use of Low Voltage Displacement Transducers (LVDTS) to create an imperfection map of the whole cylindrical shell.

Pircher and Wheeler (2003) made use of 12 LVDTS placed next to each other on a trolley perpendicular to the cylindrical shells axis of revolution. The shell was then rotated and measurements taken around the circumference till the starting points were re measured to establish closure and to account for any errors. The trolley was then moved forward and the process repeated. Pircher and Wheeler positioned the LVDTS so that there was an overlap between five of the transducers, again feeding information for possible error corrections.

The trolley had a vertical deflection; to account for this an optical levelling device was used to determine the relevant displacement at three points of the trolley. This allowed for errors to be corrected in the vertical readings of the transducers. The measurements were again taken in the circumferential direction and this continued till the entire surface was mapped. Figure 1.28 indicates the experimental set up adopted by Pircher & Wheeler (2003).

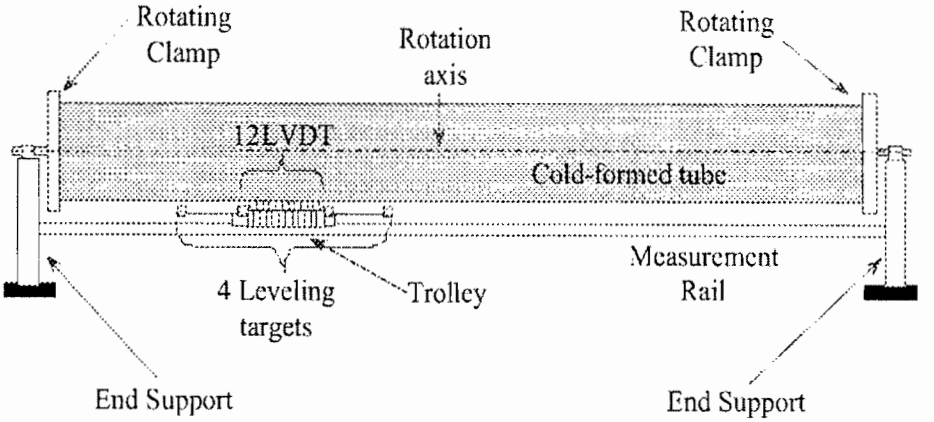

Figure 1.28: Experimental Setup (Pircher & Wheeler 2003:421)

1.3.5 Weld-Induced Imperfections in Spherical Shells

The previous sections have dealt with the effect of weld-induced imperfections on the buckling behaviour of cylindrical shells. This section will focus on some work that has been conducted on the buckling behaviour of spherical shells.

Grunitz (2002) studied the effect of a single circumferential weld-induced imperfection on the buckling behaviour of shallow spherical caps subject to a uniform external pressure loading. The shell in question had the following parameters:

$R = 5.0m$

$t = 3mm$

$H = 0.669m$

$\frac{R}{t} = 1667$

Grunitz approximated the weld-induced imperfection by applying a "prestress" force to a number of elements in the finite element model. This approximated the shrinkage behaviour due to the cooling process. As such the analysis was a two-step analysis. Step one was a static analysis allowing the formation of the geometric imperfection as well as the residual stresses. Step 2 was the nonlinear buckling analysis.

The study was conducted for the case of both pinned and fixed boundary conditions. The weld was placed at three different meridional angles. The results are recorded in Table 1.3 below.

Table 1.3: Effect of Circumferential Weld on a Shallow Spherical Cap (Grunitz 2002)

Meridional Location ϕ_w	Fixed Boundary Condition λ^*	Pinned Boundary Condition λ^*
10	0.35	0.25
15	0.4	0.30
20	0.45	0.35

The results indicate that the circumferential weld does have a significant effect on the buckling behaviour of a shallow spherical cap.

1.4 Research Aims and Methodology

The literature review has covered the buckling of shells from the derivation of the classical buckling strength to the effect of the weld imperfection on the buckling strength.

The summary of this previous research shows that the effect of imperfections on the thin walled shells is to lower the buckling capacity. As such the use of the classical buckling strength is no longer applicable from the design point of view. Taking this into account the ECCS (1988) outlined a revised approach to account for imperfection in shell buckling.

The focus of this thesis is specifically the effect of weld-induced imperfections on the buckling capacity of thin-walled shells. The previous research has been predominantly based on the cylindrical shell. The findings can be summarized as follows:

- The Circumferential Weld is an axisymmetric imperfection and reduces the buckling capacity of a conical shell under axial compression by as much as 70%.

- The main consequence of the welding process is the geometric shape imperfection due to the cooling and resultant shrinkage of the plates in the region of the weld.
- Residual stresses were in some cases shown to increase the buckling capacity.
- Adjacent circumferential weld imperfection can further reduce the buckling load.

- For the conical and spherical shells there has been relatively little work conducted on the effect of weld imperfections

The geometric shapes used in the analysis of the cylindrical shell weld imperfections were based predominantly on measured data from actual constructions. This gives a realistic shape of the imperfection for use in finite element analyses. For the conical and spherical shells there is a lack of measured data concerning the shape of the weld imperfection. Grunitz (2002) study made use of pre-stressed elements to derive the geometric weld shape.

Taking these findings into account, the following will form the basis for this dissertation. The aim is to study the effect of circumferential welds on the buckling strengths of both the spherical and conical shell. The study is to be conducted using the finite element software ABAQUS.

The approach to be adopted to solve the problem will be:

- The derivation of idealised geometric weld shapes. This will be achieved using an analytical approach as a first estimate. The analytical approach will be based on the assumptions outlined by Rotter and Teng (1989). The geometric weld shape will be determined using Geckler's approximation for the edge bending effects on spherical and conical shells.
- A verification of the finite element analysis will be conducted. This will be achieved in three parts:

  - The use of perfect shells for which the classical buckling solution of Section 1.2 can be use as a bench mark to the linear elastic eigenvalue predictions obtained form ABAQUS.
  - The re-analysis of previous problems for which there are known solutions to verify modelling assumptions and procedures.
  - The experimental testing of some fabricated specimens.
- A detailed investigation of the imperfect spherical and conical shells will then be conducted using the software ABAQUS. The invesetigation will be parametric in nature, dealing with different variables studied in the relevant chapters. The analysis will focus on the effect of circumferential weld imperfections; i.e local axisymmetric imperfections.

The study will thus deal with the weld-induced geometric imperfection and the effect of residual stresses will not be covered. This approach is followed as results of the literature review in section 1.3.2 indicated that the residual stresses accounted for an effective 10% deviation in the strength of the shell which can be considered marginal in comparison to the shape effect.

The actual shape of the weld-induced imperfection does differ from the idealised shape function. However the idealised weld-induced imperfection shape does provide a reasonable starting point as was shown by the results of Rotter and Teng (1989) and it can lend itself to future calibration with actual measured data as illustrated by Pircher and Bridge (2001).

2 THE FINITE ELEMENT METHOD

The finite element method and formulation is presented by Zienkiewicz (1971) and Cook (1974). The chapter will cover the basic background on finite elements followed by a specific focus on the two methods of analysis used for this dissertation. The methods used are the linear buckling analysis and the non linear static analysis for unstable collapse and post buckling behaviour.

2.1 The Basic Finite Element Formulation

The finite element method solves the structural response by discretizing the structure into a number of elements. The simplest example is a cable problem illustrated below.

Figure 2.1: Simple Cable with Elements

The unknowns are the displacements at the nodes. The boundary conditions are introduced at the supports and by the condition that the displacements of two elements at a shared node are equal.

The displacement of the cable in Figure 2.1 is approximated by a trial solution which commonly takes the form of a polynomial equation. The trial solution consists of the nodal parameter and the shape function and is written as:

$$u = [N_i, N_j, N_m, ...] \begin{Bmatrix} \delta_i \\ \delta_j \\ \delta_m \\ . \end{Bmatrix} \quad [2.1]$$

where:

u – is the vertical deflection

N – is the shape function

δ – is the nodal displacement/parameter

An alternative formulation of this trial solution can be written as:

$$\overline{U}(x,a) = \sum_{j=1}^{n} N_j(x) a_j \quad [2.2]$$

where:

n – is the number of nodes in the problem

a_j - is the nodal Displacement

x – is the coordinate along the cable length

Zienkiewicz (1971) and Cook (1974) make use of the energy method and the Raleigh Ritz method to formulate the finite element problem. Another method is the Galerkin method. Applying this we obtain:

$$\int_{\Omega} R_{\Omega}(x,a) W_i d\Omega = 0 \quad [2.3]$$

where:

$R(x,a)$ – is the residual equation

W_i – is the weighting factor is this case taken as the shape function N_i, $i=1.....n$

The cable problem in Figure 2.1 is governed by the ordinary differential equation:

$$\frac{-d}{dx}\left(\alpha(x)\frac{dU}{dx}\right)+\beta(x)U(x)-f(x)=0 \qquad [2.4]$$

Making use of the trail solution $\overline{U}(x,a)$ indicated earlier, the Galerkin method becomes (Balden (2003)):

$$\int\left(\frac{-d}{dx}\left(\alpha(x)\frac{dU}{dx}\right)+\beta(x)U(x)-f(x)\right)N_i dx=0 \qquad [2.5]$$

This results in the matrix form of the problem:

$$[K]\{a\}=[F] \qquad [2.6]$$

where:

$[K]$ is the stiffness matrix given by:

$$K_{i,j}=\int_{x_a}^{x_b}\frac{dN_i(x)}{dx}x\frac{dN_j(x)}{dx}dx \qquad [2.7]$$

$[F]$ is the forces matrix given by:

$$F_i=\int_{x_a}^{x_b}\frac{2}{x^2}N_i(x)dx-\left[\left(-\alpha(x)\frac{d\overline{U}}{dx}\right)N_i(x)\right]_{x_a}^{x_b} \qquad [2.8]$$

for:

$i, j = 1,2.....n$

The shape functions are mostly approximated using polynomials of differing orders. A common shape function is the Lagrange Interpolation Polynomial. The Lagrange polynomial is formulated to satisfy the condition:

$$N_1(x_1) = 1$$
$$N_1(x_2) = 0$$

Thus the nodal parameters a_i become the actual displacements of the nodes, and scale the given shape functions to obtain the overall shape of the displaced structure. This can be demonstrated by means of a simple linear polynomial:

$$N_i = a + bx \qquad [2.9]$$

Figure 2.2 indicates the Lagrange Interpolation Polynomial (Balden 2003). The formulation applies to Equation 2.2 where $\varphi = N$.

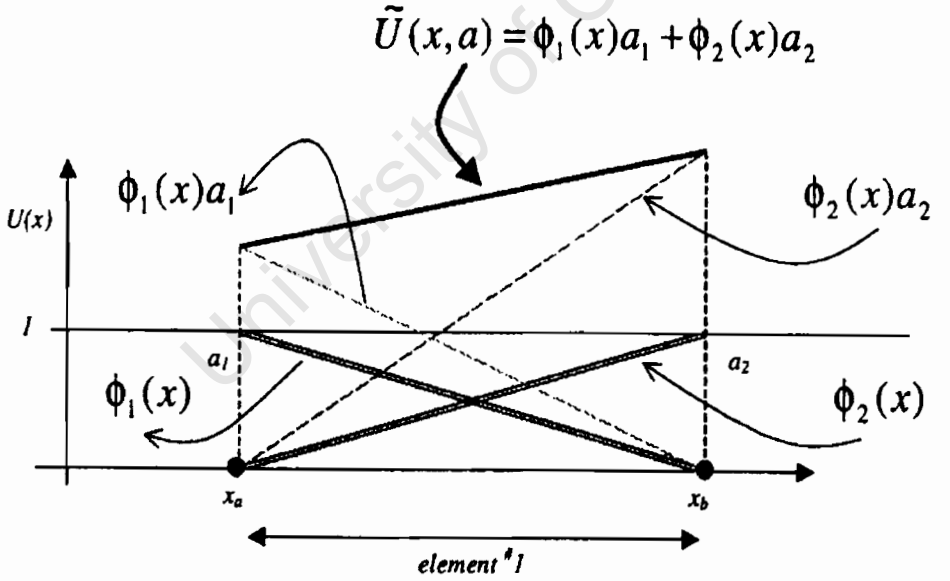

Figure 2.2: Lagrange Interpolation Polynomial (Balden, 2003)

Cook (1974) gives a generalization of the trial solution for a two dimensional element, this forms the basis for a three dimensional trial solution.

$$\overline{U} = \sum_{i=1}^{n}\sum_{j=1}^{m}\sum_{k=1}^{o} N_i(x)N_j(y)N_k(z)u_{ijk} \qquad [2.10]$$

here:

$u_{i,j,k}$ is the nodal parameter at the point x_i, y_j, z_k.

The equivalent formulation for a trial solution in a three dimensional space is given by Balden (2003) for the displacements u, v, w.

$$\overline{u}(x,y,z) = \sum_{j=1}^{n} N_j(x,y,z)u_j \qquad [2.11]$$

$$\overline{v}(x,y,z) = \sum_{j=1}^{n} N_j(x,y,z)v_j \qquad [2.12]$$

$$\overline{w}(x,y,z) = \sum_{j=1}^{n} N_j(x,y,z)w_j \qquad [2.13]$$

This can be written in the matrix format as:

$$\left[\overline{U}\right] = [N]\{a\} \qquad [2.14]$$

The stiffness matrix for a 3 dimensional linear isotropic elastic problem is given by Balden (2003) as:

$$[K] = \iiint [B]^T [C][B]dxdydz \qquad [2.15]$$

where:

$$\{\varepsilon\} = [B]\{a\} \qquad [2.16]$$

The strain for a three dimensional problem is defined as:

$$\{\varepsilon\} = \begin{bmatrix} \varepsilon_x \\ \varepsilon_y \\ \varepsilon_z \\ \gamma_{xy} \\ \gamma_{yz} \\ \gamma_{xz} \end{bmatrix} = \begin{bmatrix} \dfrac{\partial u}{\partial x} \\ \dfrac{\partial \mathrm{v}}{\partial y} \\ \dfrac{\partial w}{\partial z} \\ \left(\dfrac{\partial u}{\partial y} + \dfrac{\partial \mathrm{v}}{\partial x}\right) \\ \left(\dfrac{\partial \mathrm{v}}{\partial z} + \dfrac{\partial w}{\partial y}\right) \\ \left(\dfrac{\partial u}{\partial z} + \dfrac{\partial w}{\partial x}\right) \end{bmatrix} \qquad [2.17]$$

Thus by substituting in the trial solutions we come up with the equation:

$$\{\varepsilon\} = [B]\{a\} \qquad [2.18]$$

$$\{\sigma\} = [C]\{\varepsilon\} \qquad [2.19]$$

where:

$$[C] = \frac{E}{(1+v)(1-2v)} \begin{bmatrix} (1-v) & v & v & 0 & 0 & 0 \\ & (1-v) & v & 0 & 0 & 0 \\ & & (1-v) & 0 & 0 & 0 \\ & & & \frac{1}{2}-v & 0 & 0 \\ & & & & \frac{1}{2}-v & 0 \\ & & & & & \frac{1}{2}-v \end{bmatrix} \qquad [2.20]$$

The matrix $[C]$ is a symmetric matrix.

Cook (1974) gives the formulation in the case of general shells for which the matrix $[C]$ changes. This is due to the condition that the stress normal to the shell surface is

zero. Thus by placing the coordinate z' normal to the shell surface we have the condition

$$\sigma_{z'} = 0 \qquad [2.21]$$

Thus the new $[C]$ matrix can be written as:

$$[C] = \frac{E}{1-\nu^2}\begin{bmatrix} 1 & \nu & 0 & 0 & 0 & 0 \\ & 1 & 0 & 0 & 0 & 0 \\ & & 0 & 0 & 0 & 0 \\ & & & \frac{1-\nu}{2} & 0 & 0 \\ & & & & \frac{1-\nu}{2} & 0 \\ & & & & & \frac{1-\nu}{2} \end{bmatrix} \qquad [2.22]$$

2.2 Linear Buckling analysis with Finite Elements

Cook (1974), Gould (1985) & Zienkiewicz (1971) give a theoretical background to the stability problem with finite elements. The following section will deal specifically with a linear buckling analysis as performed by the finite element software ABAQUS.

Cook (1974) deals with the presence of linear pre buckling forces which occur in shell problems as membrane forces. It is commonly assumed that the membrane forces are a adequate description of the pre buckling condition of the shell. The linear analysis can be described in terms of two factors:

- The membrane forces can be determined through a linear elastic analysis
- Membrane forces remain constant during the deformation due to buckling

Thus the structure is subjected to a load and the corresponding membrane forces are calculated along with the relative displacements. From the know distribution of membrane forces the geometric stiffness matrix $[K_G]$ can be calculated, this is also commonly know as the initial stress matrix. The geometric stiffness matrix is described as a function of the element geometry and the initial membrane forces, it can account for the stiffening or weakening effect of the membrane forces.

Thus as the membrane stresses remain constant during buckling the final distribution of stresses can be written as a factor of the membrane stresses (λ). Cook (1974) wrote this condition by means of the following equation:

$$([K]+\lambda[K_G])\{D\}=([K]+\lambda[K_G])(\{D\}+\{\delta D\})=\{R\} \qquad [2.23]$$

where:

$[K]$ = the Global Stiffness Matrix

λ_i = the eigenvalue

$[K_G]$ = the Geometric Stiffness Matrix

$\{D\}$ = the Pre-buckling displacements

$\{\delta D\}$ = the Buckling Mode

$\{R\}$ = the Reaction Forces

By subtracting the first portion of the above equation from the second, the governing eigenvalue equation for the stability problem is obtained.

$$([K] + \lambda[K_G])\{\delta D\} = 0 \qquad [2.24]$$

This is a standard eigenvalue equation. The defining equation for the geometric stiffness matrix can be written as:

$$[K_G] = \int [G]^T [M][G] dV \qquad [2.25]$$

where:

$$\{\theta\} = [G]\{\delta\} \qquad [2.26]$$

Thus $[G]$ as illustrated by Grunitz (2001) is given in terms of the shape function, $[N]$.

$$[G] = \begin{bmatrix} \cdots & \begin{bmatrix} \frac{\partial N_k}{\partial x} & 0 & 0 \\ \frac{\partial N_k}{\partial y} & 0 & 0 \\ \frac{\partial N_k}{\partial z} & 0 & 0 \\ 0 & \frac{\partial N_k}{\partial x} & 0 \\ 0 & \frac{\partial N_k}{\partial y} & 0 \\ 0 & \frac{\partial N_k}{\partial z} & 0 \\ 0 & 0 & \frac{\partial N_k}{\partial x} \\ 0 & 0 & \frac{\partial N_k}{\partial y} \\ 0 & 0 & \frac{\partial N_k}{\partial z} \end{bmatrix} & \cdots \end{bmatrix} \qquad [2.27]$$

Here the k is a typical node with the respective shape function at that node N_k. The final displacements can be written in terms of the nodal parameters and the shape functions.

$$\begin{Bmatrix} u \\ v \\ w \end{Bmatrix} = [N]\{\delta\}^e \qquad [2.28]$$

where

$\{\delta\}^e$ = the nodal parameters for the respective element e

Finally, the matrix $[M]$ is the stress matrix describing the loading on the structure. For shell structures, Zienkiewicz (1971) indicates that the stress matrix is a nine by nine matrix arranged as follows:

$$[M] = \begin{bmatrix} [S] & [O] & [O] \\ [O] & [S] & [O] \\ [O] & [O] & [S] \end{bmatrix} \quad [2.29]$$

where:

$$[S] = \begin{bmatrix} \sigma_x & \tau_{xy} & \tau_{xz} \\ \tau_{yx} & \sigma_y & \tau_{yz} \\ \tau_{zx} & \tau_{zy} & \sigma_z \end{bmatrix} \quad [2.30]$$

$$[O] = \begin{bmatrix} 0 & 0 & 0 \\ 0 & 0 & 0 \\ 0 & 0 & 0 \end{bmatrix} \quad [2.31]$$

The extraction of the eigenvalues in ABAQUS is done using the Lancos Solver. A brief description of the solver will be presented below. The Lancos method is essentially a transformation method. Balden (2003) gives a brief overview of the technique. It is illustrated that the Lancos method will transform the problem to a standard eigenvalue problem:

$$[K']\{\delta D\} = \lambda\{\delta D\} \quad [2.32]$$

here the stiffness matrix [K'] is essentially:

$$[K'] = [K][K_G]^{-1} \quad [2.33]$$

"The converted stiffness matrix is then converted into a tridiagonal matrix. The eigenvalues of the tridiagonal may then be very efficiently computed by a separate method, such as the Strum sequence or the QR method with shifting." (Balden 2003)

2.3 Nonlinear Finite Element Analysis

The linear buckling analysis in the previous section is based upon the assumption of infinitesimal displacements and elastic behaviour in the pre buckling range. In reality a structure is often subjected to large displacements and rotations along with the possibility of inelastic behaviour. As such it is necessary to analyse the structure using a nonlinear theory. In effect the linear buckling analysis can only describe the point of bifurcation and the pre buckling behaviour and not the post buckling path. The non linear analysis can adequately give the entire pre and post buckling path. This section will focus on the basic theory behind the nonlinear finite element analysis.

Nonlinearity can occur in two forms; these are geometric and material nonlinearity. The geometric nonlinear analysis takes account of the large displacements and rotations. The material nonlinear analysis deals with the issue of inelastic behaviour. In general a nonlinear solution is achieved by applying an iterative algorithm to obtain the solution. Examples are the Newton and Newton Raphson methods. These are presented by Zienkiewicz (1971), Zienkiewicz & Taylor (2000), Cook (1974) and Bathe (1982) who give a mathematical overview.

Zienkiewicz & Taylor (2000) describes an arbitrary nonlinear problem using the equation:

$$\Psi(a) = f - P(a) = 0 \qquad [2.34]$$

"If a solution (to the nonlinear equation) is achieved it may not necessarily be the solution sought. Physical insight into the nature of the problem and, usually, small-step incremental approaches from known solutions are essential to obtain realistic answers. Such increments are indeed always required if the constitutive law relating stress and strain changes is path dependant or if the load-displacement has bifurcations or multiple branches at certain load levels." (Zienkiewicz & Taylor 2000)

Zienkiewicz and Taylor (2000) formulate the general problem as:

$$\Psi_{n+1} = \Psi(a_{n+1}) = f_{n+1} - P(a_{n+1}) = 0 \qquad [2.35]$$

A known solution point is given by:

$a = a_n$
$\Psi_n = 0$
$f = f_n$

The forcing function f is increased incrementally:

$$f_{n+1} = f_n + \Delta f_n \qquad [2.36]$$

The objective is to determine the change in a_n such that:

$$a_{n+1} = a_n + \Delta a_n \qquad [2.37]$$

It is important to keep the increments of the forcing function small; this is to allow the path dependence to be followed accurately. Thus we can conclude that non-linearity shows a high level of path dependence and the increment should be consistent with this in order to obtain an accurate solution.

Zienkiewicz and Taylor (2000) give a concise summary of the Newton-Raphson method. This will be presented here before a review of the non linear method employed by ABAQUS in its analysis. The Newton-Raphson method is an iterative method where one starts from a known equilibrium point.

$$\Psi\left(a_{n+1}^{i+1}\right) \approx \Psi\left(a_{n+1}^{i}\right) + \left(\frac{\partial \Psi}{\partial a}\right)_{n+1}^{i} da_n^i = 0 \qquad [2.38]$$

where:

i – Is the iteration counter

da - Is the solution increment

Thus the previous converged solution (a_n) is given by:

$$a_{n+1}^{1} = a_n \qquad [2.39]$$

The tangent stiffness matrix (K_T) is given as:

$$K_T = \frac{-\partial \Psi}{\partial a} \qquad [2.40]$$

Thus equation 2.40 can be written as:

$$K_T^i da_n^i = \Psi_{n+1}^i \qquad [2.41]$$

The use of successive increments is given as:

$$\begin{aligned} a_{n+1}^{i+1} &= a_{n+1}^{i} + da_{n+1}^{i} \\ &= a_n + \Delta a_n^i \end{aligned} \qquad [2.42]$$

where:

$$\Delta a_n^i = \sum_{k=1}^{i} da_n^k \qquad [2.43]$$

Figure 2.3 below is taken from Zienkiewicz and Taylor (2000) and gives a graphical overview of the Newton-Raphson method.

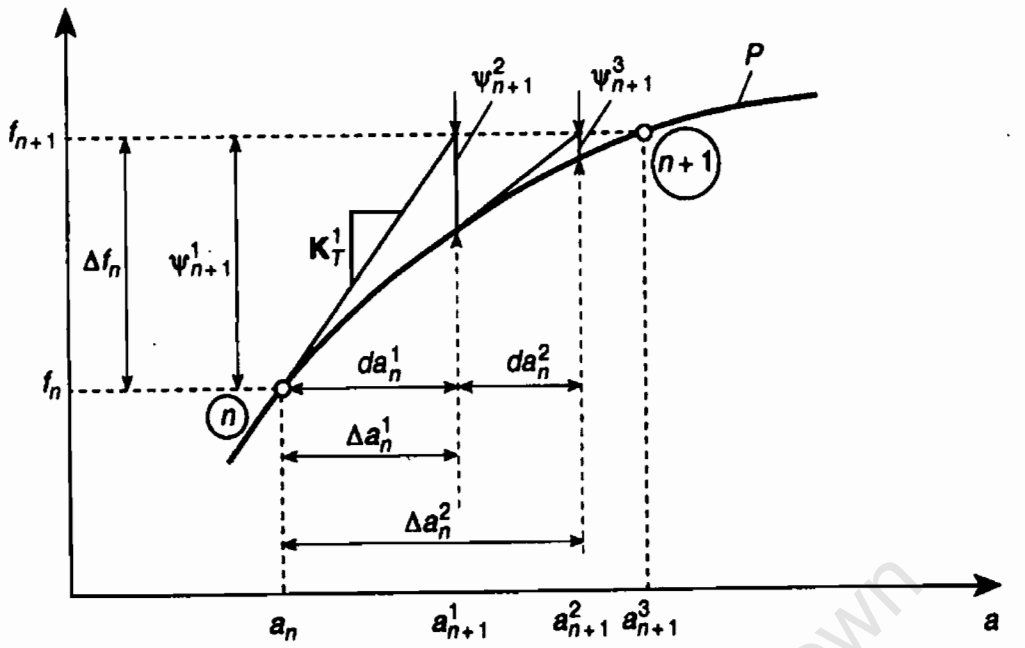

Figure 2.3: Newton-Raphson Method (Zienkiewicz & Taylor 2000)

The following deals with the basic finite element formulation for geometric non-linearity. The basic linear formulation was given as:

$$\{\psi(\{\delta\})\} = \int_V \left[\overline{B}\right]^T \{\sigma\} \mathrm{d}V - \left\{\overline{R}\right\} = 0 \qquad [2.44]$$

$$\mathrm{d}\{\varepsilon\} = \left[\overline{B}\right]\{\delta\} \qquad [2.45]$$

Zienkiewicz (1971) states that if the displacements are large the matrix $[B]$ becomes dependant on $\{\delta\}$, as the strains are nonlinearly dependant on the displacements. This is written as:

$$\left[\overline{B}\right] = [B_0] + [B_L(\{\delta\})] \qquad [2.46]$$

The elastic relation can still be given by the equation:

$$\{\sigma\} = [C]\{\varepsilon\} \qquad [2.47]$$

This can easily be altered to include the non-linear material behaviour. Zienkiewicz (1971) gives the iterative process to determine the solution using Newton's method. Thus the solution is derived below:

$$\mathrm{d}\{\psi\} = \int_V \mathrm{d}\left[\overline{B}\right]^T \{\sigma\}\mathrm{d}V + \int_V \left[\overline{B}\right]^T \mathrm{d}\{\sigma\}\mathrm{d}V \qquad [2.48]$$

Thus we can write the derivative of stress in terms of strain as:

$$\mathrm{d}\{\sigma\} = [C]\mathrm{d}\{\varepsilon\} = [C]\left[\overline{B}\right]\mathrm{d}\{\delta\} \qquad [2.49]$$

where:

$$\mathrm{d}\left[\overline{B}\right] = \mathrm{d}[B_L] \qquad [2.50]$$

Thus:

$$\mathrm{d}\psi = \int_V \mathrm{d}[B_L]^T \{\sigma\}\mathrm{d}V + \left[\overline{K}\right]\mathrm{d}\{\delta\} \qquad [2.51]$$

where:

$$\left[\overline{K}\right] = \int_V \left[\overline{B}\right]^T [C]\left[\overline{B}\right]\mathrm{d}V = [K_0] + [K_L] \qquad [2.52]$$

Here:

$[K_0]$ – Represents the small linear displacement matrix

$[K_L]$ – Represents the stiffness due to the large deflections

where $[K_L]$ is given as:

$$[K_L] = \int_V \left([B_0]^T [C][B_L] + [B_L]^T [C][B_L] + [B_L]^T [C][B_0] \right) \mathrm{d}V \qquad [2.53]$$

The first term of equation 2.53 can be written as:

$$\int_V \mathrm{d}[B_L]^T \{\sigma\} \mathrm{d}V = [K_G] \mathrm{d}\{\delta\} \qquad [2.54]$$

Thus equation 2.50 becomes:

$$\mathrm{d}\{\psi\} = \left([K_0] + [K_L] + [K_G] \right) \mathrm{d}\{\delta\} \qquad [2.55]$$

here:

$$[K_T] = \left([K_0] + [K_L] + [K_G] \right) \qquad [2.56]$$

Thus we are left with the form in which the Newton-Raphson method can be used to obtain the solution.

Imperfection sensitive and post buckling behaviour in ABAQUS is analysed with the Static Riks Algorithm. This approach is used due to its inclusion of the effects of non linear geometry.

The use of a non linear analysis is important when dealing with imperfect shells. The linear classical buckling analysis is based on the assumption of perfect geometry. The pre buckling forces in the shell are characterised by membrane forces and the corresponding displacements are infinitesimal. In the imperfect structure the geometry is no longer perfect and the imperfection causes a discontinuity in the membrane method of stress determination. Thus the shell is actually subject to both membrane and bending forces. The resulting deflections and rotations can no longer be

considered small in the pre buckling state, and as such must be taken account of through the use of a nonlinear theory (large displacements).

The finite element software ABAQUS makes use of the modified Riks algorithm for the analysis of non linear problems. "The essence of the method is that the solution is viewed as the discovery of a single equilibrium path in a space defined by the nodal variables and the loading parameter" (ABAQUS Theory Manual). The algorithm is based primarily on the Newton Method. The problem is treated as a path dependant one where the equilibrium is evaluated by taking steps of a given increment size for a given load proportion.

The following theory is directly referenced to the ABAQUS Theory Manual, and is used to give an overview of the Riks algorithm. The following definitions are given by ABAQUS Theory Manual:

P_N – Loading Pattern
N – The Degrees of Freedom
λ - The Load Magnitude Parameter
u_N – The Displacements at Given Time
λP_N – The Actual Load State

The diagram below gives a basic illustration of the Riks algorithm. The solution procedure given by ABAQUS is as follows and is referenced to the diagram for understanding.

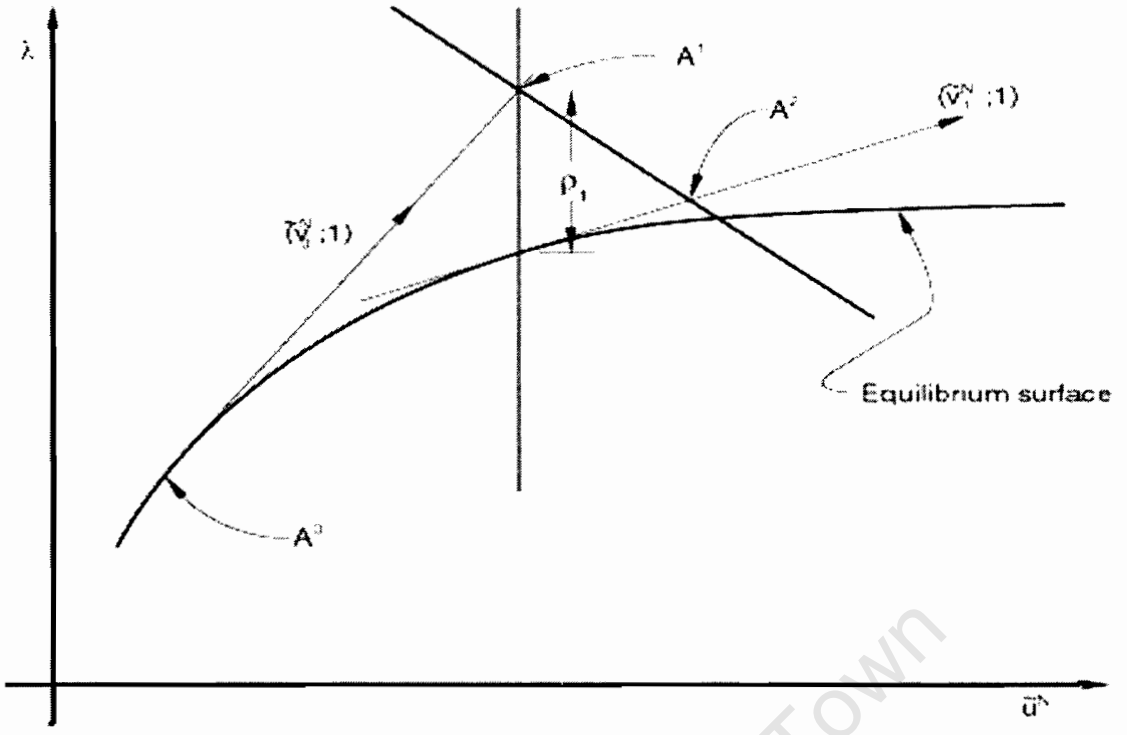

Figure 2.4: RIKS Method (ABAQUS Theory Manual)

The procedure starts at the point where the load magnitude and the displacement have been determined and equilibrium has been reached (A^0 in Figure 2.3). This point is indicated as:

$$A^0 = \left(\bar{u}^N ; \lambda_0\right) \qquad [2.57]$$

The tangent stiffness matrix is determined and ABAQUS solves for:

$$K_T^{NM} \, \mathrm{v}_0^{\,M} = P^N \qquad [2.58]$$

The solution takes a step to point A_1. The increment for this step (Δl) is adjusted automatically by ABAQUS. The solution is then corrected onto the equilibrium path in the plane orthogonal to $\left(\bar{\mathrm{v}}_0 : 1\right)$ using an iterative procedure. This is written as:

$i = 1,2,3.....$

$\Delta\lambda_i = \Delta\lambda_0$

The algorithm implemented in the ABAQUS STATIC RIKS step solves the internal forces at the nodes (I^N). A check is then made to determine the equilibrium of the problem by calculating the residual between the applied loads and the internal forces.

$$R_i^N = (\lambda_0 + \Delta\lambda_i)P^N - I^N$$

Once this has been determined a solution is obtained for the displacement vectors. The Displacement vectors are scaled so that the solution moves orthogonal to $(\bar{v}_0 : 1)$ from A^i to A^{i+1}. The iteration counter is then updated:

$$i = i + 1$$

The process continues until the residual value converges to an accepted error defined by ABAQUS. This corresponds to reaching a new equilibrium point on the equilibrium surface in Figure 2.3.

This gives a brief overview of how the finite element method is formulated. In particular this chapter gives a overview of the finite element software ABAQUS which will be used in later chapters as an analysis tool.

3 FINITE ELEMENT MODELLING OF PERFECT SHELLS

The numerical work on the buckling behaviour of shells will be conducted with the finite element software ABAQUS. This section details the choice of modelling that will be adopted for the in-depth investigation. The choice of model is dependant on the required accuracy coupled with the computational time. The modelling of a perfect shell was used to make a sound choice of elements and the mesh density. More importantly, some classical solutions for perfect shells exist in the literature (as indicated in Chapter 1), which allows the numerical modelling to be checked and adjusted if necessary, in preparation for the later simulations of the weld imperfection. The numerical analysis would have to be linear in order to be consistent with the classical approach. For the purpose of this study, a spherical shell subjected to external uniform pressure was considered.

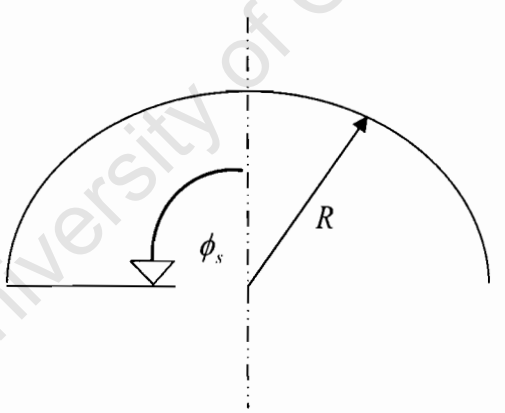

Figure 3.1:Basic Geometry of the Perfect Spherical Shell

The geometric parameters of the spherical shell are illustrated in Figure 3.1 above. The respective values used for the numerical modelling are listed below. The initial support condition was taken as fully fixed, the effect of differing conditions will be studied later in the chapter.

$R = 5m$

$t = 5mm$

$\phi_s = \frac{\pi}{2}$

$\frac{R}{t} = 1000$

The radius to thickness ratio of 1000 was chosen. The analysis of cylindrical shells with a corresponding radius to thickness ratio found that buckling occurred in the elastic range and as no real indication had been given in the literature review of the minimum radius to thickness ratio to ensure elastic buckling the values from the cylindrical shell studies were adopted. The material used was mild steel, the corresponding properties are:

$E = 200GPa$

$\sigma_y = 300MPa$

$v = 0.3$

Taking account of the above parameters, the classical buckling pressure of a spherical shell can be calculated using Equation 1.5 from Chapter 1.2.3.

$$q_{cl} = \frac{2E}{\sqrt{3(1-\nu^2)}}\left(\frac{t}{R}\right)^2$$

$$q_{cl} = \frac{2(200\times10^6)}{\sqrt{3(1-0.3^2)}}\left(\frac{0.005}{5}\right)^2$$

$$q_{cl} = 2.421\times10^5 N/m^2$$

The critical classical buckling pressure from the calculation above was found to be in the order of 242kN/m^2.

The numerical analysis was done using two distinct modelling approaches. The first was the use of an axisymmetric model and the second the use of a full 3-D model. The

axisymmetric model is based on the assumption that the buckling mode is axisymmetric with no waves forming in the circumferential direction.
The elements chosen for the modelling will be briefly discussed below. The decision was made by taking into account the later need for a nonlinear analysis which requires large rotations and finite strains to be accounted for.

The axisymmetric model was constructed using two element types as a comparison. The elements were:

- SAX2 – 2 Noded Axisymmetric Stress Element
- SAX3 – 3 Noded Axisymmetric Stress Element

Each element will be illustrated by means of a diagram and their respective properties will be discussed.

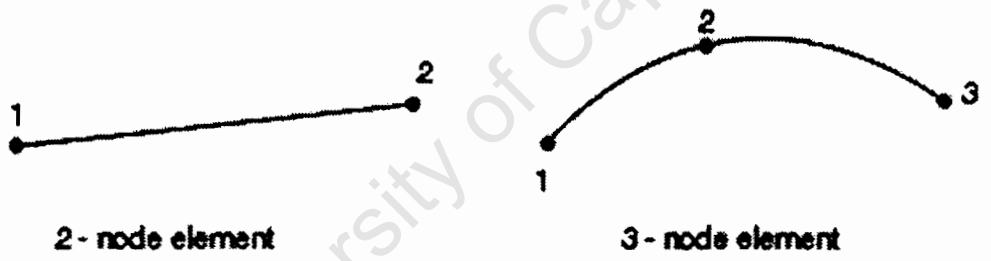

Figure 3.2: SAX2 and SAX3 Axisymmetric Shell Elements

The computational time is not affected by the choice of element. The difference between the two elements is indicated in Figure 3.2 above. This can be listed as:

- SAX2 – It is two nodded with integration of the stiffness matrix at a single point between the nodes. The displacements and rotations between the nodes are deduced by linear interpolation.
- SAX3 – This three nodded axisymmetric element has the stiffness matrix integrated at two points. The displacement and rotations between the nodes are given by quadratic interpolation.

Both elements will account for finite stresses and displacements, as such they can be used in the later nonlinear analysis. The integration points are illustrated in Figure 3.3 below.

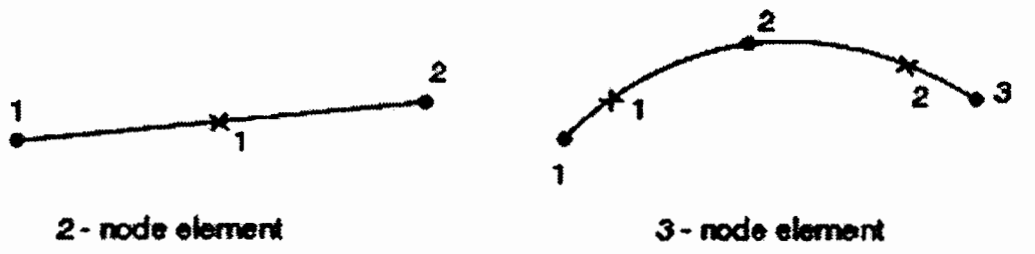

Figure 3.3: Integration Points for Axisymmetric Elements

The full 3-D model was constructed using a single element only. The element used was a S4R element, which is a 4 nodded curved shell element with reduced integration. There are other elements that could be applied to the 3-D model however the S4R was chosen due to its capacity to reduce the computational time taken to analyse the problem when compared with the S4 element. This time reduction is due to the integration of the stiffness matrix [*K*] occurring at a single point in the S4R element. Figure 3.4 below gives an overview of the S4R element. The advantages will be discussed too.

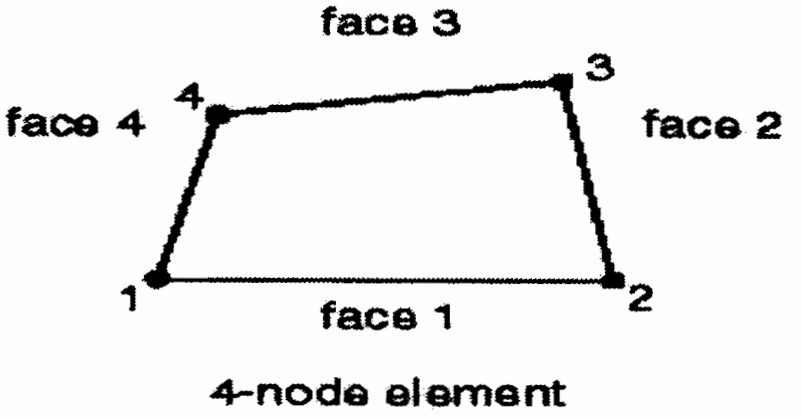

Figure 3.4: S4R – General Shell Element

The S4R element is also adequate for later analysis of the nonlinear behaviour. It accounts for the development of large rotations and displacements. The element has 6 degrees of freedom at each node accounting for all the rotations and displacements in a three dimensional model. The displacements and rotations at interior points in the shell element are determined through linear interpolation. An effect of the S4R element is the possibility of distortion (Hour glassing) the results should be examined bearing this in mind. The solution is the refinement of the mesh density in the area where distortion (hour glassing) is occurring. The integration point for the S4R element can be seen in Figure 3.5.

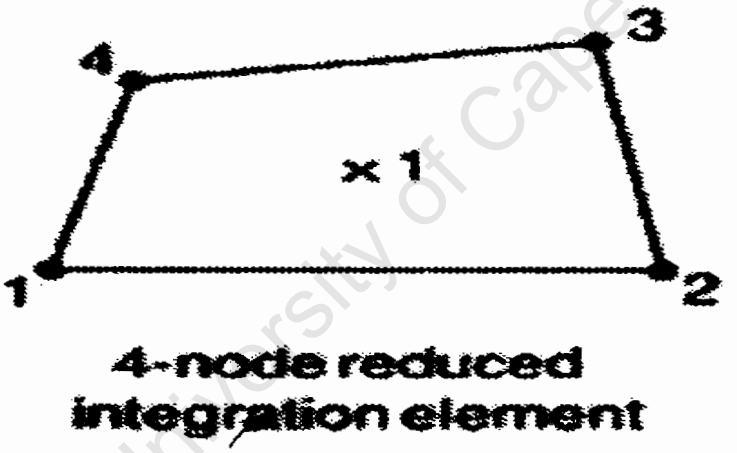

Figure 3.5: S4R Element indicating the point of Integration for the Element

The final three dimensional model is given in Figure 3.6 below. The figure is an indication of the mesh used for the linear buckling analysis. The Sweep meshing algorithm was used in ABAQUS to develop a regular mesh around the circumference of the shell.

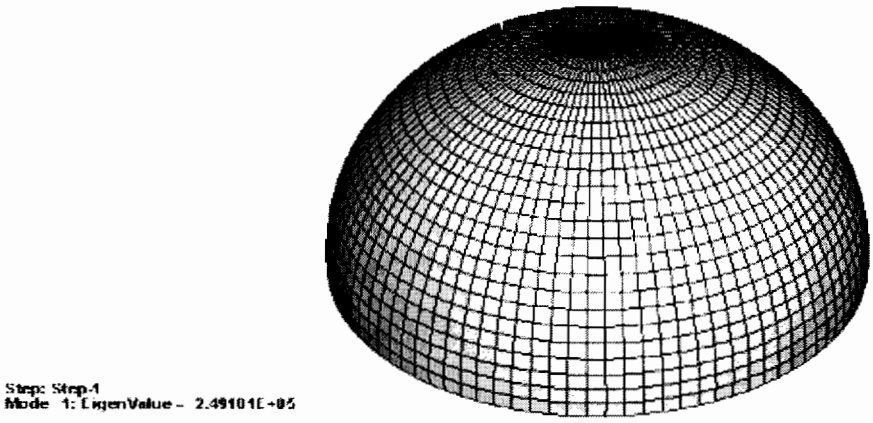

Figure 3.6: Mesh Arrangement for Perfect 3-D Spherical Shell

The classical buckling strength given in Chapter 1.2.3 allows the mesh density to be refined, thus calibrating the numerical model. Figure 3.7 gives the convergence of the eigenvalue to the classical buckling pressure with the refinement of the mesh size.

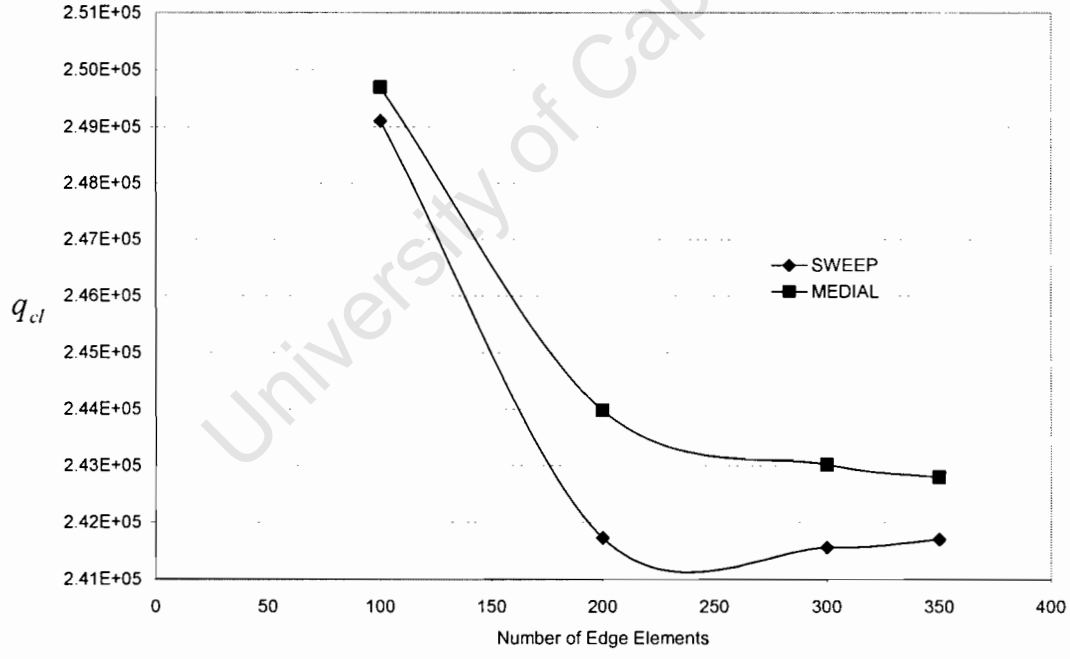

Figure 3.7: Mesh Refinement for 3-D Model

The full 3-D shell model was meshed by defining the number of elements occurring along the lower edge/perimeter of the shell. The meshing algorithms in ABAQUS were the sweep and medial axis algorithms. The sweep method of meshing gave a

consistent regular mesh pattern, but the later densification of the mesh around the weld imperfection was not supported by this algorithm.

The increase in mesh density has a resultant increase in the computational time. The mesh density of 200 elements was thus chosen to model the shell. This is supported as there is no real gain in accuracy when increasing the element number to 300. The associated error for the mesh convergence study when compared to the classical buckling solution is given in Figure 3.8 below.

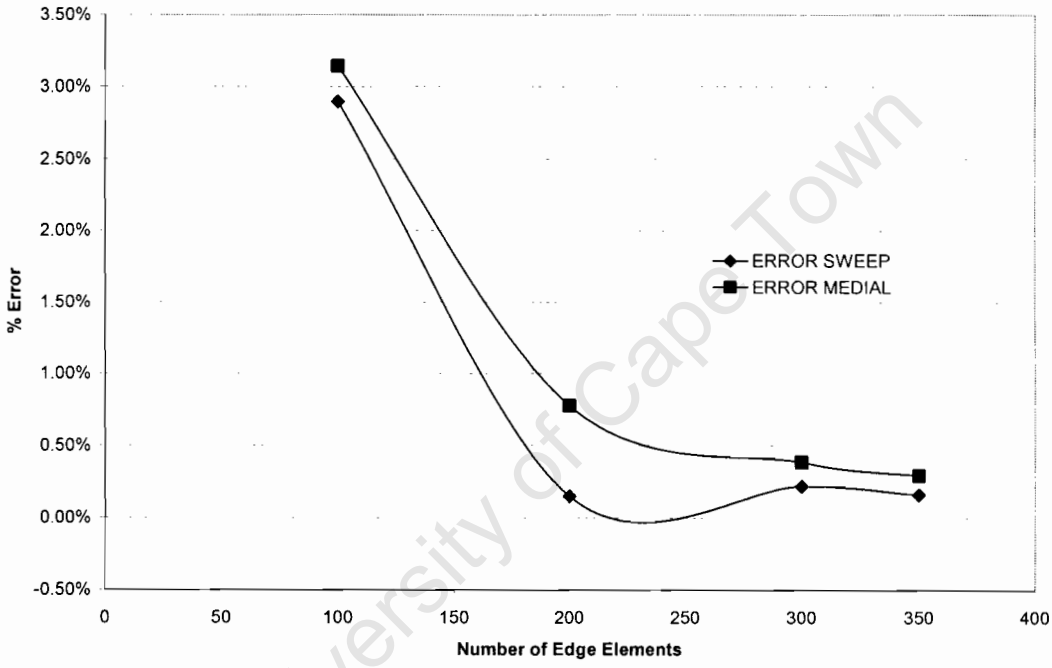

Figure 3.8: Error Associated with Mesh Convergence

The results of the analysis are presented in Table 3.1 below.

Table 3.1: Finite Element Results

Element	SAX1	SAX2	S4R
Eigenvalue	2.4212 x 105	2.421 x 105	2.4286 x 105

The results above indicate that we do have a good correlation between the numerical model and the classical buckling strength for a spherical shell. The computational time for the axisymmetric models is small compared to the full three dimensional

model. The 2 & 3 nodded axisymmetric shell stress element used in a wire model gave the best agreement. It is important that the mode shapes are also consistent. The full model presented more asymmetric modes shapes; however the above load is given for an axisymmetric mode. The figures below illustrate the buckling modes of the respective eigenvalue analysis. The plots are all for the lowest eigenvalues and correspond to the buckling strength given above.

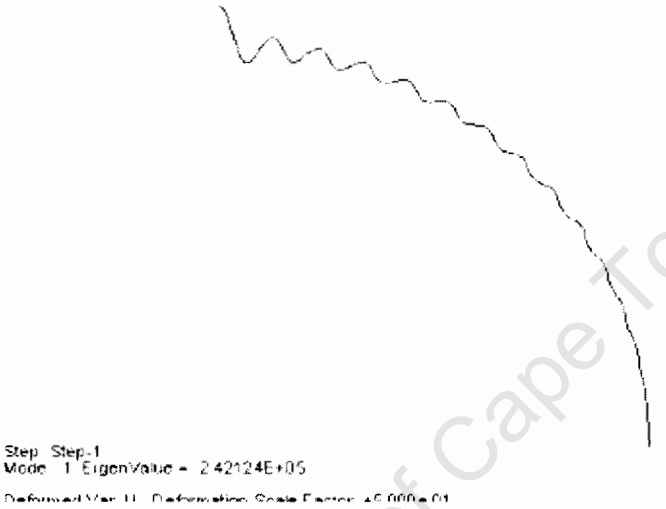

Figure 3.9: First Buckling Mode for the Wire Model – SAX2

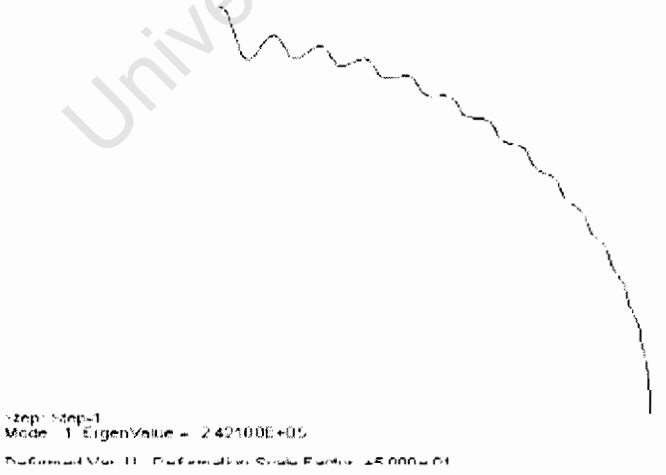

Figure 3.10: First Buckling Mode for the Wire Model – SAX3

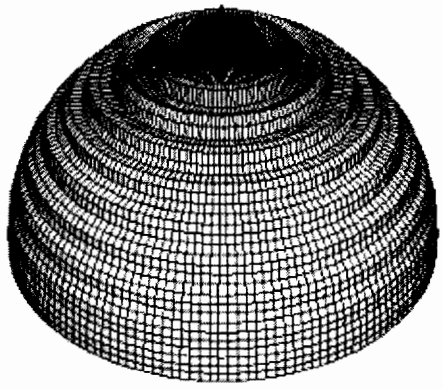

Figure 3.11:First Buckling Mode for the Full 3D Model – S4R

The buckling values and the mode shapes all show good agreement with each other. The other important factor to consider is the computational time taken; the axisymmetric models were quicker in comparison with the full model. As the lowest buckling mode of the three dimensional model is axisymmetric, one approach would be to use the axisymmetric wire model in future analyses, reducing the computational time. This however would limit the final deformation state to an axisymmetric one, whereas one could have the case where the asymmetric buckling mode is more critical.

All the linear buckling analysis results presented above where for the case of a fixed boundary condition. To determine the effect of boundary conditions, a further study was done on two more boundary types; the membrane-type boundary and the pinned boundary. Figure 3.12 below gives a concise illustration of the different boundary conditions.

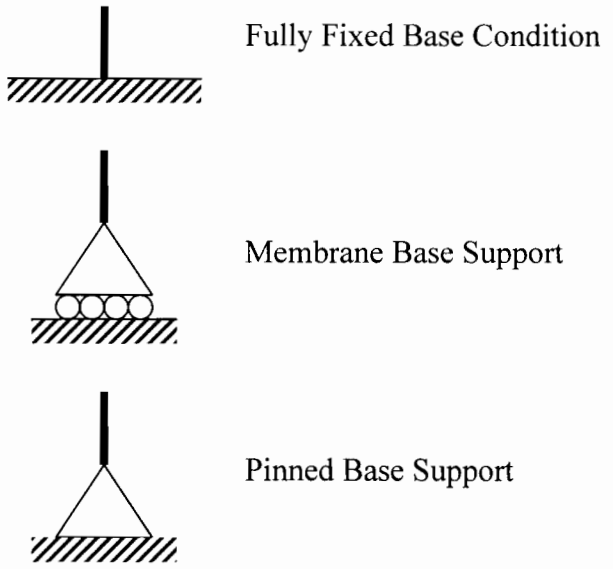

Figure 3.12: Support Conditions at Shell Edge

The initial investigation was to make use of the predefined ABAQUS linear elastic buckling analysis. The calculated value of the buckling strength through linear elastic analysis for the pinned supports is:

$$q_{cl} = 2.4197\, kN/m^2$$

This analysis was conducted on the axisymmetric shell model making use of the SAX3 element in ABAQUS. The Buckling Mode for the pinned shell is similar to the fixed condition apart from the area immediately at the base as the condition of the $\frac{dw}{d\phi} = 0$ is no longer applicable. The figure below illustrates the buckling mode for the pinned shell.

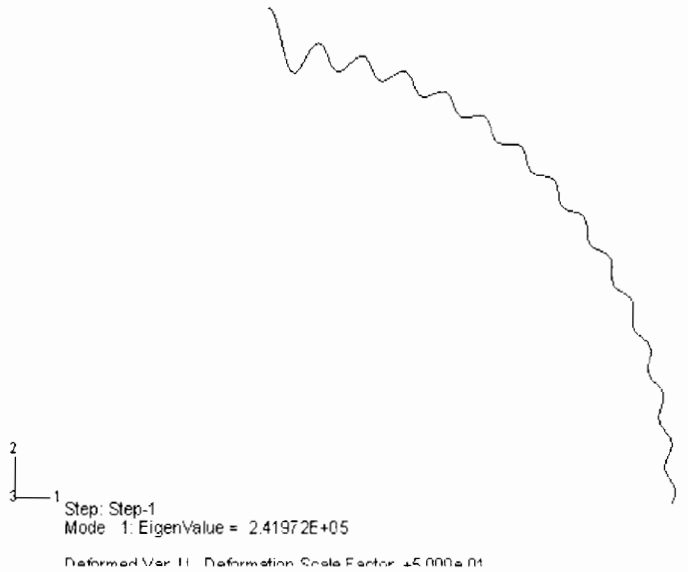

Figure 3.13: Buckling Mode for the Pinned Support Condition

This indicates that in terms of the linear buckling analysis, there is very little difference in the buckling strength due to the change of the support condition. This is to be expected as the model used was a hemispherical model where the support location is largely negated due to its location as it is isolated from the shell apex where the buckling begins. This effect is also due to the thin nature of the shell as the radius to thickness ratio is greater than 1000.

To provide coherent conclusions of the effect of the weld imperfection it is necessary to have an idea of the respective effects of the boundary conditions on the buckling strength. The previous linear analysis showed little effect, thus the next step involved the study of the boundary conditions using a nonlinear analysis. This nonlinear analysis would account for the effect of large rotations or displacements resulting from the boundary conditions. The boundary conditions are in effect discontinuities with in the membrane theory; they result in the inclusion of bending moments through edge effects. These bending moments result in increased stresses which could lower the buckling capacity of the spherical shell.

The nonlinear analysis was conducted in ABAQUS using the "STATIC RIKS" step. This analysis step has been discussed in Chapter 2.0, it accounts for the nonlinear effect of geometry and material. The results of the analysis are given in Figure 3.14 below. The figure indicates the variation of the parameter λ^* ;which is a measure of

the actual load over the classical buckling load; with the arc length used in the incremental analysis.

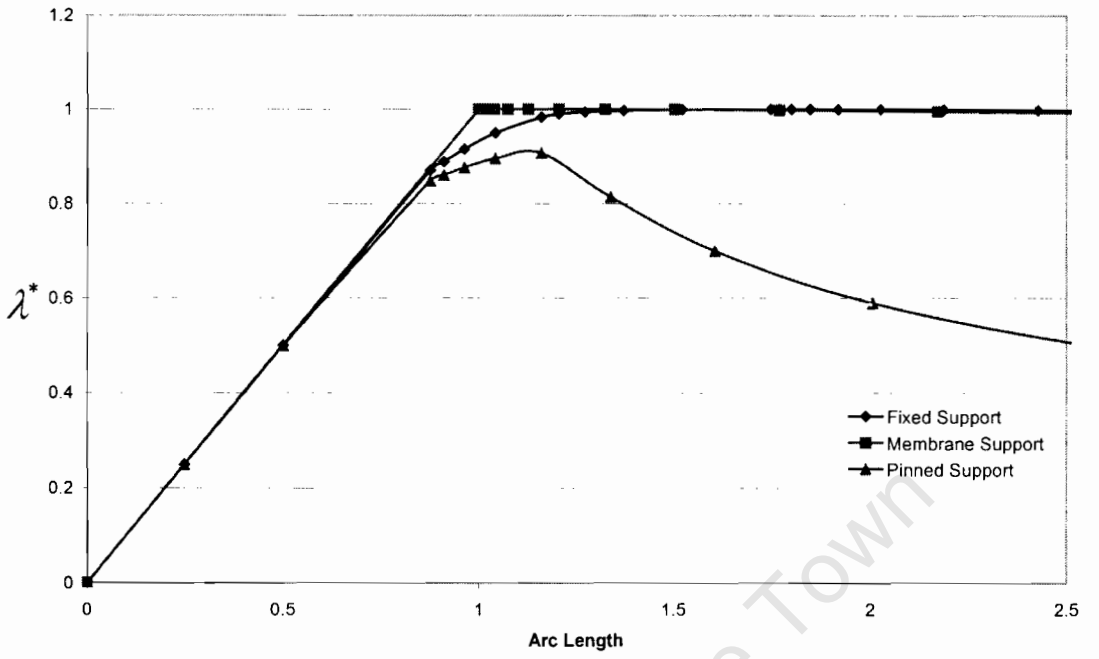

Figure **3.14: Nonlinear Analysis of Boundary Conditions for Spherical Shell**

The results indicate that the boundary conditions have little or no effect on the buckling strength of the spherical shell. Again this is a consequence of the location of the supports. The hemispherical shell isolates/reduces the effect of the boundary conditions. It is clear when comparing these results with those of the shallow spherical shell given in Chapter 1.0 that the location of the supports is critical. The location at meridional angles of 30° results in a snap through buckling of the spherical shell and a significant reduction of the buckling capacity. This effect will be studied later with a single circumferential weld.

4 WELD SHAPE MODELLING

This chapter deals with the modelling of the weld shape. In order to effectively understand the impact of welding on the buckling strength of shells, an approximation of the geometric weld shape must be sought. The derivation of weld shapes for both non shallow spherical and conical shells is detailed below.

Much of the work in this line is based upon the approach laid out by Rotter & Teng (1989) in which they derived shape functions for cylindrical shells. The assumptions will be briefly revisited here. The basic assumption is that the weld can behave in a manner which reflects either full moment continuity or none. Thus the weld can be regarded effectively as "fixed" or "pinned".

Rotter & Teng (1989) made use of the bending behaviour of cylindrical shells in the derivation of their shape functions. The weld was subject to certain boundary conditions. These are given for the two cases Rotter & Teng A (fixed) and Rotter & Teng B (pinned). The derivation and subsequent equations were given in Section 1.4.1.

The approach adopted for this thesis is to assume the boundary conditions stated by Rotter & Teng (1989), and apply them to spherical and conical shells through their respective bending equations.

Zingoni (1997) gives the development of the Reissner-Meissner governing equations for the bending of an arbitrary shell of revolution. The edge conditions are governed by Geckler's approximation, also given in a concise form by Zingoni (1997). Geckler's approximation is only valid for shells were the angle of the meridional edge is not very small.

For a spherical shell, the governing equations for axisymmetric bending are written in terms of the meridional shear force (Q_ϕ) and the rotation parameter (V).

$$\frac{d^2V}{d\phi^2} + (\cot\phi)\frac{dV}{d\phi} - (\nu + \cot^2\phi)V = \frac{-a^2}{D}Q_\phi \qquad [4.1]$$

$$\frac{d^2Q_\phi}{d\phi^2} + (\cot\phi)\frac{dQ_\phi}{d\phi} + (\nu - \cot^2\phi) = EtV \qquad [4.2]$$

Zingoni (1997) shows that the above can be reduced, through Geckler's approximation, to the following equation which governs bending:

$$\frac{d^4Q_\phi}{d\phi^4} + 4\lambda^4 Q_\phi = 0 \qquad [4.3]$$

where:

$$\lambda^4 = 3(1-\nu^2)\left(\frac{a}{t}\right)^2 \qquad [4.4]$$

The solution for the above differential equation can be written in the form:

$$Q_\phi = e^{\lambda\phi}(C_1\cos\lambda\phi + C_2\sin\lambda\phi) + e^{-\lambda\phi}(C_3\cos\lambda\phi + C_4\sin\lambda\phi) \qquad [4.5]$$

However, for the calculation of edge effects, we are interested in the decaying function only, which can be re-written as:

$$Q_\phi = Ce^{-\lambda\psi}\sin(\lambda\psi + \beta) \qquad [4.6]$$

$$\psi = \phi_e - \phi \qquad [4.7]$$

Here C and β are constants to be deduced from the boundary conditions, and ϕ_e is the angle of the edge measured from the axis of revolution.

The conical shell is also presented by Zingoni (1997). The differential equations governing the bending solution for conical shell can be written as:

$$\frac{d^2V}{ds^2}+\frac{1}{s}\frac{dV}{ds}-\frac{1}{s^2}V=\frac{Q_s}{D} \qquad [4.8]$$

$$\frac{d^2Q_s}{ds^2}+\frac{3}{s}\frac{dQ_s}{ds}=\frac{1}{s^2}\left(\tan^2\alpha\right)EtV \qquad [4.9]$$

Zingoni (1997) indicates that by applying a similar approximation to that of Geckler, we derive the governing equation for conical bending similar to that of spheres and cylinders. The approximations are:

$$\frac{d^2V}{ds^2}\approx\frac{-Q_s}{D} \qquad [4.10]$$

$$\frac{d^2Q_s}{ds^2}\approx\frac{1}{s^2}EtV\left(\tan^2\alpha\right) \qquad [4.11]$$

This leads to:

$$\frac{d^4Q_s}{ds^4}+4\eta^4Q_s=0 \qquad [4.12]$$

where:

$$\eta^4=\frac{3\left(1-v^2\right)}{s^2\left(\cot^2\alpha\right)t^2} \qquad [4.13]$$

We assume $s = l$ at the edge of the conical shell, to fix the value of the denominator in η. The solution to the above equation is similar to that of a spherical shell. The edge disturbance tends to die down, thus the use of a decaying function:

$$Q_s=Ce^{-\eta x}\sin\left(\eta x+\xi\right) \qquad [4.14]$$

where:

$$x=l-s \qquad [4.15]$$

and ξ and C are constants of integration.

The edge deformation δ and V can be written as:

$$\delta = \frac{-1}{Et}\left(l^2 \cot^2 \alpha\right)\eta\sqrt{2}\left(\sin\alpha\right)Ce^{-\eta x}\sin\left(\eta x + \xi - \frac{\pi}{4}\right) \qquad [4.16]$$

$$V = -\left(l^2 \cot^2 \alpha\right)\frac{2\eta^2}{Et}Ce^{-\eta x}\cos\left(\eta x + \xi\right) \qquad [4.17]$$

Thus having established the theory behind the bending behaviour of shells, we can use Geckler's approximation to determine shape functions for the weld. The shape functions are derived for both shells assuming firstly that the weld is "pinned" and secondly that the weld is "fixed".

4.1 Modelling of "Pinned" Weld Shape

The weld shape for the non-shallow spherical shell will be derived first, followed by that of the conical shell. The assumption of zero moment capacity for the weld leads to the following boundary conditions:

$M_e = 0$

Thus applying only the edge forces H_e we obtain the following solutions for the constants C and β.

$$C = -\sqrt{2}H_e \sin\phi_e \qquad [4.18]$$

$$\beta = -\frac{\pi}{4} \qquad [4.19]$$

We are able to write down the general terms for the rotation (V) and the shear (Q).

$$V^b = -\frac{2\lambda^2}{Et} C e^{-\lambda\psi} \cos(\lambda\psi + \beta) \qquad [4.20]$$

$$\delta^b = \frac{-a}{Et} \lambda\sqrt{2}(\sin(\phi_e - \psi)) C e^{-\lambda\psi} \sin\left(\lambda\psi + \beta - \frac{\pi}{4}\right) \qquad [4.21]$$

We need to take into account the amplitude of the weld imperfection, which has been defined as w_0. The deflection w is measured in the direction normal to the meridian. There is also the assumption that the meridional displacment v is negligible. Thus the following condition applies:

$$\left(\delta^b\right)_{\phi=\phi_e} = w_0 \sin\phi_e + \mathrm{v}\cos\phi = w_0 \sin\phi_e \qquad [4.22]$$

Using this condition coupled with the known values of the constants, we can calculate the value of H_e in terms of the imperfection amplitude. Substituting this result back into our deflection (δ) leads to the shape of the weld imperfection in terms of the angle ϕ. Substituting Equations 4.18 and 4.19 into 4.21 and using the boundary condition 4.22 we obtain:

$$w_0 \sin\phi_e = \frac{-a}{Et} \lambda\sqrt{2}(\sin\phi_e)\left(-\sqrt{2}H_e \sin\phi_e\right)\sin\left(\frac{-\pi}{2}\right) \qquad [4.23]$$

that is,

$$w_0 \sin\phi_e = \frac{-2a\lambda \sin^2(\phi_e) H_e}{Et} \qquad [4.24]$$

so that

$$H_e = \frac{w_0 Et}{2\lambda \sin\phi_e} \qquad [4.25]$$

Substituting the value for H_e back into Equation 4.18 and correspondingly 4.21, we determine the shape of the weld imperfection as:

$$w(\phi) = \frac{\delta}{\sin\phi} = \frac{w_0(\sin(\phi_e - \psi))e^{-\lambda\psi}\sin\left(\lambda\psi - \frac{\pi}{2}\right)}{\sin\phi} \qquad [4.26]$$

The conical shell derivation is much the same. The boundary conditions can be written as:

$$M_e = 0$$
$$\delta_e^b = -w_0 \sin\alpha$$

Zingoni gives the solutions for a shell subjected to an edge load. The values of the constant are given as:

$$C = -\sqrt{2}H_e \sin\alpha \qquad [4.27]$$

$$\xi = -\frac{\pi}{4} \qquad [4.28]$$

The solution procedure is similar to that adopted for spherical shells. By substituting in the boundary conditions into equation 4.12, the value of H_e can be determined as:

$$H_e = \frac{w_0 \sin\alpha Et}{2l^2 \cos^2\alpha\eta} \qquad [4.29]$$

And accordingly the deflection can be written as:

$$w(s) = \frac{\delta}{\sin\alpha} = w_0 e^{-\eta x}\sin\left(\eta x - \frac{\pi}{2}\right) \qquad [4.30]$$

4.2 Modelling of "Fixed" Weld Shape

The approximation of the "fixed" weld shape is a more tedious process. The boundary conditions for the spherical shell are given below.

$$\delta_e^b = w_0 \sin\phi_e$$

$$\left(\frac{dw}{d\phi}\right)_{\phi=\phi_e} = 0$$

The equations for the displacement and rotation both have to be solved simultaneously to obtain the approximate weld shape. The calculations are given below. For the spherical shell the edge rotation and the radial displacement are both a function of the meridian displacement v. The relationships are given by Zingoni (1997) as:

$$V = \frac{1}{a}\left(\mathrm{v} - \frac{dw}{d\phi}\right) \qquad [4.31]$$

taking account of the previous assumption:

$$\mathrm{v} = 0 \qquad [4.32]$$

and including the boundary condition:

$$V = -\frac{1dw}{ad\phi} = 0 \qquad [4.33]$$

The shell edge is subject to both a lateral force H_e and a moment M_e. The relevant solutions or Geckler's approximation for these conditions are represented in Zingoni (1997). For the case where the lateral force is zero we have:

$$C' = \frac{2\lambda}{a} M_e \qquad [4.34]$$

$$\beta' = 0 \qquad [4.35]$$

The case where the edge moment is zero we have:

$$C'' = -\sqrt{2} H_e \sin\phi_e \qquad [4.36]$$

$$\beta'' = -\frac{\pi}{4} \qquad [4.37]$$

The values of the constants above must be substituted into the relevant equations describing the meridional and circumferential forces. These equations at the shell 'edge' are given as:

$$V_e = -\frac{4\lambda^3}{Eat} M_e + \frac{2\lambda^2}{Et} \sin\phi_e H_e \qquad [4.38]$$

$$\delta_e = \frac{2\lambda^2}{Et} \sin\phi_e M_e - \frac{2\lambda a}{Et} \sin^2\phi_e H_e \qquad [4.39]$$

Rearranging Equation 4.38 and including the boundary condition 4.33 we can solve the two simultaneous equations above. This is given as:

$$H_e = \frac{2\lambda}{a \sin\phi_e} M_e \qquad [4.40]$$

Substituting this along with the initial boundary condition regarding the radial deflection *w*, we obtain a solution:

$$M_e = \frac{w_0 Et}{2\lambda^2} \qquad [4.41]$$

thus:

$$H_e = \frac{w_0 Et}{a\lambda \sin\phi_e} \qquad [4.42]$$

Substituting these results into Equation 4.21 we can calculate the lateral deflection in terms of the edge force and the edge moment. This is given below:

$$\begin{aligned}\delta^b &= \frac{-a}{Et}\lambda\sqrt{2}(\sin(\phi_e-\psi))Ce^{-\lambda\psi}\sin\left(\lambda\psi+\beta-\frac{\pi}{4}\right)\\ \delta^b &= \frac{-a}{Et}\lambda\sqrt{2}(\sin(\phi_e-\psi))C'e^{-\lambda\psi}\sin\left(\lambda\psi+\beta'-\frac{\pi}{4}\right)\\ &+\frac{-a}{Et}\lambda\sqrt{2}(\sin(\phi_e-\psi))C''e^{-\lambda\psi}\sin\left(\lambda\psi+\beta''-\frac{\pi}{4}\right)\end{aligned} \quad [4.43]$$

Thus the final deflected shape of the weld is given by:

$$\delta = w_0\sin(\phi_e-\psi)e^{-\lambda\psi}\left(2\sin\left(\lambda\psi-\frac{\pi}{2}\right)-\sqrt{2}\sin\left(\lambda\psi-\frac{\pi}{4}\right)\right)$$

$$w(\phi) = \frac{w_0\sin(\phi_e-\psi)e^{-\lambda\psi}\left(2\sin\left(\lambda\psi-\frac{\pi}{2}\right)-\sqrt{2}\sin\left(\lambda\psi-\frac{\pi}{4}\right)\right)}{\sin\phi} \quad [4.44]$$

The solution procedure for the conical shell is again much the same. For the conical shell the values dictating the radius of curvature are written as:

$$r_2 = s\cot\alpha \quad [4.45]$$

$$r_1 \to \infty \quad [4.46]$$

$$d\phi = \frac{ds}{r_1} \quad [4.47]$$

Thus the edge rotation V is a function of ds.

$$V = \frac{dw}{ds} \quad [4.48]$$

The boundary conditions for the conical shell are given below. These are:

$$\delta_e^b = -w_0 \sin\alpha$$

$$\left(\frac{dw}{ds}\right)_{s=l} = 0$$

thus:

$$V_e^b = 0 \qquad [4.49]$$

The equations are in a simplified version to the spherical shell equations and can be solved symbolically.

$$V_e^b = \left(l^2 \cot^2\alpha\right)\frac{2\eta^2}{Et}(\sin\alpha)H_e - \left(l^2 \cot^2\alpha\right)\frac{4\eta^3}{Et}M_e \qquad [4.50]$$

$$\delta_e^b = \left(l^2 \cot^2\alpha\right)\frac{2\eta^2}{Et}(\sin\alpha)M_e - \left(l^2 \cot^2\alpha\right)\frac{2\eta}{Et}\left(\sin^2\alpha\right)H_e \qquad [4.51]$$

The equations above can again be solved simultaneously to determine the values for M_e and H_e. From Equation 4.50 we can determine the relationship:

$$H_e = \frac{2\eta}{\sin\alpha}M_e \qquad [4.52]$$

By substituting the value for H_e into Equation 4.51, we can derive the values of M_e. This is given as:

$$M_e = \frac{w_0 Et}{2\eta^2 l^2\left(\cot^2\alpha\right)} \qquad [4.53]$$

and correspondingly;

$$H_e = \frac{w_0 Et}{\eta\left(l^2 \cot^2\alpha\right)(\sin\alpha)} \qquad [4.54]$$

Zingoni (1997) derives the values of the constants for Geckler's approximation.

$$C' = 2\eta M_e$$

$$C' = \frac{w_0 Et}{\eta\left(l^2 \cot^2 \alpha\right)} \qquad [4.55]$$

$$\xi' = 0 \qquad [4.56]$$

and the corresponding deflection is given as:

$$\delta_M = -w_0\sqrt{2}(\sin\alpha)e^{-\eta x}\sin\left(\eta x - \frac{\pi}{4}\right) \qquad [4.57]$$

The deflection for the lateral force H_e is determined through the constants below:

$$C = -\sqrt{2}H_e \sin\alpha \qquad [4.58]$$

$$\xi = \frac{-\pi}{4} \qquad [4.59]$$

The corresponding deflection due to the lateral force H_e is given as:

$$\delta_h = 2w_0(\sin\alpha)e^{-\eta x}\sin\left(\eta x - \frac{\pi}{2}\right) \qquad [4.60]$$

The total deflection of the shell due to the edge moment and force is written as:

$$\delta = \delta_M + \delta_H$$

$$\delta = 2w_0(\sin\alpha)e^{-\eta x}\sin\left(\eta x - \frac{\pi}{2}\right) - w_0\sqrt{2}(\sin\alpha)e^{-\eta x}\sin\left(\eta x - \frac{\pi}{4}\right)$$

$$w(s) = w_0 e^{-\eta x}\left(2\sin\left(\eta x - \frac{\pi}{2}\right) - \sqrt{2}\sin\left(\eta x - \frac{\pi}{4}\right)\right) \qquad [4.61]$$

4.3 Summary

The two sections above involved the use of Geckler's approximation to develop shape functions for the weld imperfections. This section will give a brief graphical representation of the equations.

Geckler's approximation solved the bending disturbances for the edge of shells of revolution. To depict the weld shape the derived equations must be made symmetrical about the edge (in our case the centre of the weld). The original terms used in the analysis are indicated in Figures 4.1 and 4.2 below, where the edge of the spherical and conical shell is defined respectively.

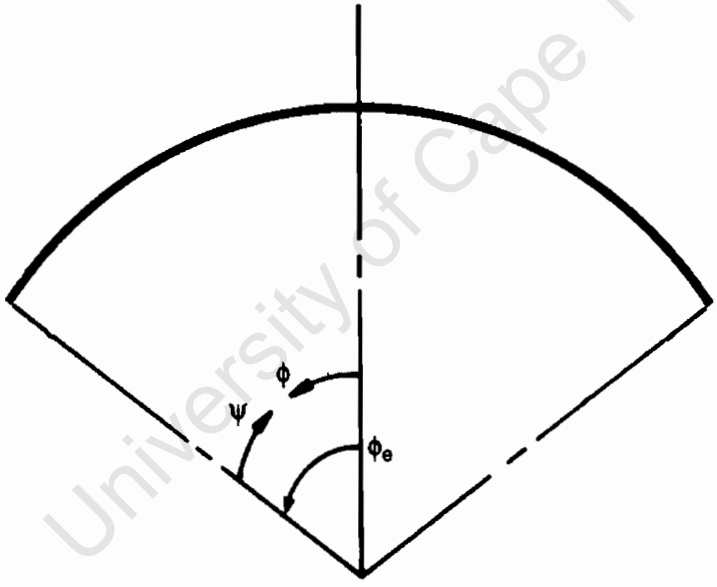

Figure 4.1: Spherical Shell Location of Edge Angle

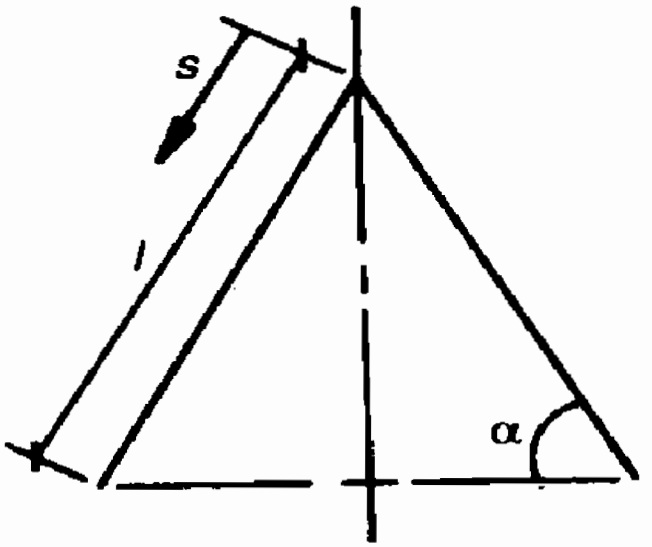

Figure 4.2: Edge Location of Conical Shell

Thus the new definitions are:

$$\phi_w = \phi_e \qquad [4.62]$$

$$l_w = l \qquad [4.63]$$

where:

ϕ_w is the meridional angle at the weld centre for the spherical shell

l_w is the location of the weld on the conical shell generator

thus the parameters ψ and x become:

$$\psi = \phi_w - \phi \qquad [4.64]$$

$$x = l_w - s \qquad [4.65]$$

The weld shapes will be summarised below to account for the parameter change and the symmetrical requirement. The spherical shell weld shapes are:

"Pinned"

$$w(\phi) = \frac{w_0\left(\sin(\phi_w - |\psi|)\right)e^{-\lambda|\psi|}\sin\left(\lambda|\psi| - \frac{\pi}{2}\right)}{\sin\phi} \qquad [4.66]$$

"Fixed"

$$w(\phi) = \frac{w_0\sin(\phi_w - |\psi|)e^{-\lambda|\psi|}\left(2\sin\left(\lambda|\psi| - \frac{\pi}{2}\right) - \sqrt{2}\sin\left(\lambda|\psi| - \frac{\pi}{4}\right)\right)}{\sin\phi} \qquad [4.67]$$

The conical shell equations become:

"Pinned"

$$w(s) = w_0 e^{-\eta|x|}\sin\left(\eta|x| - \frac{\pi}{2}\right) \qquad [4.68]$$

"Fixed"

$$w(s) = w_0 e^{-\eta|x|}\left(2\sin\left(\eta|x| - \frac{\pi}{2}\right) - \sqrt{2}\sin\left(\eta|x| - \frac{\pi}{4}\right)\right) \qquad [4.69]$$

The graphical representation of the weld shapes is given in Figures 4.3 and 4.4 below. The graphs have been drawn up for conical and spherical shells of arbitrary dimensions. It indicates the symmetrical shape of the weld imperfection with respect to the generator of the cone (*s*) and the meridional angle of the sphere (ϕ).

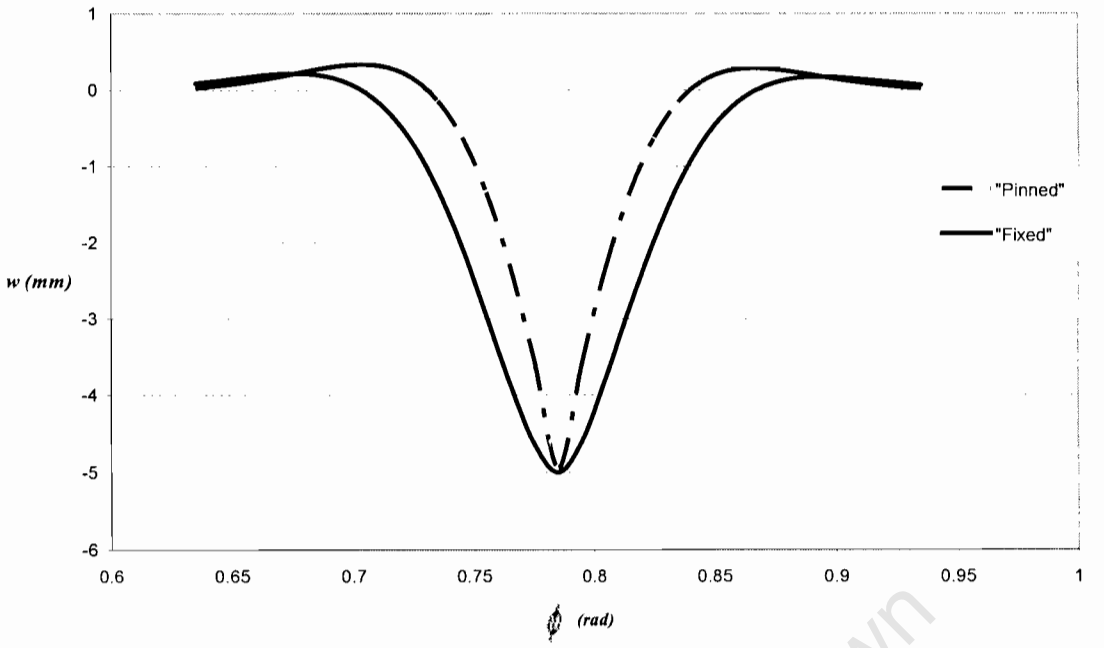

Figure 4.3: Weld Imperfection Shape; Spherical Shell

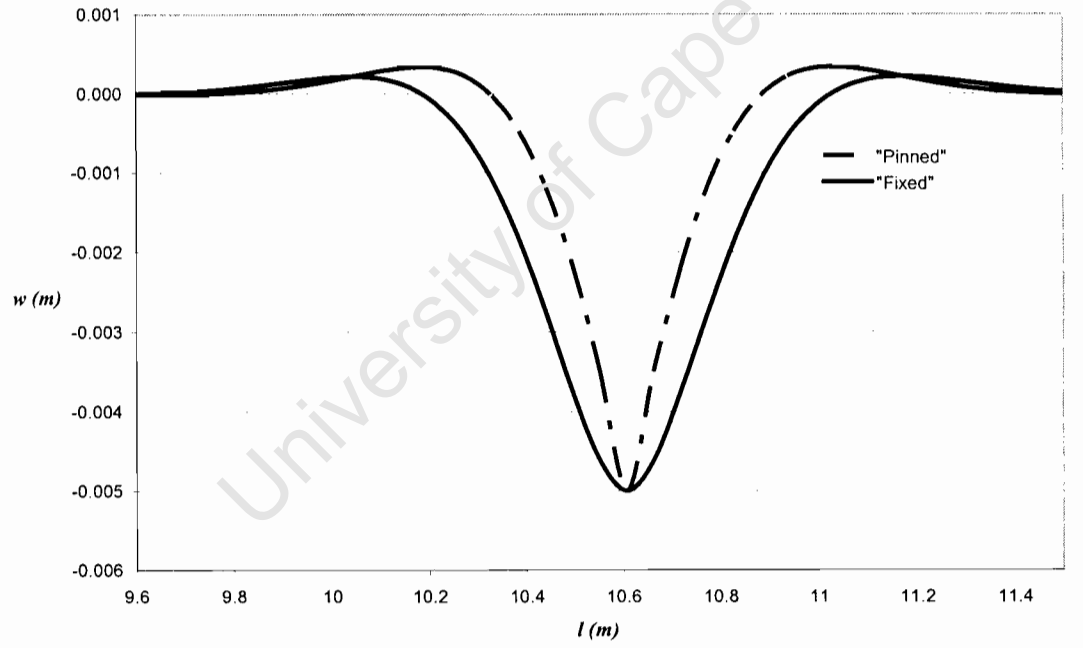

Figure 4.4: Weld Imperfection Shape; Conical Shell

The figures represent the weld shapes that will be adopted in the future chapters of this dissertation to examine the effect of the circumferential weld-induced imperfection on the buckling capacity of the spherical and conical shells.

5 FINITE ELEMENT ANALYSIS OF IMPERFECT SPHERICAL AND CONICAL SHELLS

The previous chapter involved the determination of approximate geometric shapes for the weld imperfection. The current chapter will deal with the effect of the geometric weld imperfection on the buckling behaviour of the spherical and conical shells of revolution.

The literature review in Chapter 1.0 identified that the axisymmetric imperfection results in a reduction of the load carrying capacity. The research on cylindrical shells indicated that the circumferential weld (Axisymmetric imperfection) resulted in a reduction of 70 % of the axial load. Taking this into account the investigation will focus on the effect of a circumferential geometric weld imperfection in the spherical and conical shells.

The analysis will be performed using the finite element software ABAQUS. Due to the presence of the imperfection the analysis will be a nonlinear analysis that takes account of the material and geometric nonlinearity.

The material used in this investigation will constitute mild steel. The properties have been listed in Chapter 3. The respective geometries and results will be discussed in the relevant sections that follow.

5.1 Imperfect Spherical Shell

This section deals with the analysis of an imperfect spherical shell. The dimensions of the spherical shell will be taken to be equivalent to those laid out in Chapter 3. The geometric parameters will be repeated here for convenience:

$R = 5.0m$

$t = 5mm$

$\phi_s = \frac{\pi}{2}$

The aim of the analysis is to determine the effect of a circumferential weld on the buckling behaviour of a spherical shell under uniform external pressure. The following areas will be investigated:

- The effect of the "Pinned" and "Fixed" geometric weld imperfection shapes
- The effect of the imperfection amplitude w_0
- The effect of the meridional location of the circumferential weld (ϕ_w)
- The effect of the adjacent circumferential welds
- The effect of the radius to thickness ratio (R/t)
- The effect of the boundary support location (ϕ_s)

The classical buckling pressure for a sphere of the described proportions was dealt with in Chapter 3. The classical buckling pressure was found to be:

$q_{cl} = 241.2\,kN/m^2$

The analysis of the imperfect shell was initially done using a full 3 dimensional model. This was to ensure that any asymmetric buckling modes would be accounted for. A mesh convergence study was done for a spherical containing a single "Pinned" geometric shape. This was then followed by an analysis of a spherical shell containing a single "Fixed" geometric shape. The parameters used were:

- "Pinned" and "Fixed" geometric weld shapes
- $\phi_w = 45$
- $\frac{w_0}{t} = 1.0$
- Fully fixed boundary supports

The weld imperfection was created in the ABAQUS CAE environment using a spline to model the weld shape. The spline was chosen as it ensures a smoother more continuous surface. An initial study was conducted by describing the geometry as a series of straight lines; this yielded a lower capacity however it was felt that the more angular nature increased the associated bending stresses. The geometry was described by calculating the X and Y coordinates at intervals of 0.025 radians in the meridional direction. This equates to a point every 125mm along the arc length.

The mesh size in the region of the weld imperfection would have to be smaller than 125mm to account for the geometry and change in curvature of the weld shape. For the prefect shell with 200 elements, this equates to a size of 157mm. This is still adequate to discretize the perfect geometry. A mesh convergence was done by using a square mesh in the vicinity of the weld. Figure 5.1 below indicates the convergence of the mesh to a size of 40mm, the computational expense is however extensive. The mesh size of 40mm also relates to a parameter used by Rotter and Teng (1989):

$$mesh\,size = 0.25\left(\sqrt{(Rt)}\right)$$

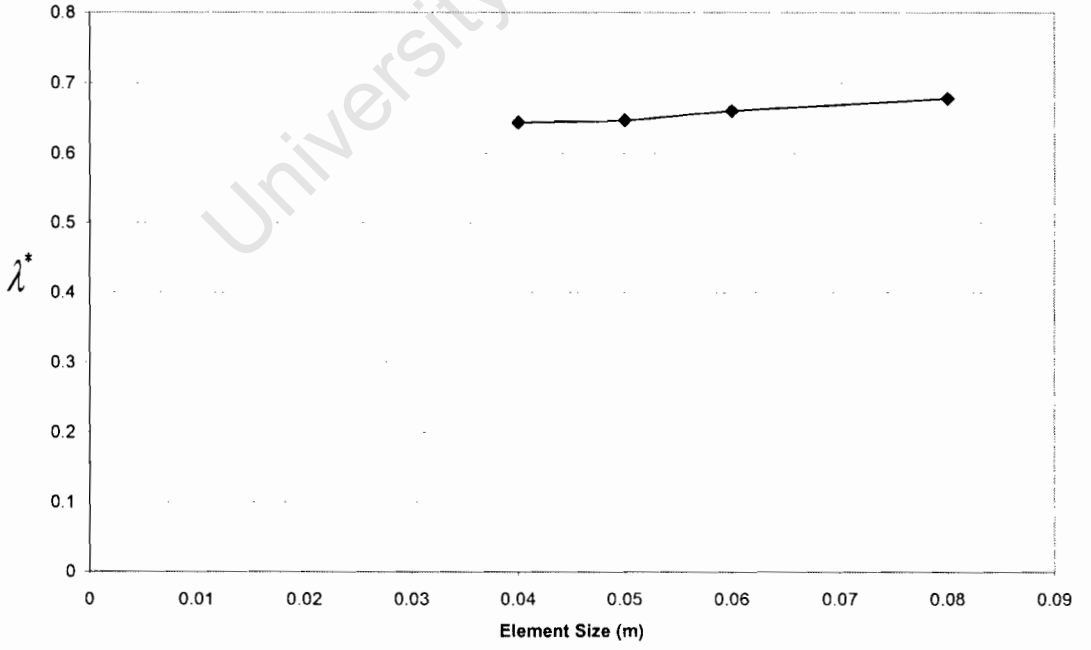

Figure 5.1: Convergence of Solution with Increasing Mesh Density

The axisymmetric model gave a rapid convergence with a mesh size of 0.01m in the vicinity of the weld imperfection and 0.15m for the perfect shell regions. The result obtained was 0.617 which is lower than the result for the 3-D model. The result for the axisymmetric model containing a "Fixed" geometric imperfection was lower than the equivalent 3-D model.

The stress distribution along with the vertical and lateral displacement of the full model indicates that failure occurs due to the development of plasticity in the region of the weld imperfection. The lateral deflection indicates that $n = 0$, lateral expansion in the hoop direction. As such the failure can be adequately described by the axisymmetric model which has a better convergence and far less computational time. The figures below give a comparison of the deflections for the axisymmetric and full spherical models at the point of Bifurcation.

Table 5.1: Comparison of Axisymmetric and 3-D model

	λ^* **"Pinned"**	λ^* **"Fixed"**
Axisymmetric	0.617	0.653
3-Dimensional	0.644	0.692

Table 5.1 shows the results obtained for the full 3-D analysis compared with the axisymmetric stress analysis. The axisymmetric model provides a consistently lower buckling capacity for both geometric shapes.

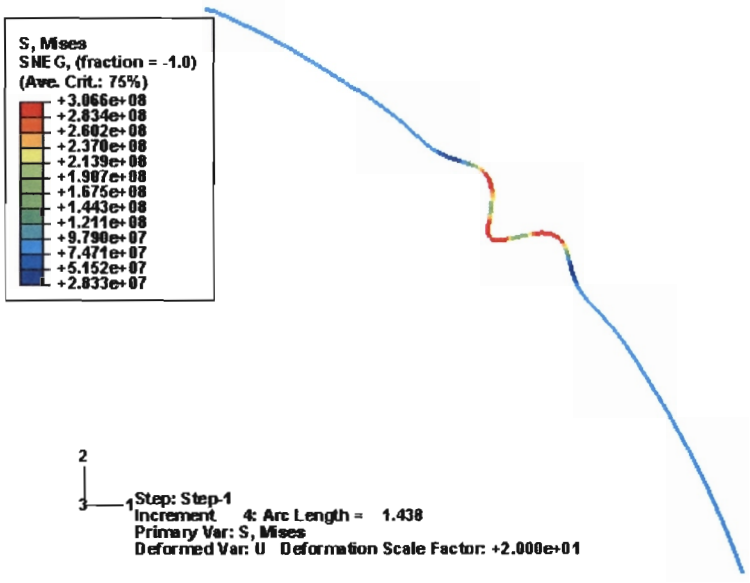

Figure 5.2: Magnification of Weld Shape Showing Mises Stresses

Figure 5.3: Mises Stresses and Buckled Mode 3-D Model

From the above diagrams, we can conclude that the axisymmetric model represents an accurate picture of the effect of the weld imperfection. The Mises Stresses indicate that yielding has occurred at the weld centre. Figure 5.3 also indicates that the deflected shape of the 3-D model at the point of bifurcation is axisymmetric. The remainder of the investigation will be conducted using the axisymmetric model. The parametric study will be conducted with a single circumferential weld.

The first focus was to determine the effects of the "Pinned" and "Fixed" geometric weld shapes and their respective amplitudes. This was combined with the effect of the imperfection amplitude (w_0). The parameters used were:

- $\phi_w = 45$
- $\frac{w_0}{t} = 0;\ 0.5;\ 1.0;\ 1.5;\ 2.0$
- Weld Shape: "Fixed" and "Pinned"
- Boundary Conditions: Membrane

The results of the numerical analysis are presented for the case of the membrane support.

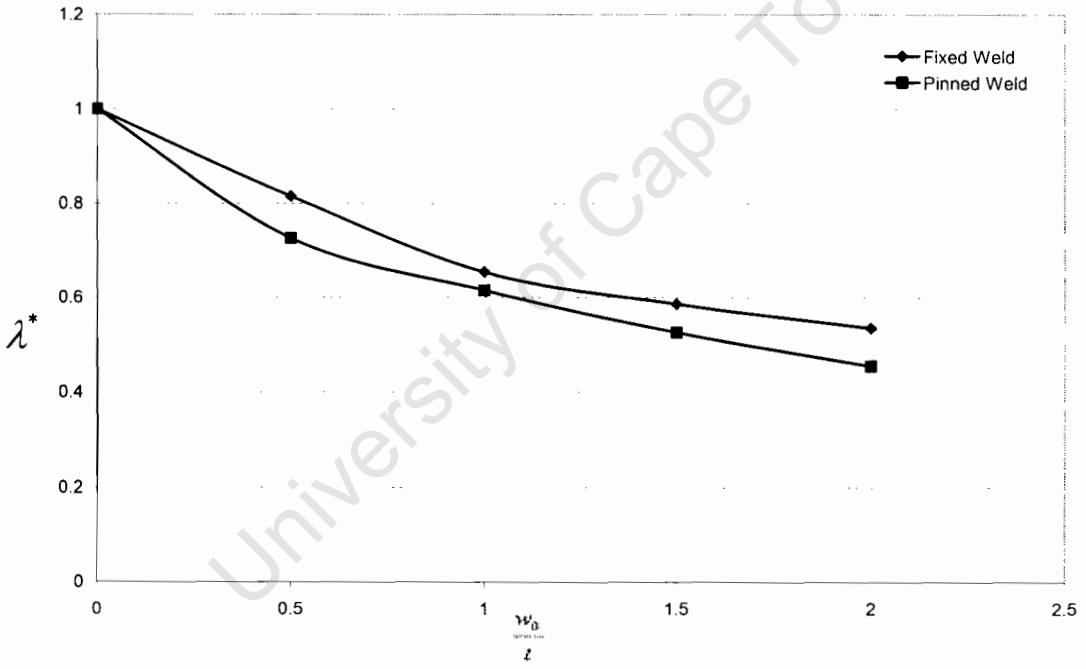

Figure 5.4: Spherical Shell with Circumferential Weld at 45 Degrees

From Figure 5.4 above it is clear that there is a general trend in the behaviour of a spherical shell containing a single circumferential weld imperfection. The graphical results allow the following observations:

- There is a decrease in the buckling capacity of the spherical shell with an increase in the imperfection amplitude.

- The "Pinned" weld gives a lower bound solution for the two idealised analytical weld imperfection shapes.

The Mises Stress from the ABAQUS analysis indicates that at the point of bifurcation the yield strength of the mild steel has been reached. This is illustrated by the Mises stress diagrams in Figures 5.5 and 5.6. The effect of yield is clear in the deflected diagrams Figure 5.2 and 5.3, where the upper portion of the shell goes through a uniform deflection and the weld imperfection experiences the largest deflection indicating this effect of inelastic behaviour.

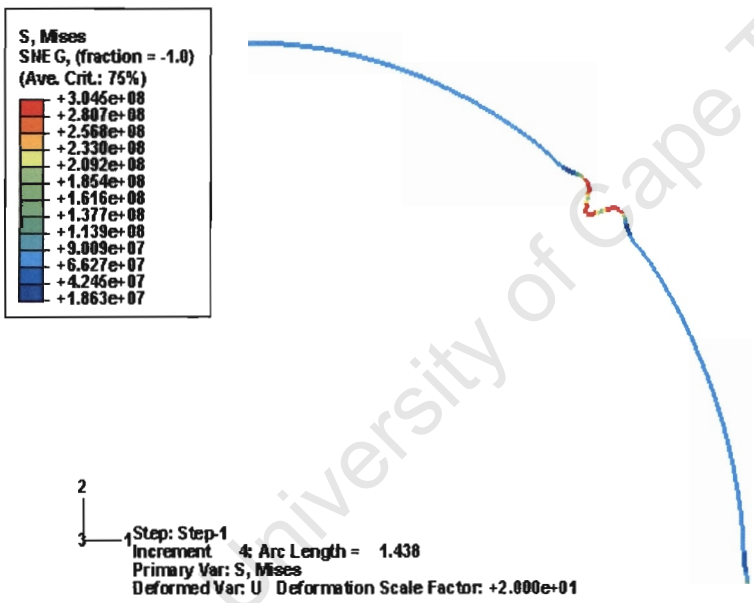

Figure 5.5: Mises Stresses for "Pinned" Weld, $w_0/t = 1.0$

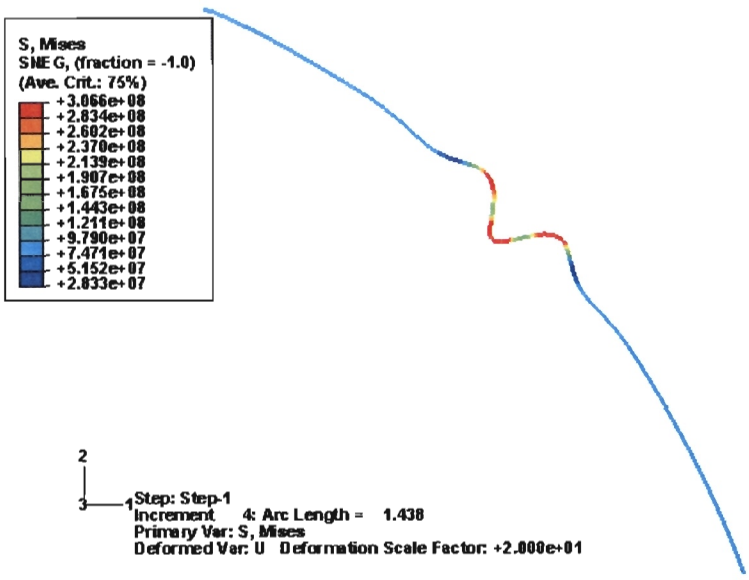

Figure 5.6: Mises Stresses for "Fixed" Weld, $w_0/t = 1.0$

The meridional location of the circumferential weld imperfection was altered to determine its effect on the buckling capacity. The following parameters were used for this analysis:

- $\phi_w = 20; 45; 60$
- $\frac{w_0}{t} = 0;\ 0.5;\ 1.0;\ 1.5;\ 2.0$
- Weld Shape: "Fixed"
- Boundary Conditions: Membrane

The results are presented in Figure 5.7, as a plot of the imperfection amplitude versus the classical reduction factor (λ^*).

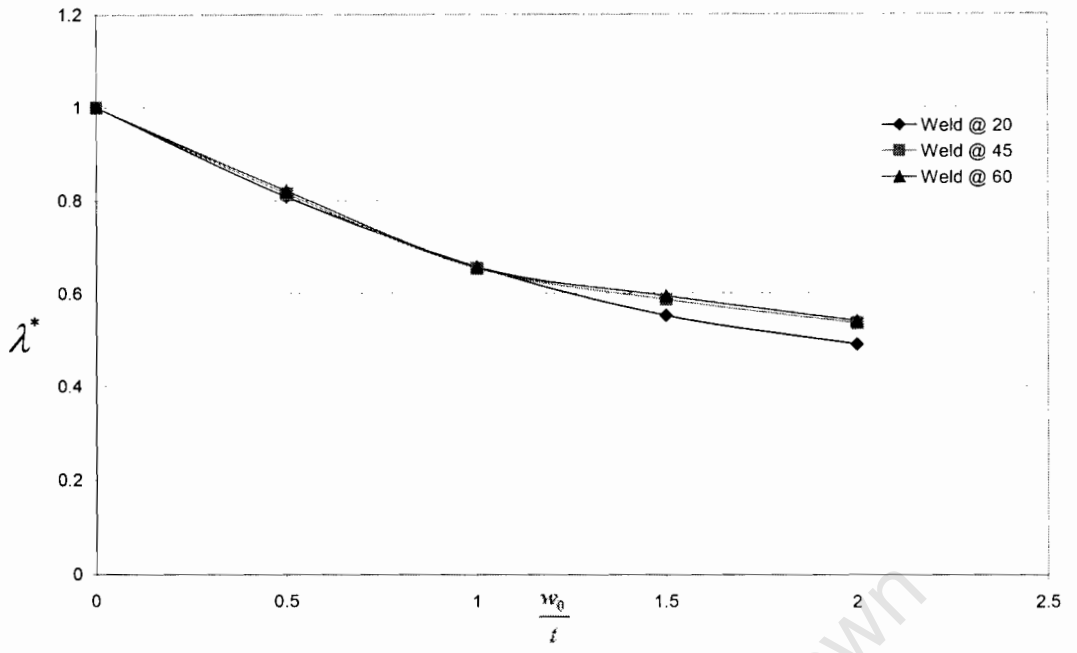

Figure 5.7: Comparison of Results for Meridional Location of Imperfection

The results indicate that the closer the circumferential weld to the apex the more critical the buckling capacity. This is true for all values of imperfection amplitude for the weld placed at 20 degrees. The difference is not significant except for values of imperfection amplitude greater than one wall thickness.

This can be better viewed by taking account of the "Pinned" imperfection at a defined value of imperfection amplitude. Figure 5.8 illustrates the effect of the meridional location on the buckling capacity for and imperfection amplitude, $w_0\backslash t = 1.5$, with membrane type boundary conditions.

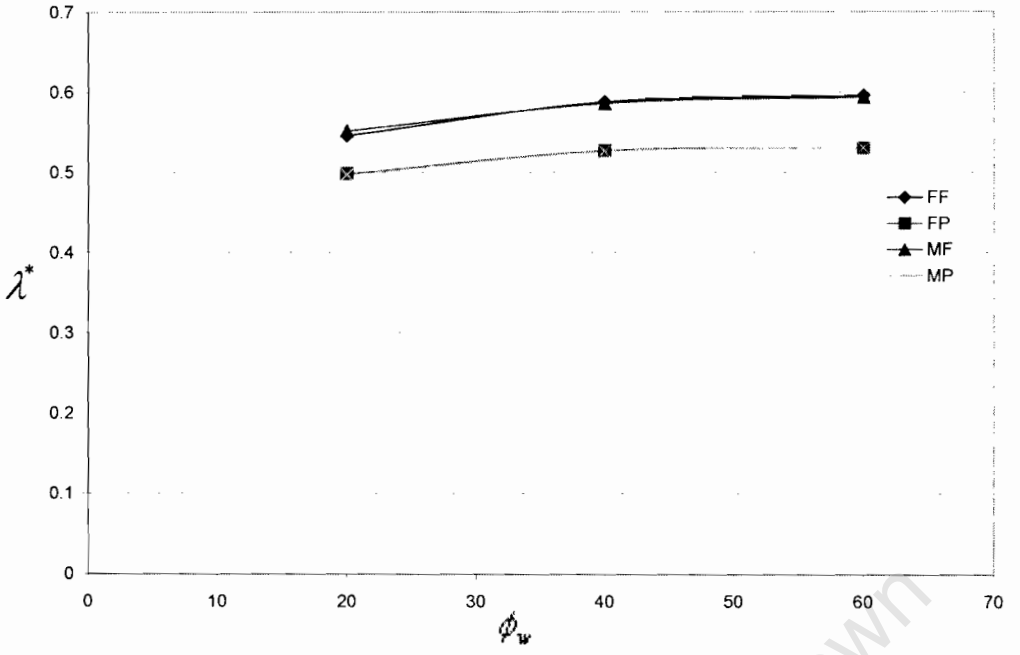

Figure 5.8: Comparison of Meridional Weld Location

Figure 5.8 illustrated the reduction of the buckling capacity when moving the location of the circumferential weld closer to the apex of the spherical shell. The difference is 1.5% between a weld at 60 and 20. The reduction of buckling capacity is still approximately 50% of the classical.

The material behaviour is nonlinear in all off the analysis conducted. To determine the effect of the radius to thickness ratio on the buckling capacity, and the possibility of elastic buckling the thickness of the shell was altered. The analysis was conducted for shells:

- $\frac{R}{t} = 500;1000;1500;2000$
- $\frac{w_0}{t} = 1.0$
- "Pinned" Geometric Weld Imperfection

The results are given in the Figure 5.9.

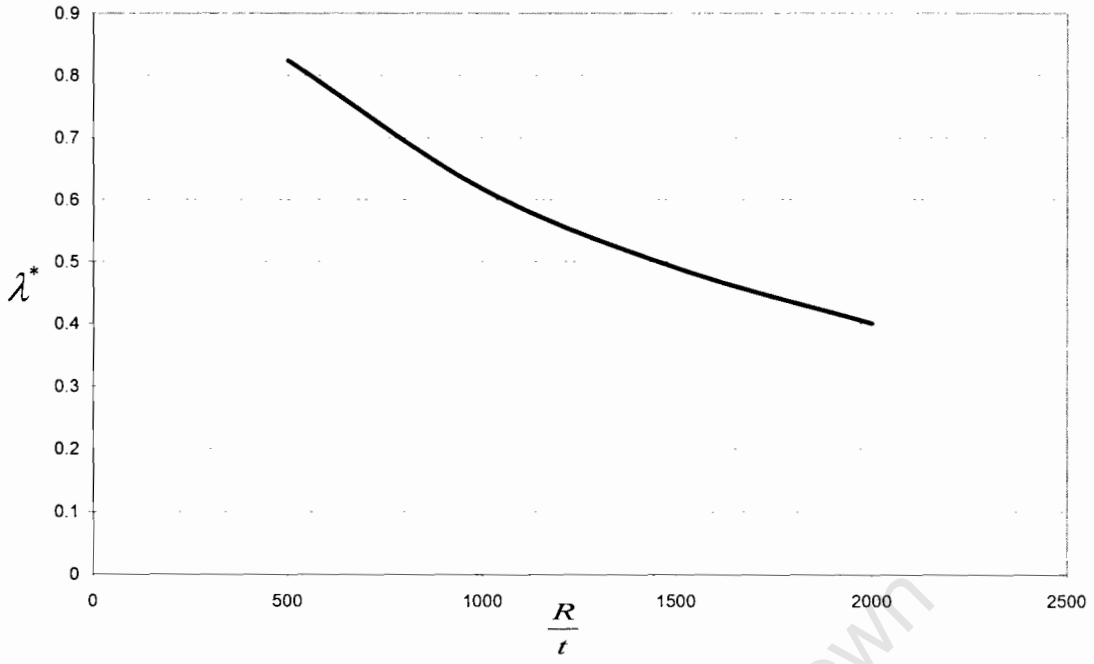

Figure 5.9: The Effect of Radius to Thickness Ratio on Buckling Capacity

The results are better viewed in tabular form to indicate the classical buckling strength of each shell.

Table 5.2: Radius to Thickness Ratios

R/t	q_{cl} (N/m^2)	λ^*
500	484180	0.824
1000	242100	0.617
1500	161320	0.49
2000	121046	0.4

An increase in the radius to thickness ratio results in a decrease of the buckling capacity of the spherical shell concerned. In all cases the material showed nonlinear behaviour at the point of bifurcation. The thinner the shell becomes the more critical the effect of the weld imperfection.

The construction of shells in civil engineering applications often sees the introduction of more than one circumferential weld imperfection. The following section is thus

aimed at studying the effect of two adjacent c ircumferential welds on the buckling capacity.

The study was conducted using a parametric study. The details are again given here for completeness. The adjacent welds were placed at the following locations:

- $\phi_{w1} = 30$; $\phi_{w2} = 60$
- $\phi_{w1} = 20$; $\phi_{w2} = 45$

The parametric study involved the increase in the imperfection amplitude in the manner applied to the previous studies. The results are given in Figure 5.10.

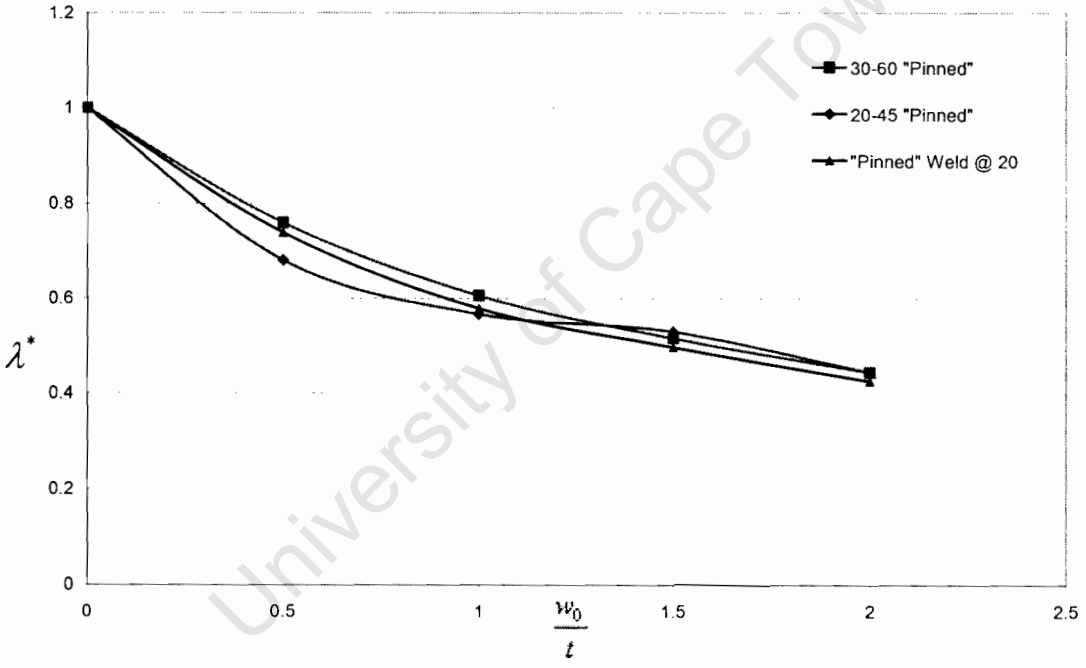

Figure 5.10: Effect of Adjacent Welds on the Buckling Capacity

Figure 5.10 shows a comparison between the adjacent weld results and the results of a single circumferential weld at 20 degrees. It is clear that the adjacent weld at 30 and 60 degrees does not reduce the buckling capacity dramatically. The effect of adjacent welds at 20 and 45 however does result in a reduction below the values obtained for a a single weld with an imperfection amplitudes of less than one wall thickness.

The final analysis to be conducted was the location of the supports. The literature review on shallow spherical shells in Chapter 1.1.3 indicates that there can be an associated reduction of classical buckling capacity due to increased bending stresses resulting from the fully fixed support conditions. As such the location of the support was altered to determine the combined effect of a fully fixed support and a geometric weld imperfection. The parameters are:

- $\phi_w = 20$
- $\phi_s = 90; 75; 60; 55; 45; 35$
- $\frac{w_0}{t} = 1.0$
- Boundary Support Fully Fixed

The results of the ABAQUS analysis are plotted below. Figure 5.11 plots the reduction of buckling capacity versus the location of the fixed support conditions.

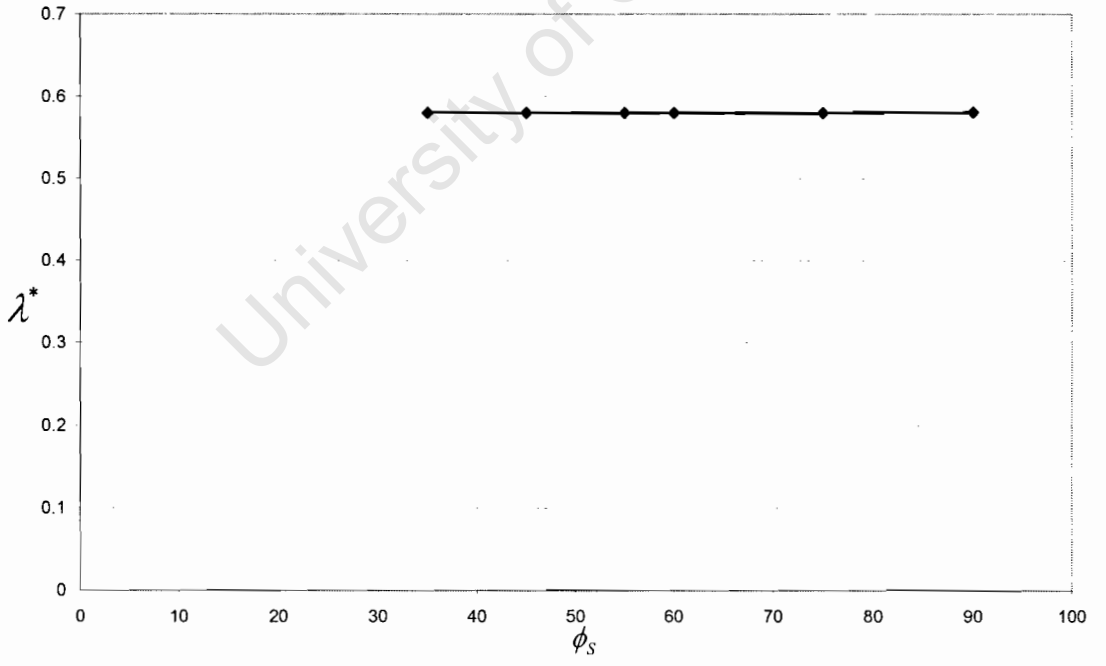

Figure 5.11: Effect of Support Location

The results indicate that there is little effect felt due to the location of the fixed support. This indicates that the weld imperfection at 20 degrees is the overriding factor influencing the reduction of buckling capacity for the spherical shell.

All the previous analysis results indicate that the material yield stress is a dominant contributing factor to the reduction of strength. To determine the effect of the material properties it was decided to conduct a nonlinear elastic buckling analysis. This was conducted for the case:

- Axisymmetric and 3-D Models
- "Pinned" and "Fixed" Welds
- $\frac{w_0}{t} = 1.0$
- Fixed Boundary Conditions

The results of the analysis are recorded in Table 5.3. The 3-D model was done using a S4 element with a mesh size of 40 x 40 mm in the region of the weld shape.

Table 5.3: Elastic Buckling Analysis

Model	**Axisymmetric Model**		**3-D Model**	
Weld Shape	**"Pinned"**	**"Fixed"**	**"Pinned"**	**"Fixed"**
λ^*	0.897	0.915	0.819	0.791

The elastic analysis results were not as low as those obtained earlier. In this case the 3-D model was consistently lower than the axisymmetric model. This is because the critical buckling mode was in the circumferential direction. The 3-D model buckled with approximately 5 waves in the hoop direction. The buckled modes and Mises stresses are given in the figures below.

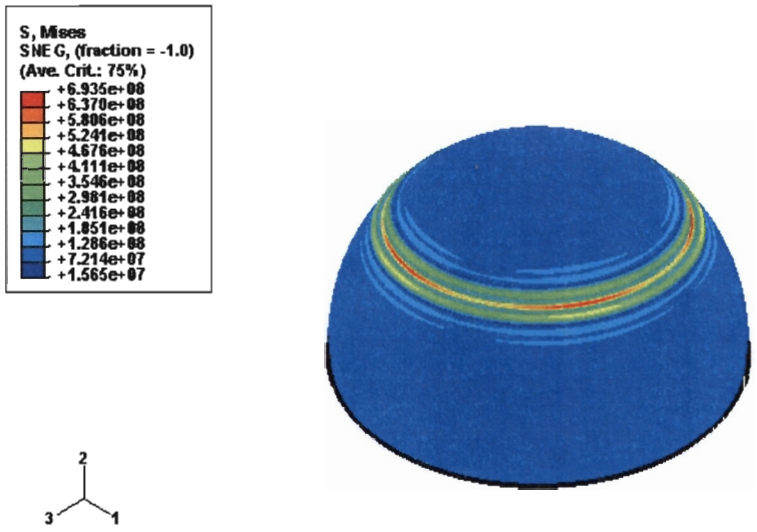

Figure 5.12: Buckling Mode and Mises Stress for 3-D Model, "Pinned" Shape

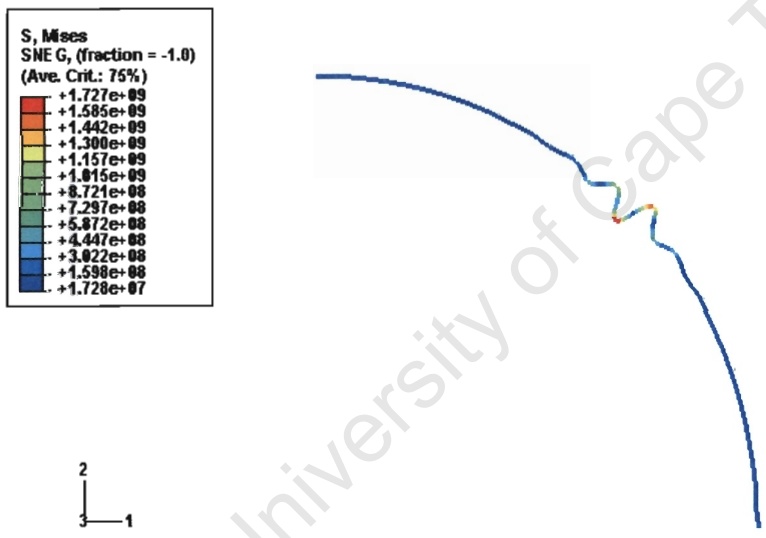

Figure 5.13: Axisymmetric Buckling Mode and Mises Stresses

Figure 5.12 and 5.13 indicate that the stress level is above the yield stress of 300MPa. This indicates that the results obtained for the spherical shell are a result of material nonlinearity rather than typical buckling behaviour. The Elastic Buckling analysis does not significantly reduce the carrying capacity of a spherical shell under uniform external pressure.

The results of the elastic analysis and the effect of the yield stress should be taken into account in the next section on the conical shell

5.2 Imperfect Conical Shell

The following section deals with the effect of the geometric weld imperfection on the buckling behaviour of an axially compressed conical shell. The investigation will be conducted to determine the following characteristics of the buckling behaviour of an imperfect conical shell. These are:

- The effect of the "Pinned" or "Fixed" geometric weld shapes
- The effect of the imperfection amplitude w_0
- The effect of the angle α
- The Effect of the meridional location of the weld
- The effect of adjacent weld imperfections

The geometric parameters for the truncated conical shell are given below along with a schematic of the conical shell in Figure 5.13.

$R_u = 5.0m$

$R_l = 10.0m$

$t = 5mm$

thus:

$$\frac{R_u}{t} = 1000$$

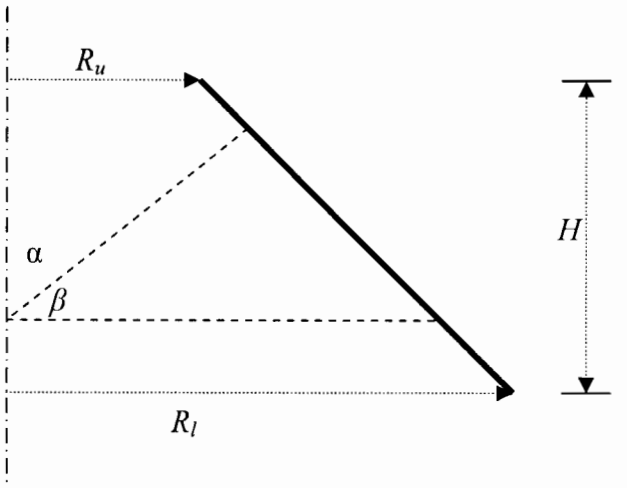

Figure 5.14: Schematic of Truncated Conical Shell

The mesh size/convergence for the perfect conical shell was determined using the linear elastic eigenvalue buckling procedure within ABAQUS. The analysis was conducted on a full model to account for the event of a asymmetric buckling mode. The shell element, S4R, was used and the summary on its properties can be seen in Chapter 3.0. This element accounts for the finite strains and rotations that result from the nonlinear material and geometric behaviour.

The linear buckling analysis was conducted on a shell with an apex angle of $\beta = 45$ degrees. The shell was meshed by defining the number of elements along the upper and lower edges. The classical buckling solution for an axially loaded conical shell is given by Seide (1956) and provides an adequate means for comparison. The shell had fixed boundary conditions which will be applied for the rest of the analysis. These are illustrated in Figure 5.15 below.

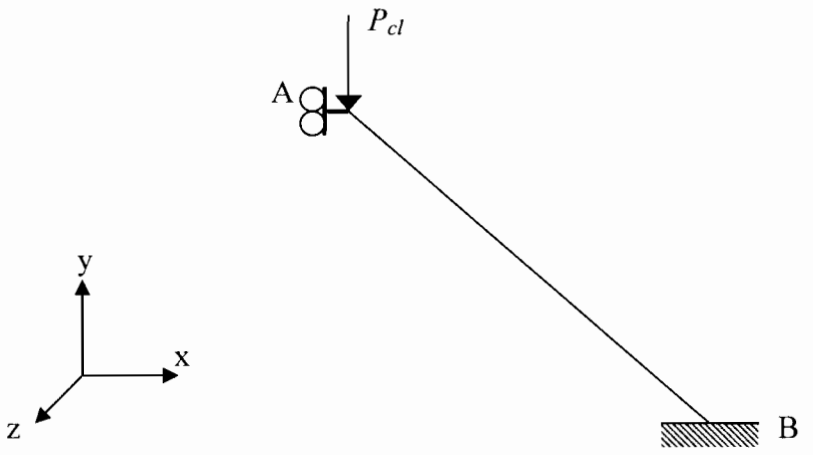

Figure 5.15: Conical Shell Boundary Conditions

All the degrees of freedom were fixed except for the translation in the direction of the y axis. The figure indicates the respective boundary conditions, these are better described:

- A: fixed against rotation and translation for all degrees of freedom except for translation in y
- B: Encastre, all degrees of freedom fixed against rotational and translational movement.

The classical buckling load from Chapter 1.1.4 can be calculated as:

$P_{cl} = 9.5MN$ (total axial load)

The convergence for different mesh sizes to Seide (1956) classical buckling solution is given in Figure 5.17. The figure plots the total classical axial load versus the number of edge elements used to mesh the conical shell. The mesh arrangement of the conical shell is given in Figure 5.15 and the buckling mode corresponding to the lowest eigenvalue is given in Figure 5.16.

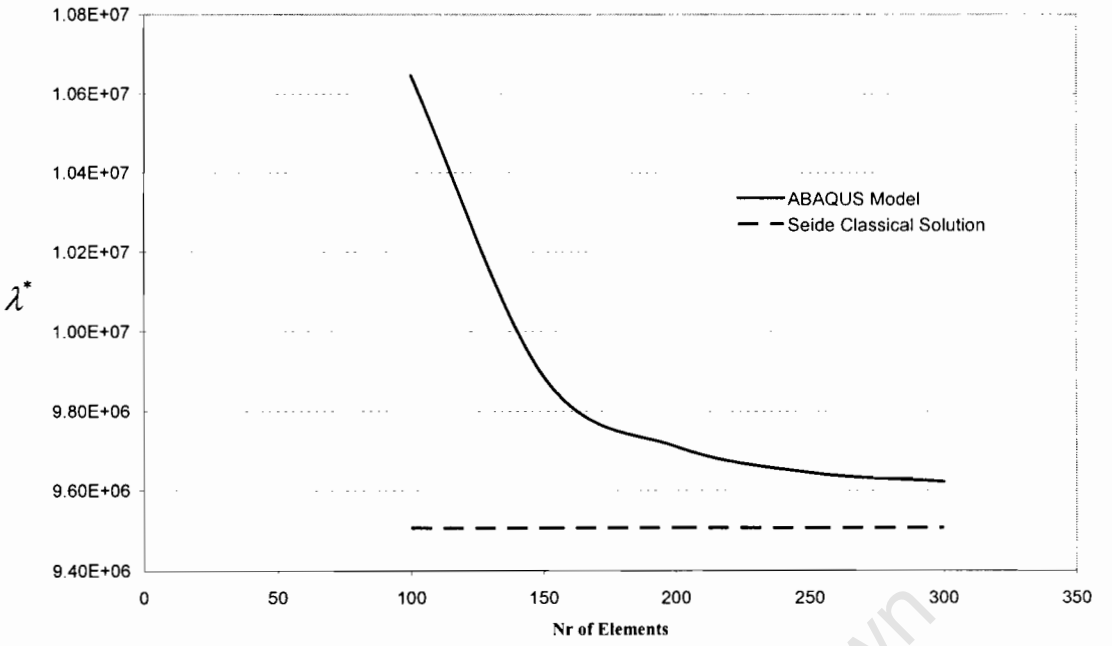

Figure 5.18: Mesh Convergence Perfect Conical Shell

It is visible that the increase of edge elements results in a solution converging to the classical buckling strength. The results corresponding to the use of 300 edge elements will be used for the remainder of the analysis. It was felt that this was within the required accuracy of 5%, a further refinement of the mesh would only increase the computational time.

The second step involved inserting the geometric shape of the weld imperfection defined in Chapter 4, these will be summarised here for completeness.

- "Pinned" Weld

$$w(x) = w_0 e^{-\eta x} \sin\left(\eta x - \frac{\pi}{2}\right) \qquad [5.1]$$

- "Fixed" Weld

$$w(x) = w_0 e^{-\eta x}\left(2\sin\left(\eta x - \frac{\pi}{2}\right) - \sqrt{2}\sin\left(\eta x - \frac{\pi}{4}\right)\right) \qquad [5.2]$$

The geometry in ABAQUS was achieved by using a spline to model the geometric shape at intervals. This was then used to generate the X and Y global coordinates for the model using a total of 40 points distanced every 55mm along the conical shell generator.

The mesh needed to be refined in the region of the weld imperfection to account for the high localised bending stresses that would occur due to the shape discontinuity. The number of elements on the upper and lower edge would be kept consistent with the results form the linear buckling analysis; at 300 elements. From the literature review Rotter and Teng (1989) made use of a geometric parameter to determine the mesh size for a cylindrical shell. This is given as:

$$Mesh\,size = 0.25\sqrt{(Rt)}$$

Thus by making use of the upper radius R_u we can determine the mesh size for the conical shell as:

$$0.25\sqrt{(5.0\times 0.005)} = 0.04m$$

This equates to a square mesh of 40mm x 40mm. The mesh could be refined further however this would increase the computational expense of the problem. Thus all the models will be meshed using the defined size of 40x40mm in the region of the weld and 300 elements on the upper and lower edge.

The Finite Element Analysis was conducted to determine the respective effects of the "Pinned" and "Fixed" geometric weld shapes. The parameters involved in the study are listed below:

- $\alpha = 45$
- $w_0 = 0.5t; 1.0t; 1.5t; 2.0t$

The boundary conditions used for the analysis are kept fixed as indicated in Figure 5.14.

The imperfect shell was analysed using the STATIC RIKS step in ABAQUS, this was discussed in Chapter 2.0. This step takes account of both the material and geometric nonlinearity associated with the problem. The analysis was again conducted with the mild steel material properties The applied load for the perfect shell determined through a linear elastic buckling analysis is given as:

$$P_{cl} = \frac{9.6MN}{2\pi R_u}$$

The analysis results are given in Figure 5.19. The graph records the reduction in the classical buckling strength versus the increase in the weld imperfection amplitude.

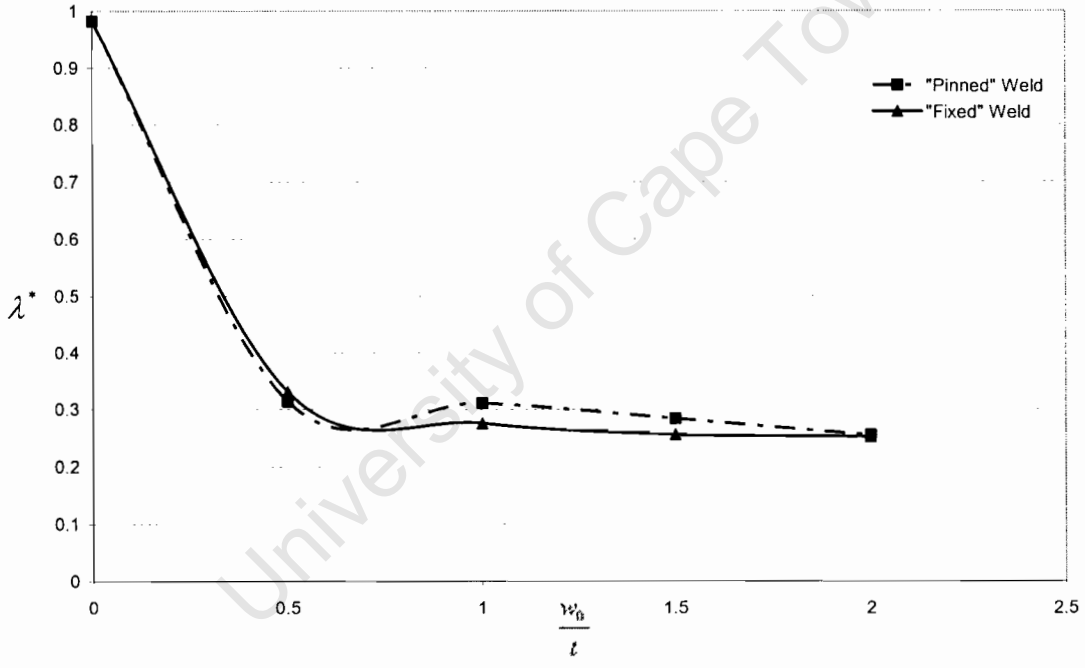

Figure 5.19: Circumferential Weld Imperfection

The graphical results indicate that there is a loss in the buckling capacity for an imperfect conical shell. The effect of a weld imperfection with an amplitude of *0.5t* can result in a 68% reduction in the applied axial load.

The "Fixed" weld appears to be a lower bound solution which is consistent with results obtained by Rotter & Teng (1989) for their shapes A and B for the cylindrical shells. The respective solutions appear to converge with the increase of the imperfection amplitude.

Further differences can be seen in the stress states of the finite element models. The following diagrams are illustrated for the cases of a "pinned" and "fixed" weld imperfection at the amplitude of *1.0t* and *2.0t*. The diagrams will illustrate the Mises stress plots to indicate the formation of plasticity, the meridional stress state and the buckled mode.

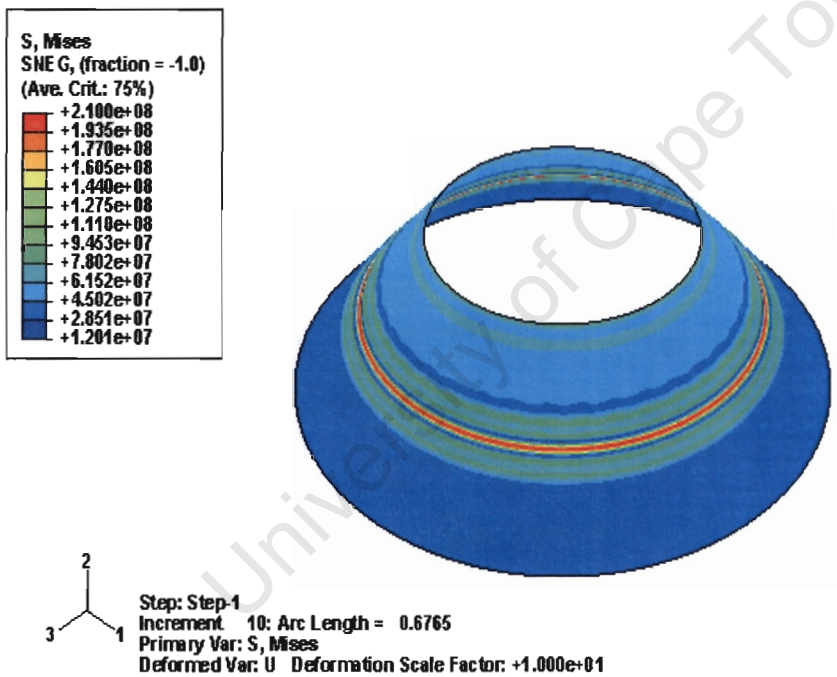

Figure 5.20: Mises Stress for a "Fixed" Weld, $w_0/t = 1.0$

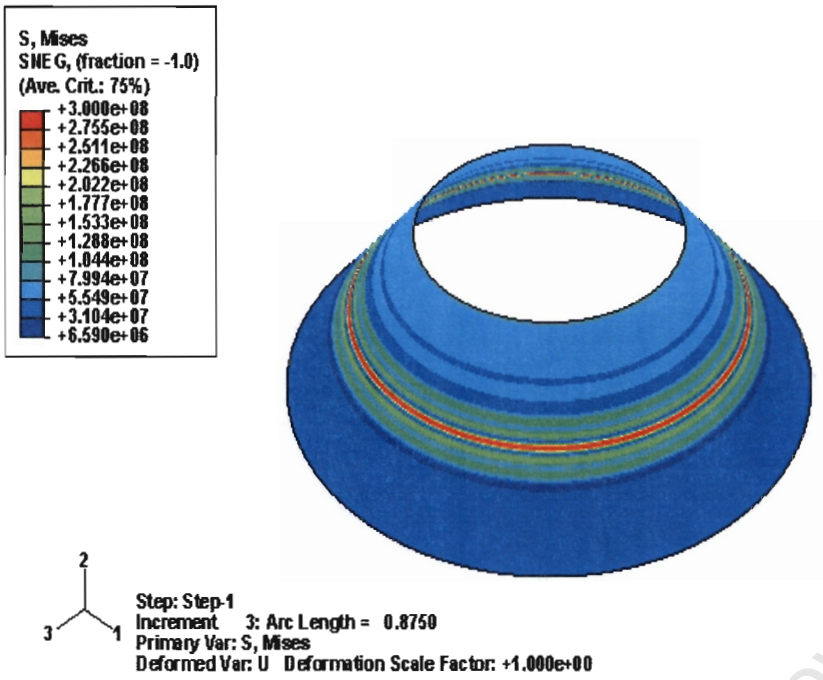

Figure 5.21: Mises Stress for a "Pinned" Weld, $w_0/t = 1.0$

The figures indicate that the "Pinned" weld models reach the yield stress at the point of bifurcation. The buckling is thus a nonlinear inelastic buckling where as the "Fixed" weld model is still with in the elastic range of the material.

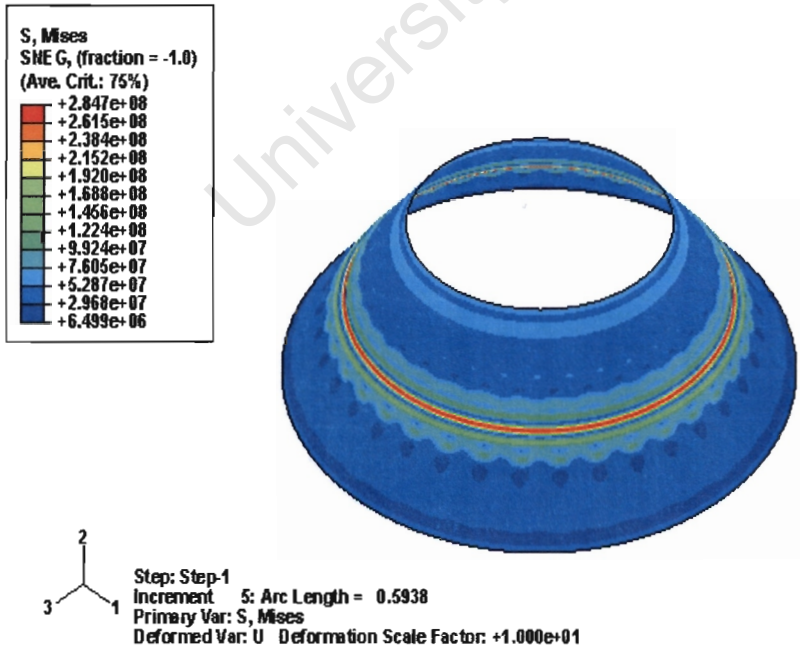

Figure 5.22: "Fixed" Weld, Mises Stresses, $w_0/t = 2.0$

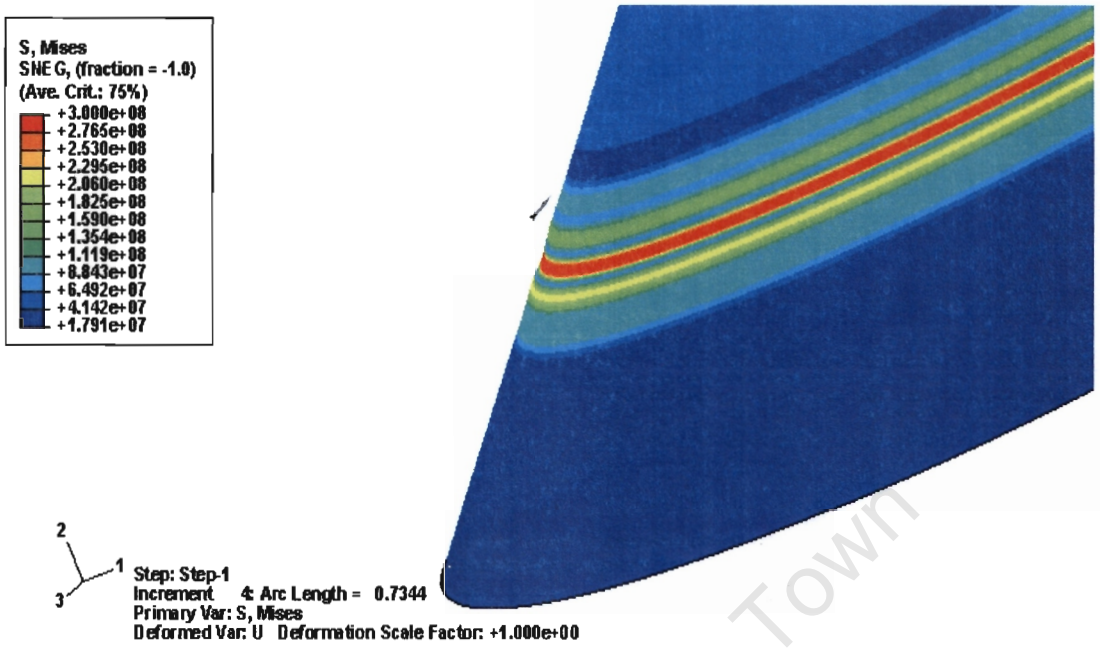

Figure 5.23: "Pinned" Weld Mises Stresses, $w_0/t = 2.0$

The effect of the two geometric shapes can be seen again at the increased imperfection amplitude. Again the "pinned" shape indicates the onset of material nonlinearity whilst the "Fixed" shape is still within the elastic region at the point of bifurcation.

The respective meridional stress patterns can be seen in the figures below. It is visible that the meridional stresses in the region of the "Pinned" geometric weld imperfection are higher than those encountered for the case of the "Fixed" imperfection. The stress patterns for both cases do correspond to each other as well as the same basic pattern encountered in the spherical shells.

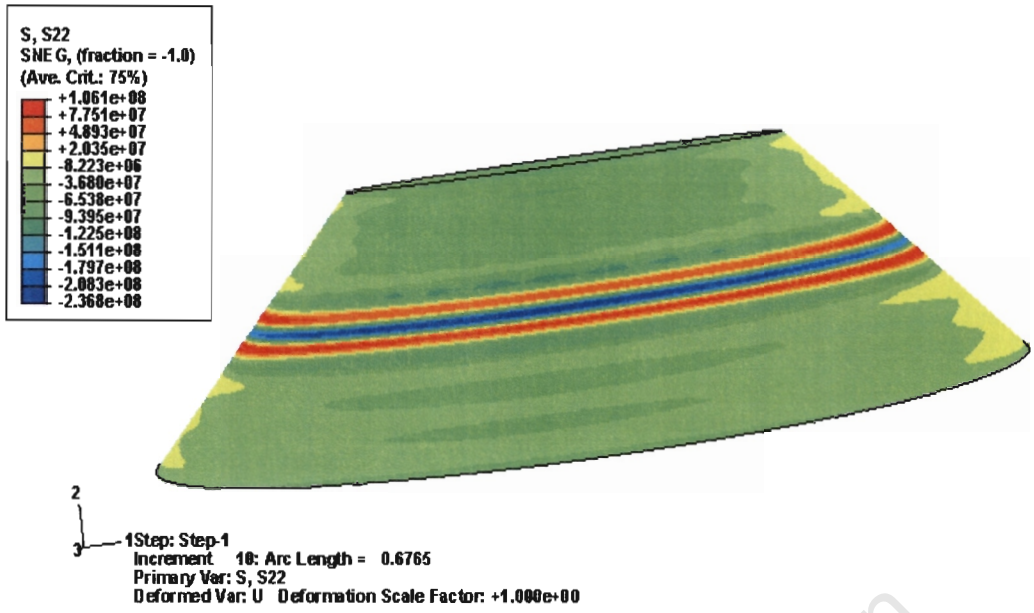

Figure 5.24: "Fixed" Weld - $w_0/t = 1.0$

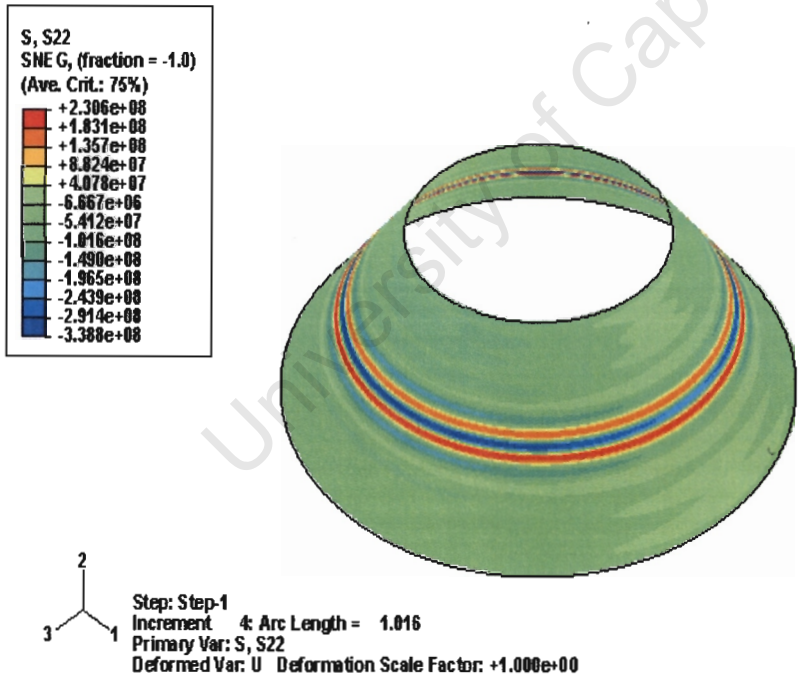

Figure 5.25: "Pinned" Weld, $w_0/t = 1.0$

The final buckled shapes of the conical shells differ as a result of the material nonlinearity. The "Fixed" geometric imperfection results in the formation of buckles

in the circumferential direction, along the upper and lower edges and the centre of the weld-induced imperfection.

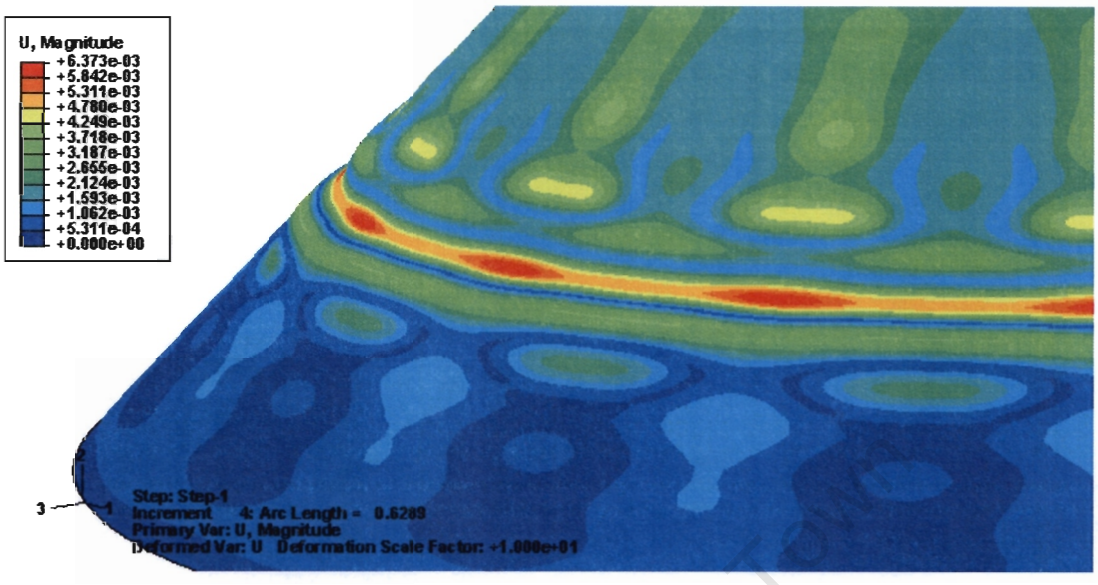

Figure 5.26: Buckling Mode – "Fixed" Weld, $w_0/t = 1.0$

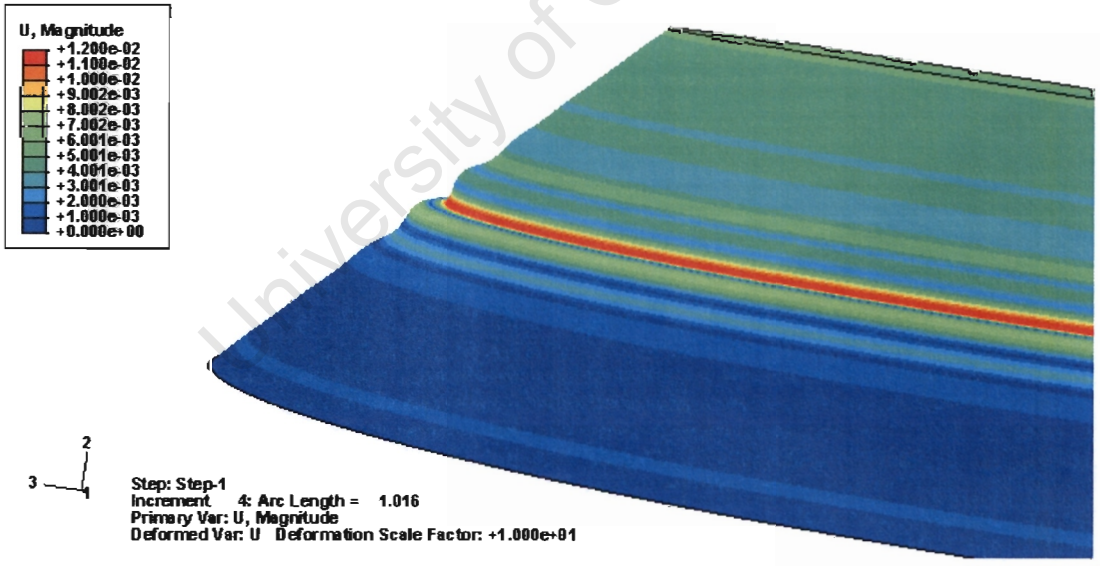

Figure 5.27: Buckling Mode, "Pinned" Weld, $w_0/t = 1.0$

The "Pinned" geometric shape is just amplified at the point of bifurcation and no buckles develop in the circumferential direction due to the onset of material nonlinearity. The "fixed" weld induces buckling in the circumferential direction.

Figure 5.26 highlights the occurrence of buckles adjacent to the weld-induced imperfection as well as at the weld centre. The model indicates that there are a total of 17 buckling waves in the circumference, this is agreeable with the findings of Rotter and Teng (1989) who found 18 waves for the cylindrical shell.

A further study was conducted on the pinned model assuming an elastic material. The models were meshed with an S4 element. To draw a better comparison of the results the "fixed" weld model was also evaluated. The results are given in Table 5.4 below.

Table 5.4: Comparison of Results for Elastic and Inelastic Material

Imperfection Amplitude	"Fixed" Weld Imperfection		"Pinned" Weld Imperfection	
	S4R σ_y = 300MPa	S4 Elastic	S4R σ_y = 300MPa	S4 Elastic
1.0t	0.285	0.277	0.311	0.335
2.0t	0.251	0.244	0.255	0.299

The results for the "fixed" imperfection show good agreement for the two element types. The S4 element shows a further reduction in the buckling capacity. The results for the "pinned" imperfection differ by a greater margin; the nonlinear elastic analysis indicates a lesser reduction in the load carrying capacity. The view of the Mises Stresses for the "pinned" weld is given in Figure 5.29.

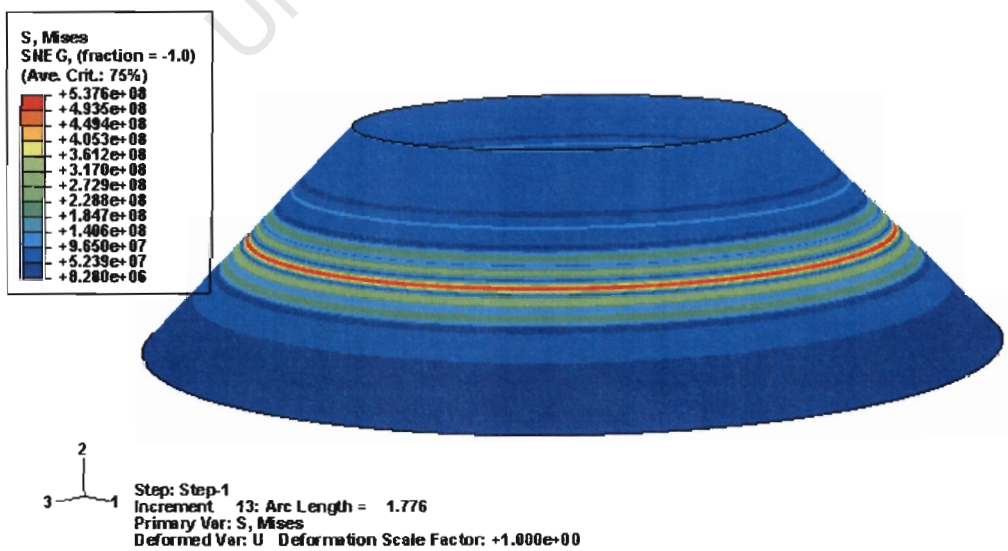

Figure 5.28: Mises Stresses "Pinned" Weld

It is visible that the stresses are a value of 537 MPa at the weld centre. This is well above the assumed yield stress for a mild steel of 300 MPa. The buckled shape is not consistent with that found in the cylindrical shells. The final shape appears to be a magnification of the weld-induced imperfection shape rather than having buckles in the circumferential direction as found with the "Fixed" weld shape. This can be seen in Figure 5.29 below and is more indicative of progressive failure.

Figure 5.29: Buckled Mode "Pinned" Weld Imperfection $w_0/t = 1.0$

The rest of the analysis for the conical shell deals with the use of the mild steel. This is a more realistic representation of the actual behaviour in an engineering environment. The results for the "pinned" weld imperfection indicate the effect of instability combined with the material nonlinearity. All the analysis were conducted with the S4R element.

A secondary analysis was conducted to determine the effect of the angle α. The finite element analysis was conducted using the following:

- "Pinned" Weld
- $\frac{w_0}{t} = 1.0$
- $\alpha = 30; 45; 60$
- Fixed Boundary Conditions

The results of the analysis are presented in Table 5.5 below. The table lists the classical linear buckling strength derived using ABAQUS and the loss of capacity for an imperfect conical shell.

Table 5.5: Circumferential Weld Imperfection in Conical Shells

α	q_{cl} *(MN)*	λ^*	q_{actual} *(MN)*
30	4.85	0.318	154.4
45	9.63	0.311	299.2
60	1433.9	0.28	401.5

The "Pinned" weld reduces the buckling capacity by up too 72%. The effect is visibly worse in the 60 degree truncated conical shell.

The location of the circumferential weld imperfection has been kept at *H/2* for all the previous analysis. A further analysis was conducted to determine the effect of the circumferential weld located at different points along the conical generator. The locations were taken at the quarter points *(H/4)* along the generator. The analysis was conducted using:

- "Pinned" Weld Imperfection
- $\alpha = 45$
- $\frac{w_0}{t} = 1.0$

The results of the finite element analysis are given in Figure 5.30 below. The diagram is a plot of the buckling parameter versus the location along the conical generator (l_s).

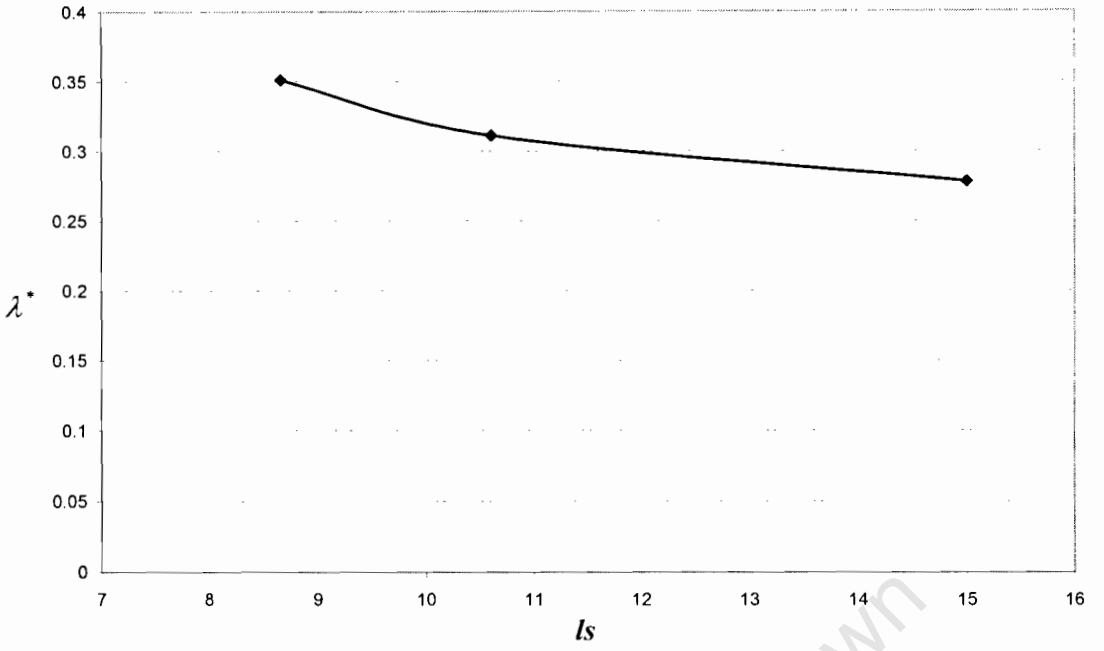

Figure 5.30: Effect of Weld Location on the Buckling Capacity

The figure indicates that the closer the circumferential imperfection is to the lower edge of the truncated conical shell, the more critical the reduction of the classical buckling load. This could be due to the interaction of the weld imperfection and the fully fixed support conditions at the base of the truncated conical shell.

The previous sets of analysis results have been conducted for the case of a single circumferential weld imperfection. In actual civil engineering applications the construction might result in the presence of more circumferential welds. As such an analysis was conducted on a conical shell containing two circumferential welds. The parameters for this analysis are:

- "Pinned" Weld
- $\alpha = 45$
- $\frac{w_0}{t} = 1.0$
- Fixed boundary conditions

The placement of the weld imperfections is best given by means of graphical representation.

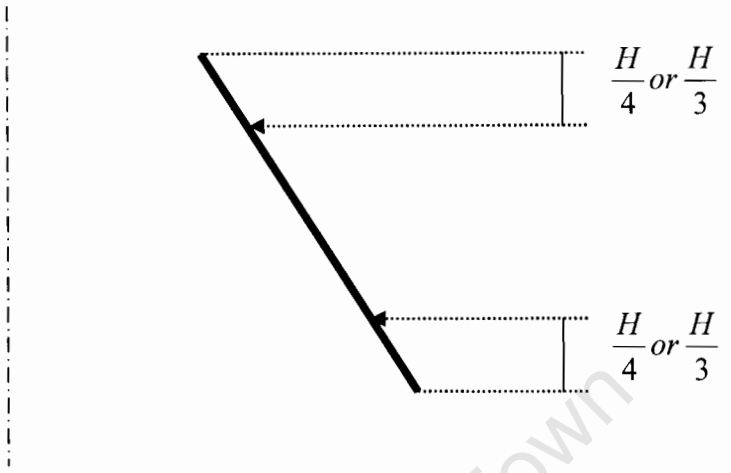

Figure 5.31: Schematic Showing Location of Adjacent Welds

The results of the nonlinear analysis are given in Table 5.6 below. The table shows the reduction of classical buckling strength for the two cases of adjacent welds.

Table 5.6: Results of Nonlinear Analysis, Adjacent Welds

H	λ^*
H/3	0.246
H/4	0.247

Both results indicate a further reduction of the buckling capacity of the conical shell. The results can be compared with those given in Figure 5.30 concerning the weld location. The weld location study was done with the upper and lower welds place at a third of the distance along the conical generator. The comparison can be seen in Table 5.7.

Table 5.7: Comparison of Results

Model	Adjacent Welds *H/3*	Upper Weld *H/3*	Lower Weld *H/3*
λ^*	0.246	0.351	0.278

It is clear that more than one circumferential weld combine to increase the loss of buckling capacity for the conical shell. The result of 0.246 is equivalent to a loss of 75% of the original buckling capacity compared with the of 72% for a weld placed in the lower portion of the conical shell.

A final study was conducted to see the approximate gain in strength due to the effect of internal pressure. In most applications the conical shell will be subjected to internal pressure, most commonly its use as a junction in silos. The investigation was done using the "Fixed" weld imperfection subject to varying degrees of internal pressure (p_r). The results can be seen in Figure 5.32.

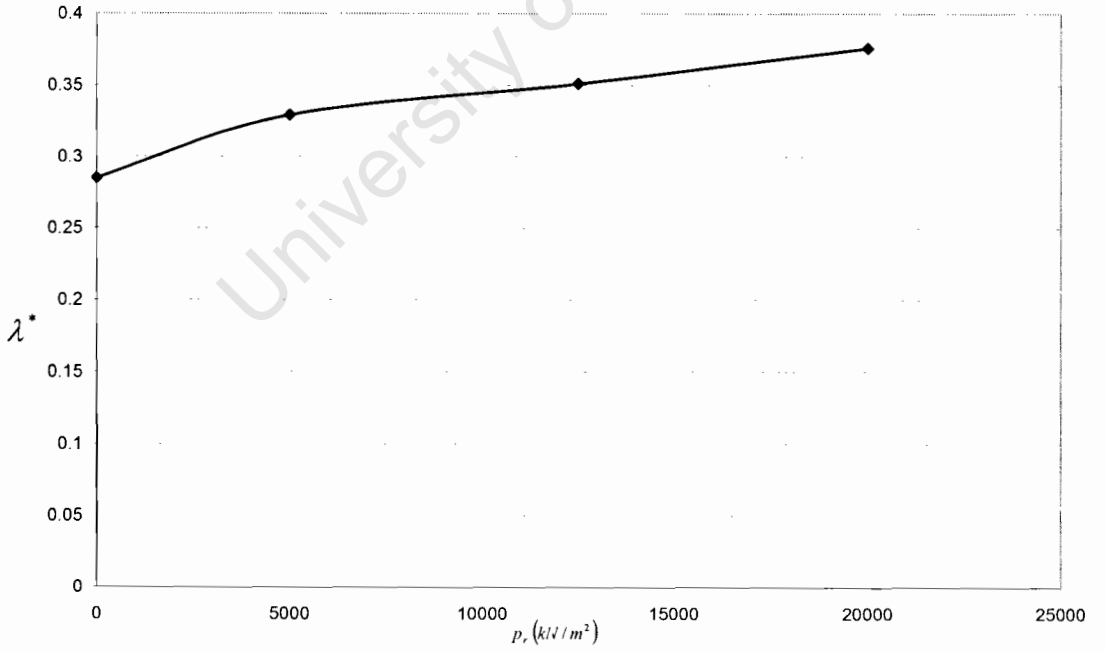

Figure 5.32: Effect of Internal Pressure, "Fixed" Weld, $w_0/t = 1.0$

It is clear that the internal pressure increases the load capacity of the conical shell under axial compression. The internal pressure places the hoop in tension which counters the compressive hoop stresses resulting from the axial load hence the increase in capacity.

The results determined from the nonlinear numerical analysis indicate that the conical shell is sensitive to the presence of imperfections. In particular the weld-induced imperfection can vastly reduce the axial carrying capacity of a conical shell. These results will be discussed along with previous researcher's results in Chapter 7.0. Prior to this discussion some experimental validation was conducted to give confidence in the modelling methodology, this is covered next in Chapter 6.0.

6 EXPERIMENTAL TESTING OF TRUNCATED CONICAL SHELLS

The results obtained in previous chapters have been based purely on numerical methods. This chapter will focus on experimental work conducted using truncated conical shells. The aim was to provide some experimental validation to the numerical results.

The experiments were conducted using four conical shells. This consisted of two control shells and two component shells containing a single circumferential weld. The fabrication, testing procedure and results will be discussed accordingly in the following sections.

6.1 Fabrication of Test Specimens

All four truncated conical shells were designed to the same measurements. Figure 6.1 outlines the dimensions adopted.

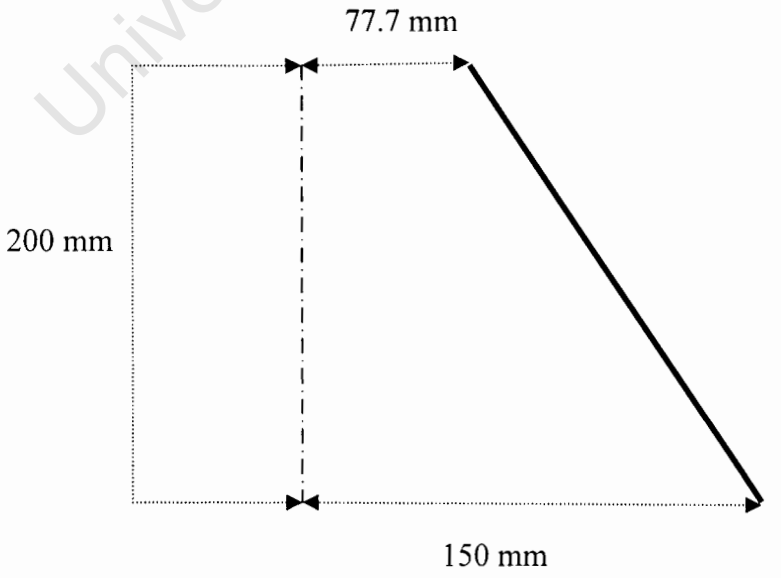

Figure 6.1: Dimensions of Truncated Conical Shell

The shells were all rolled circular conical shells and contained a single longitudinal seem weld. The shells were fabricated from electronic galvanised sheet metal, with a nominal thickness of 1.6mm. The relevant alterations will be discussed for each class of conical shell.

6.1.1 Control Specimen

The control specimens were kept unchanged for the experimental testing. The shells were measured to obtain the actual dimensions after fabrication to accurately inform the finite element model. The measured dimensions are recorded in Table 6.1 below for the control shells C1 and C2.

Table 6.1: Measured Dimensions for Control Shells

SHELL	C1		C2	
	Inner	**Outer**	**Inner**	**Outer**
Upper Diameter (mm)	152	154.7	152.97	156.17
Lower Diameter (mm)	294	297.5	295.18	298.38
Height (mm)	200.5		202.3	
Apex Angle (Degrees)	19°36'30"		19°21'54"	

The control specimens were not measured for imperfections and were treated as prefect in the numerical modelling. An initial test was conducted on the specimen C2 with no lateral restraint provided at the upper or lower edges. This led to a localised inelastic buckling failure in the upper region of the conical shell. In an attempt to avoid this, corrective measures were added to the specimen C1. The corrective measures consisted of top and bottom end plates, the dimensions are:

- Upper Plate: 200 x 200 mm mild steel plate, t = 4mm
- Lower Plate: 350 x 350 mm mild steel plate t = 4mm

These end plates will also be for the component models discussed in the next section.

6.1.2 Component Specimen

The component specimens were fabricated to obtain experimental results for an axially compressed conical shell containing a circumferential weid. The process is listed is a step by step manner.

- *Separate truncated conical shell into two halves*
  This involved the construction of a wooden chuck for the lathe. The shell was then separated into two halves on the lathe. The separation was done at a height of 100mm. Figure 6.2 illustrates the cutting procedure and Figure 6.3 illustrates the conical shell.

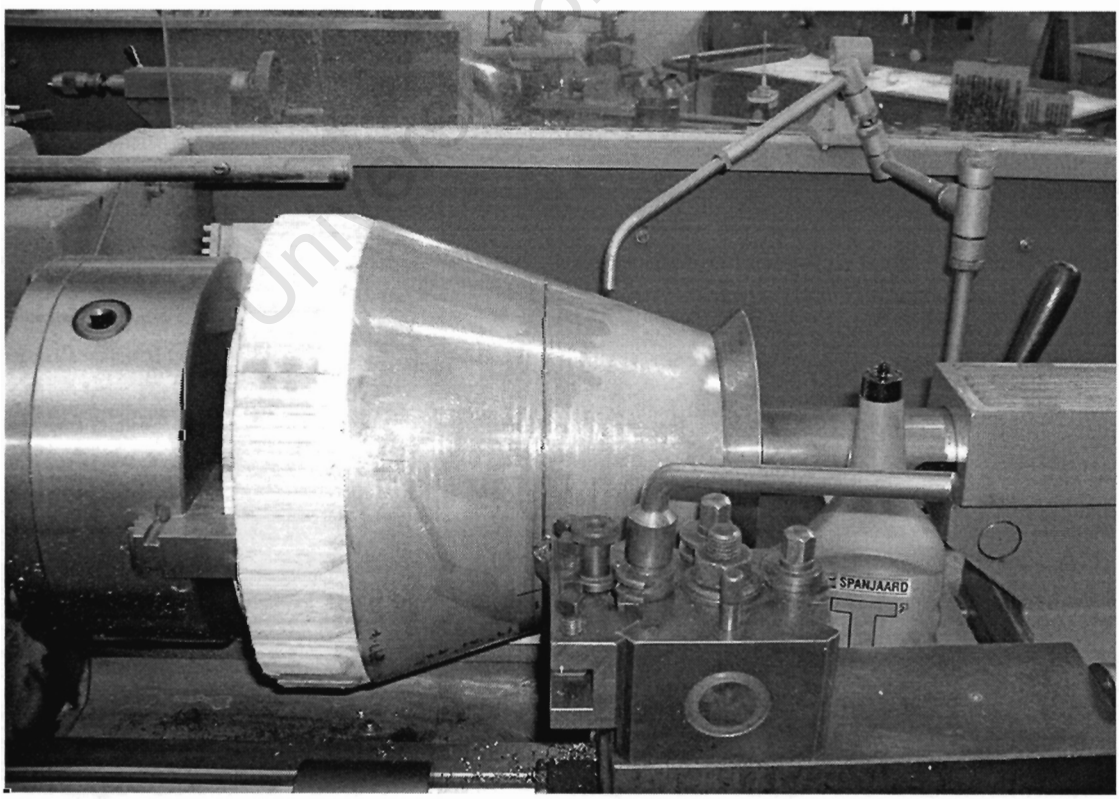

Figure 6.2: Cutting of Conical Shell on Lathe

Figure 6.3: Separated Conical Shell

- *Rejoin Conical Shell using a single Circumferential Weld*
  The two halves of the imperfect conical shells were rejoined using a single circumferential weld. The respective diameters were realigned using red markers (Figure 6.3). A butt weld was used to rejoin the two halves.

The final dimensions of the component shells were then taken for use in the finite element models. The dimensions are given in Table 6.2.

Table 6.2: Dimensions of Component Shells

SHELL	I1		I2	
	Inner	**Outer**	**Inner**	**Outer**
Upper Diameter (mm)	152	155.4	151.8	155.7
Lower Diameter (mm)	294	297.8	293.7	297.4
Height (mm)	199		199	
Apex Angle (Degrees)	19°41'11"		19°35'50"	

After the introduction of the circumferential weld, the top plate was added to provide restraint. The shell was placed on the lathe to allow profiles of the inner surface to be taken in the region of the weld.

The profiles were measured over 25 mm above and below the weld centre. The radial measurement w was taken every 1mm and a total of three profiles were taken for each component shell. The results can be seen in Figures 6.4 and 6.5 below. The figures also include the idealised geometric weld shapes from Chapter 4. The plots are for the radial deflection (w) versus the conical coordinate (s).

The figures reveal that there is an imperfection at the circumferential weld. The imperfection in this case consists of both the shrinkage deformation as well as some misfit between the two diameters. The misfit is illustrated by the sudden jump between the upper and lower sections of the conical shell in Figure 6.4, the lower being the blue portion. It must be noted that the deflection of 0.7mm corresponds to the point above the weld material and is an outlier unrepresentative of the plate middle surface. This has been corrected for in Figure 6.5.

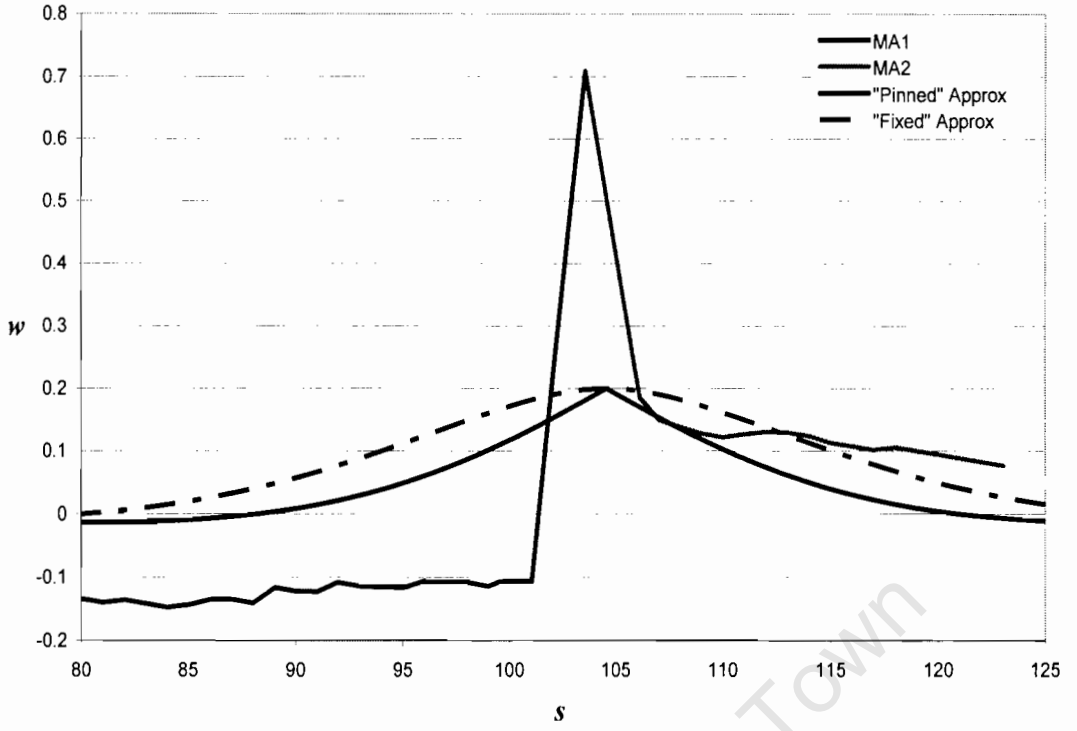

Figure 6.4: Single Weld Profile, Shell I1

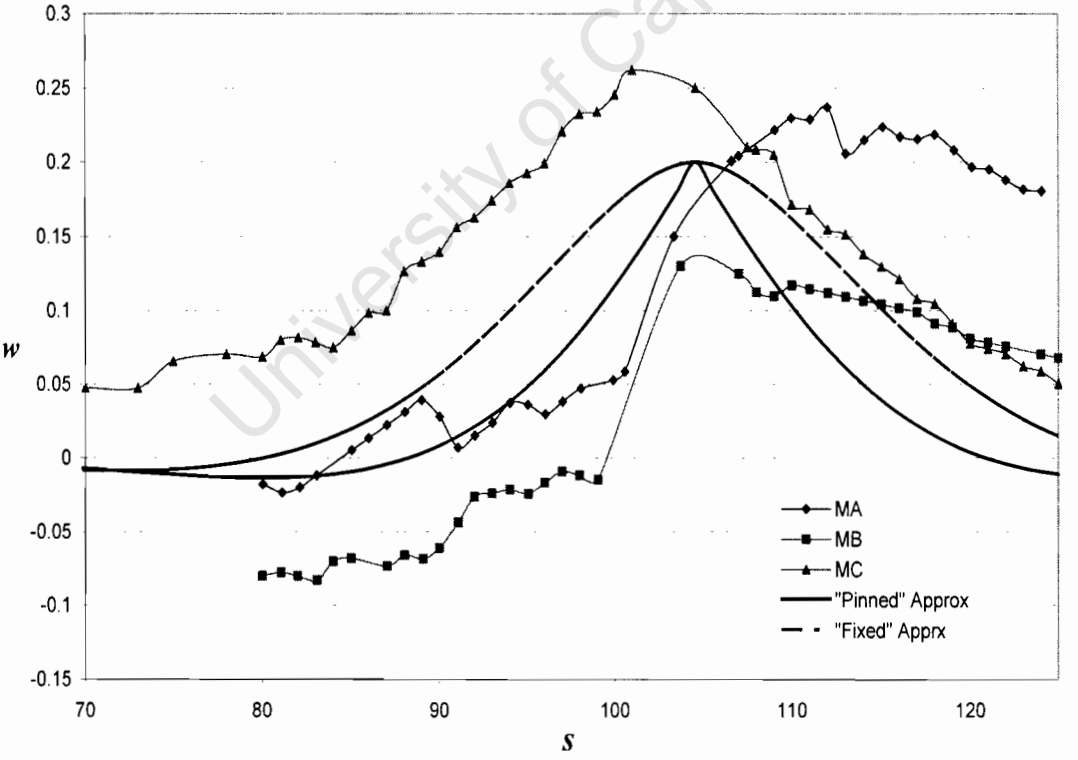

Figure 6.5: Weld Profiles, Shell I2

The imperfection profiles indicate that the average amplitude of imperfection can be taken as w_0 = 0.2 mm. This is below the norm for thin shells where the amplitude is nominally one wall thickness. This is an indication of the stiffness of the test specimens.

A good agreement does not exist between the measured profiles and the analytically derived geometric shapes. The approximate radius to thickness ratio for the experimental shells is 50. This indicates that the shell is stiff in comparison to normal thin shell theory; as such there would be more resistance to the formation of the analytical derived geometric shapes. This is supported by the low imperfection amplitude discussed previously.

6.2 Experimental Results

The experimental testing was done by applying an axial load to the truncated conical shells. The information obtained from the testing procedure was:

- The Final Buckling Load
- A Plot of Axial Load Versus the Vertical Displacement
- The Buckling Mode

The apparatus used is listed here for reference. The main equipment is:

- 1 x Amsler Axial Compression Tester
- 1 x 50mm Dial Gauge
- 2 x 10mm Dial Gauge
- 3 x Magnetic Dial Gauge Stands

The testing procedure can be listed in a few short steps as well:

- Insert the test specimen centrally between the compression plinths
- Apply the load incrementally, taking dial gauge readings every 10 kN until the point of bifurcation.
- Take photos of the final buckled shape of the conical shell

The control shell C2 which did not have the upper and lower end plates was tested initially. The test made no use of dial gauges and only measured the approximate final axial buckling load. The setup can be seen in Figure 6.6 below and the final buckled shape can be seen in Figure 6.7.

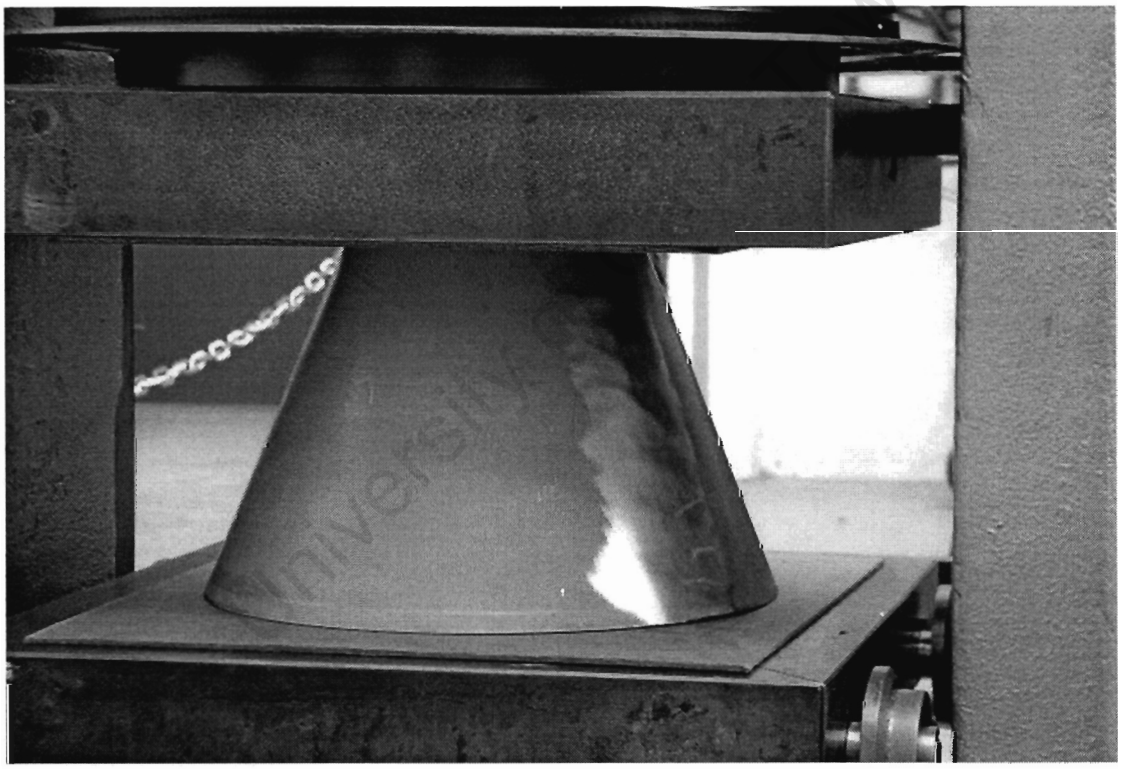

Figure 6.6: C2 in the Amsler Test Apparatus

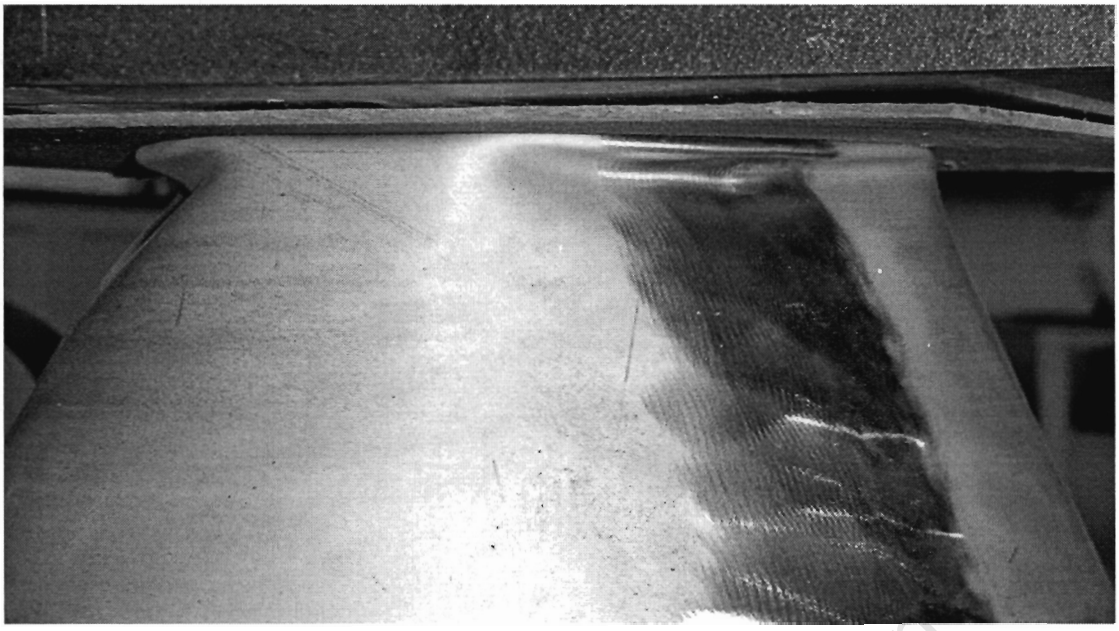

Figure 6.7: Buckled Shape Shell C2

Shell C2 had no lateral restraint on the upper or lower edge. The failure was thus a progressive crumpling/buckling of the upper region. The final shape consisted of three waves in the circumferential direction and one wave in the meridional direction. This progressive failure prompted the use of the end pates in all other shells as a means of stiffening the edge zones.

The tests were then conducted on the shells C1, I1 and I2. Figure 6.8 shows the initial setup of the respective dial gauges prior to the application of axial load.

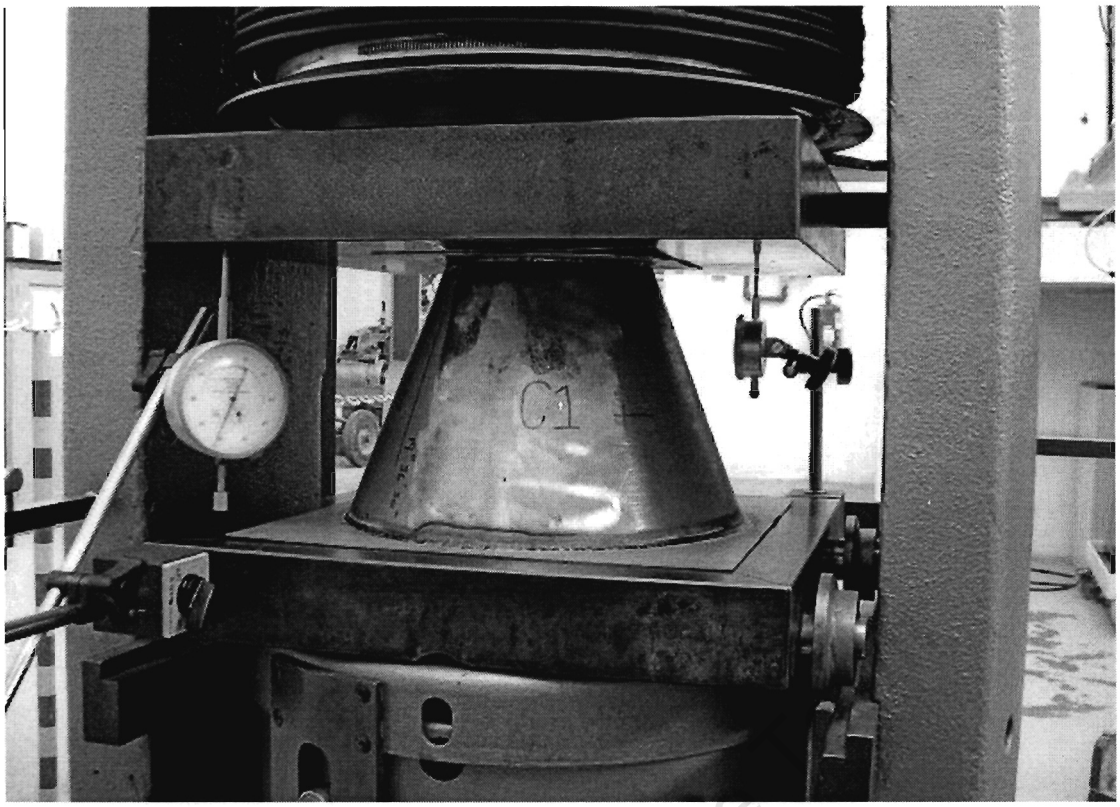

Figure 6.8: Experimental Setup Shell C1

The results of the tests are given in Figure 6.9 which represents the vertical deflection of the shells versus the applied load.

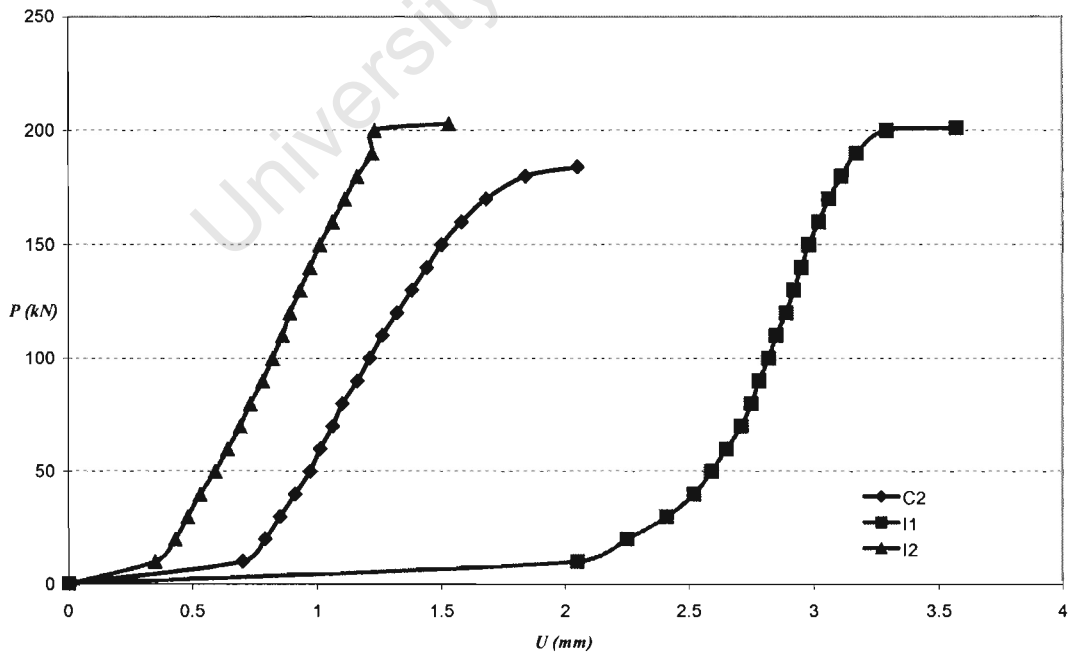

Figure 6.9: Load vs. Deflection Curves Test Shells C1, I1 and I2

Figure 6.8 indicates that there was a certain amount of slippage in the initial stages of load application. It is also visible that the circumferential weld does not reduce the buckling capacity of the test specimens. The final buckling loads are given in Table 6.3.

Table 6.3: Final Buckling Loads C1, C2, I1 and I2

Test Shell	Buckling Load P (kN)
C1	184
C2	85
I1	201
I2	203

The results indicate that apart from shell C2 which had no lateral restraint the buckling loads are within 10%. The imperfect shells in the test results achieve a higher buckling capacity than the control specimens. The buckling mode is however consistent for the three tests C1, I1 and I2, with a predominantly axisymmetric dimple forming next to the upper edge/support of all three cones. The buckling modes are illustrated in the figures below for each of the test specimens.

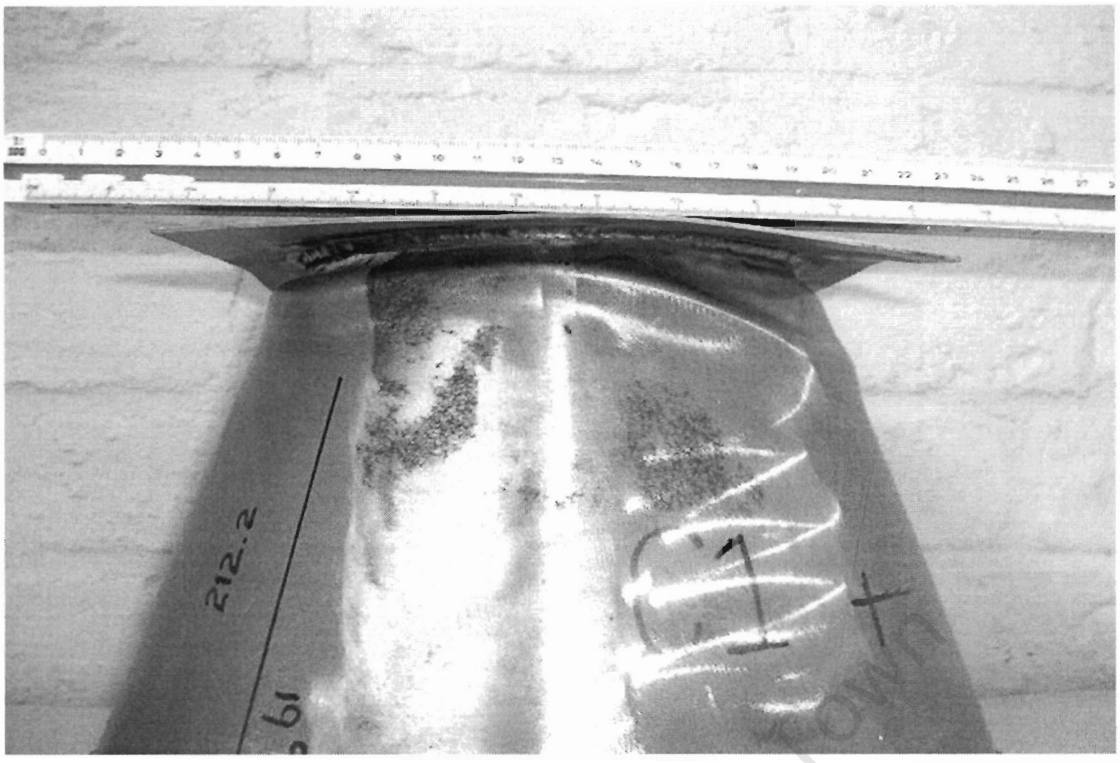

Figure 6.10: Buckling Mode; C1

Figure 6.11: Buckling Mode Shell C1

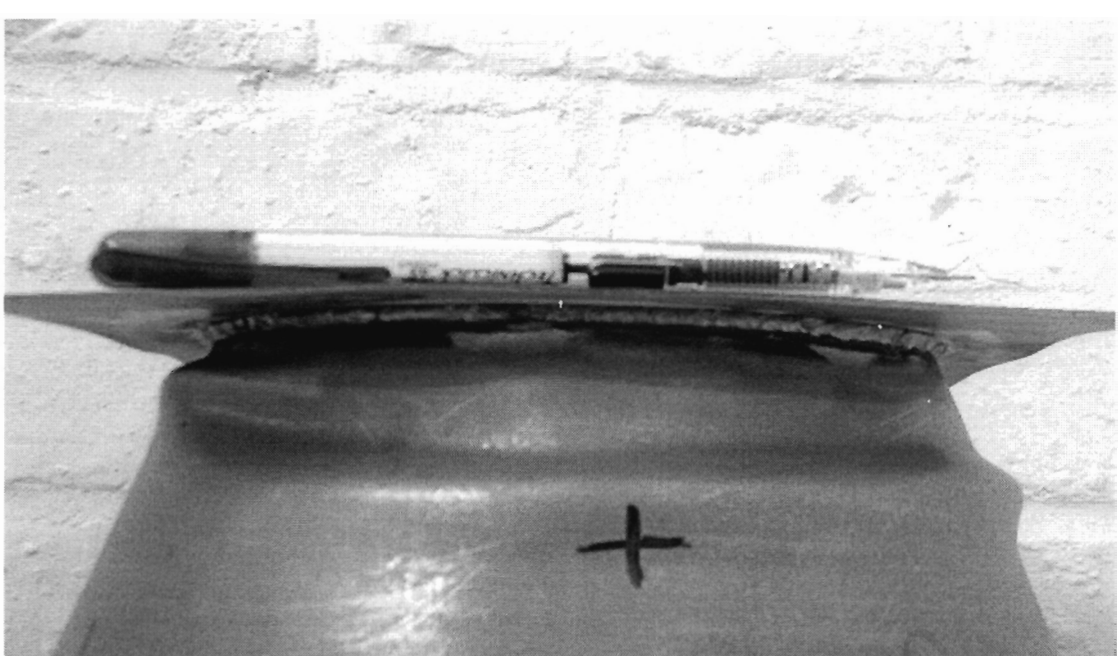

Figure 6.12: Buckling Mode Shell I1

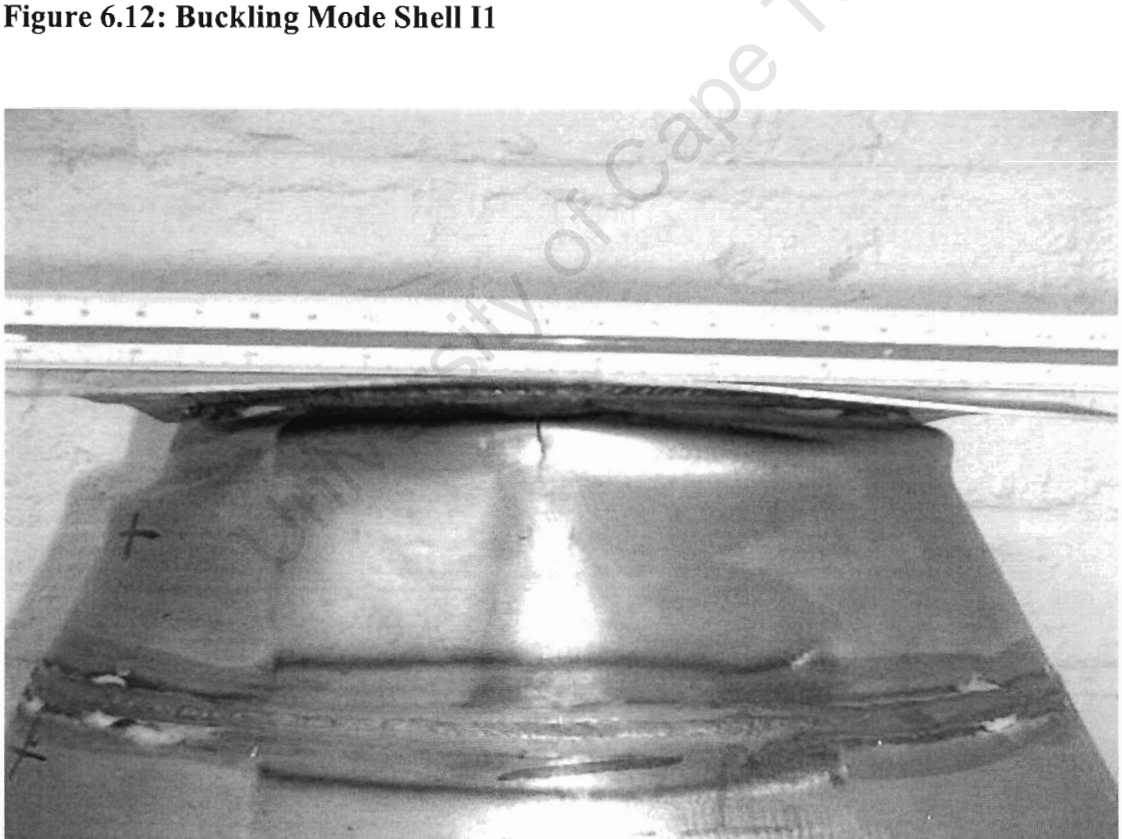

Figure 6.13: Buckling Mode Shell I1

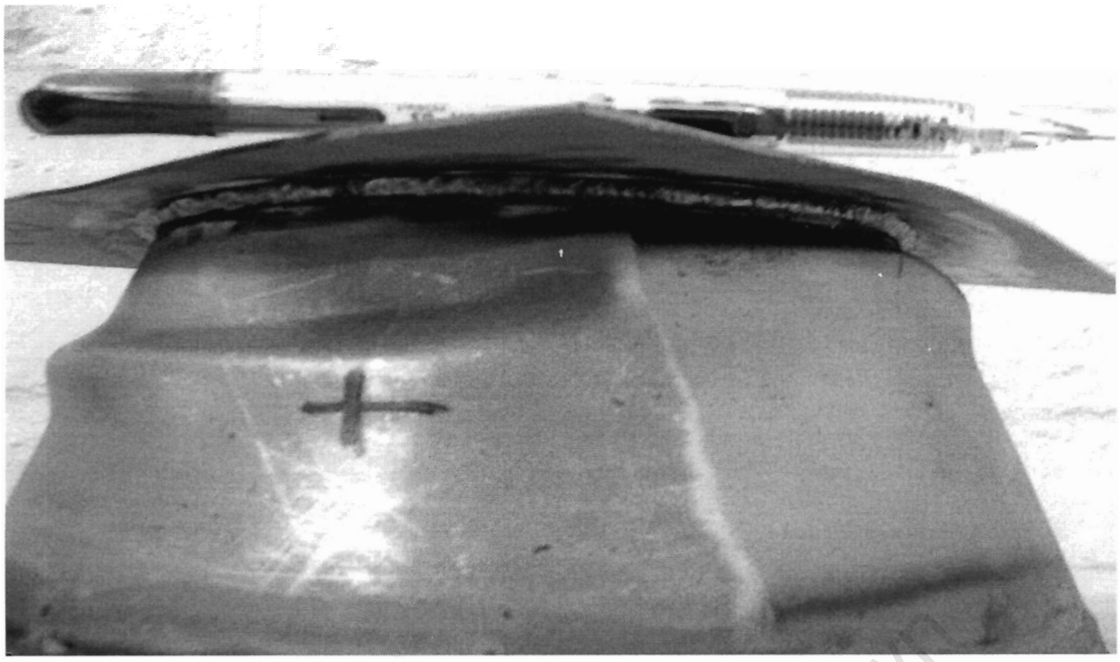

Figure 6.14: Buckling Mode Shell I1

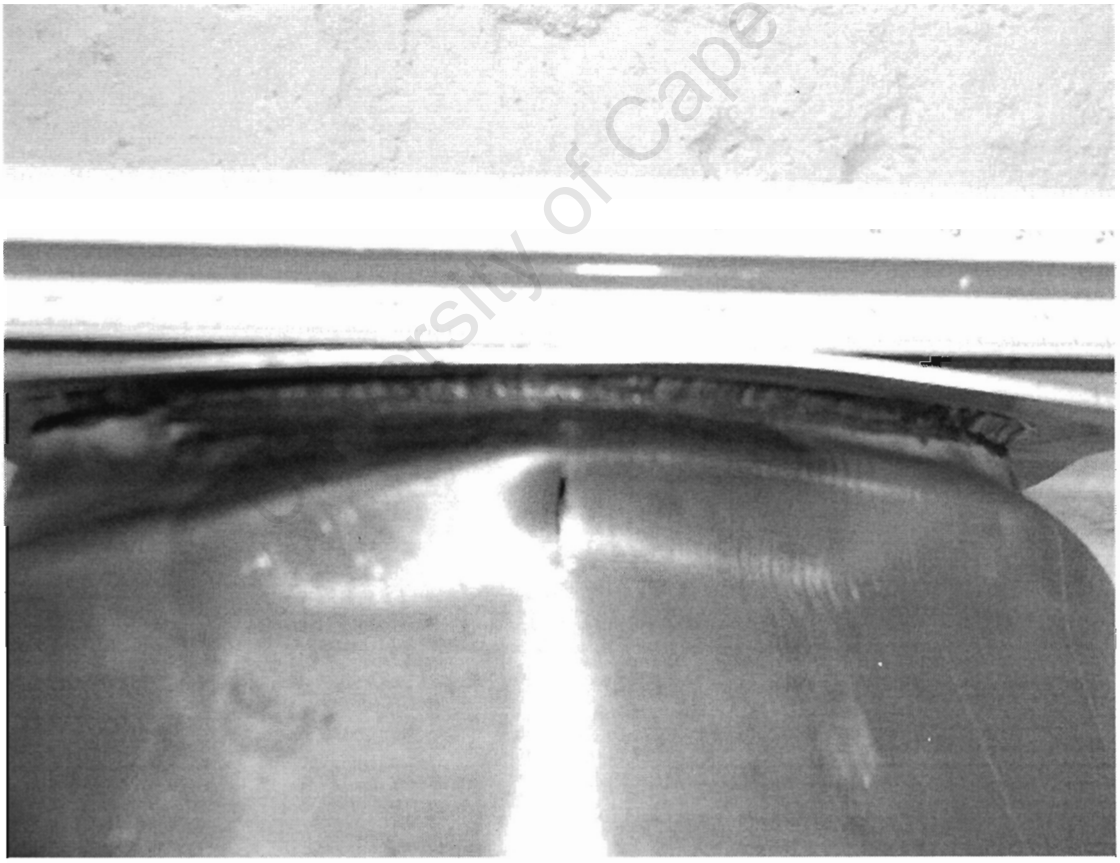

Figure 6.15: Buckling Mode Shell I2

Figure 6.16: Buckling Mode Shell I2

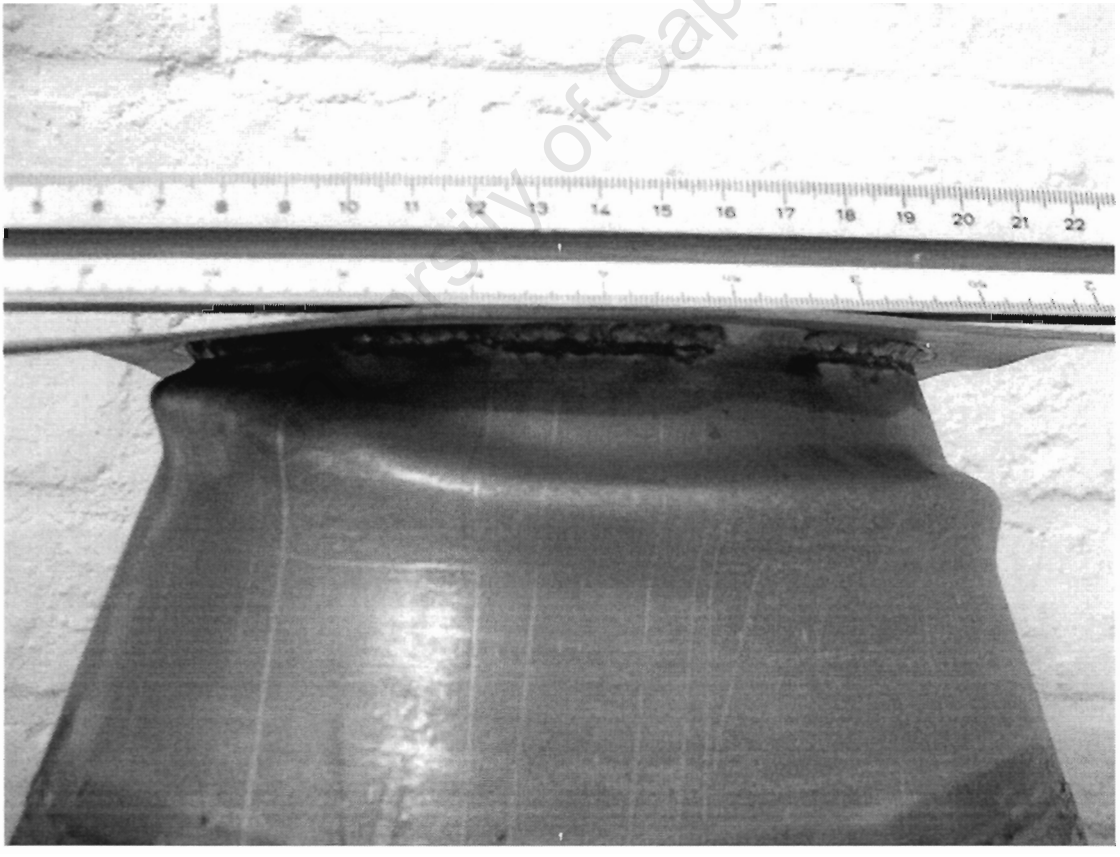

Figure 6.17: Buckling Mode Shell I2

6.3 Finite Element Modelling of Experimental Models

The experimental results will be used as a means to validate the finite element modelling. This section will focus on the development of the finite element models. The results of the finite element analysis will then be related to the experimental values obtained.

The experimental buckle was predominantly axisymmetric and axisymmetric models were used to predict the buckling load. Three dimensional models were also made, firstly to ensure the use of the S4R & S4 element is adequate for the nonlinear inelastic buckling and secondly in the case of the conical analysis the need to pick up asymmetric buckling modes. Thus it is important that there is a match between the axisymmetric, 3-D and experimental models.

The axisymmetric model comprised SAX3 elements and the 3-D model comprised S4R elements, both of which have been discussed in Chapter 3. The axisymmetric model was used to determine the classical linear elastic buckling strength for the case of the shell dimensions C1. The boundary conditions were taken to be fully fixed or pinned. The results are given in Table 6.4.

Table 6.4: Classical Buckling Load from Axisymmetric Models

Support Condition	P_{cl} (kN)
Fully Fixed	1756.64
Pinned	17158.9

To determine the realistic behaviour of the shells a nonlinear analysis needed to be performed. The experimental results indicated that the buckling was due to the inelastic behaviour of the material. Thus the material and geometric nonlinearity had to be accounted for. This was done using the STATIC RIKS step in ABAQUS, this has been discussed in Chapter 2.

The shells were made up off Electronic Galvanised sheet metal. The typical values for mild steel will be adopted for the analysis. The properties are given as:

$E = 200GPa$

$v = 0.3$

$\sigma_y = 300MPa$

$t = 1.6mm$

The finite element models were constructed using the measurements listed in Tables 6.1 and 6.2. The axisymmetric model made use of a mesh size of 0.001m while the 3-D model was meshed using 250 elements on the upper and lower edges. In the case of the imperfect shell the mesh in the region of the geometric weld imperfection in the 3-D model was taken as 0.00277m. This corresponds to the parameter used by Rotter and Teng (1989) and defined in Chapter 5. This is given as:

$$0.25\sqrt{(Rt)} = 0.25\sqrt{(0.077)(0.0016)} \approx 0.00277m$$

The linear elastic buckling loads from Table 6.4 where applied in the STATIC RIKS step. The results of the finite element analysis are recorded in Table 6.5, for the experimental model C1.

Table 6.5: Finite Element Analysis Model C1

Model	**Axisymmetric**		**3-Dimensional**	
Support Condition	**Fixed**	**Pinned**	**Fixed**	**Pinned**
Buckling Load (kN)	232	213	235	217

The models in Table 6.5 show good agreement with the results obtained. For the imperfect models it was decided that the fully fixed support condition would be used as its buckling mode is more realistic.

The analysis of the imperfect models was done using the geometric weld imperfection shapes. The imperfection amplitude was taken to be 0.2mm from the profile measurements in the previous section. Both the "Pinned" and "Fixed" geometric shapes were used. The results are shown in Table 6.6 for both the models I1 and I2. The analysis was conducted on the 3-D models only.

Table 6.6: Finite Element Analysis of Imperfect Models I1 and I2

	"Fixed" Geometric Weld Shape	"Pinned" Geometric Weld Shape
I1	236	225
I2	236	236

There appears to be little difference between the buckling loads for the 4 imperfect models. All three models show consistent behaviour in terms of the buckling modes. All the buckling modes occur in the upper region of the conical shell adjacent to the fixed support condition on the upper edge. The boundary condition is thus introducing high bending moments increasing the local stress state and resulting in inelastic buckling under axial compression. The respective buckling modes for the finite element models C1, I1 and I2 can be seen in the figures below.

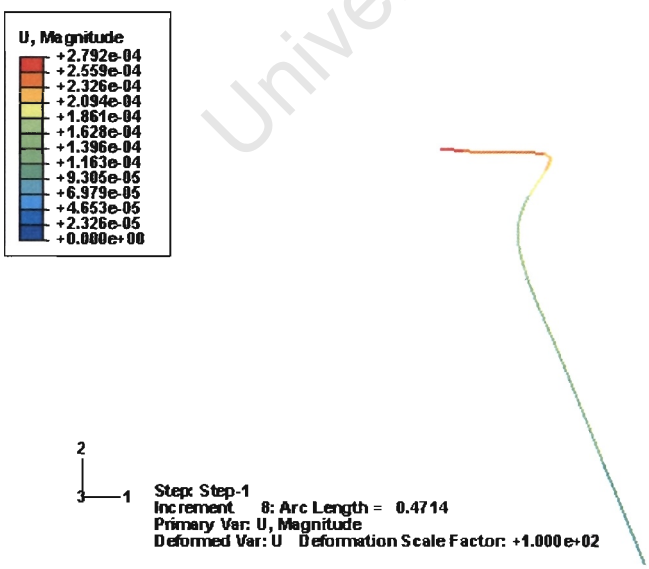

Figure 6.18: Axisymmetric Buckling Mode Shell C1

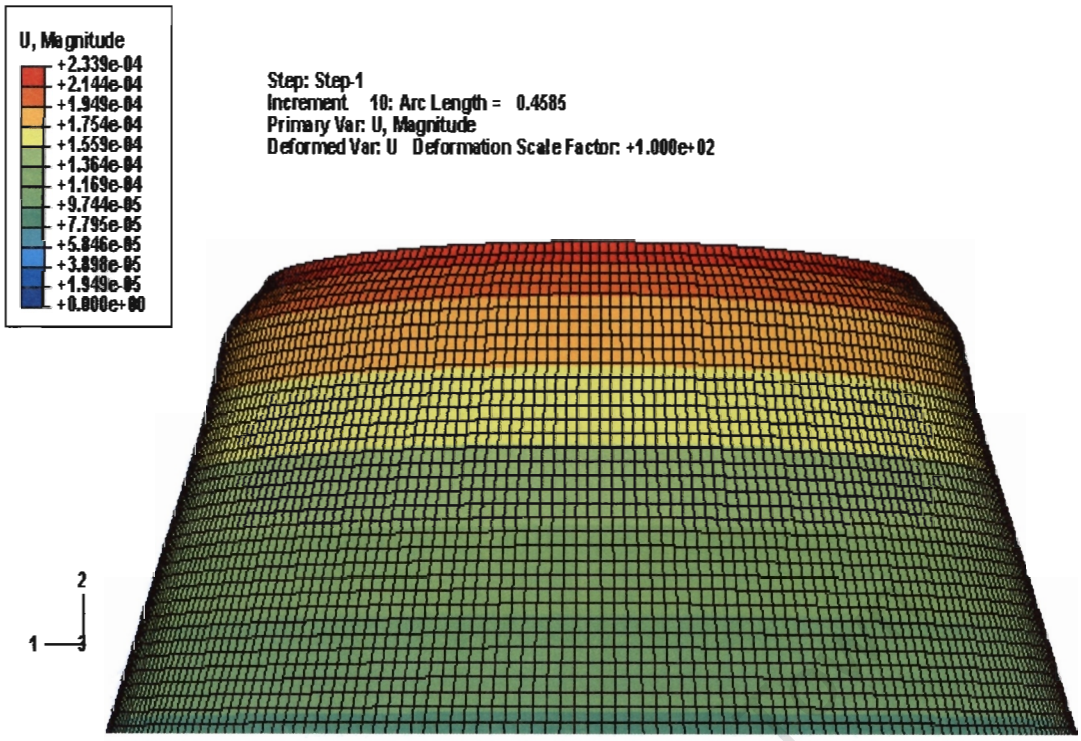

Figure 6.19: 3-D Buckling Mode Shell C1

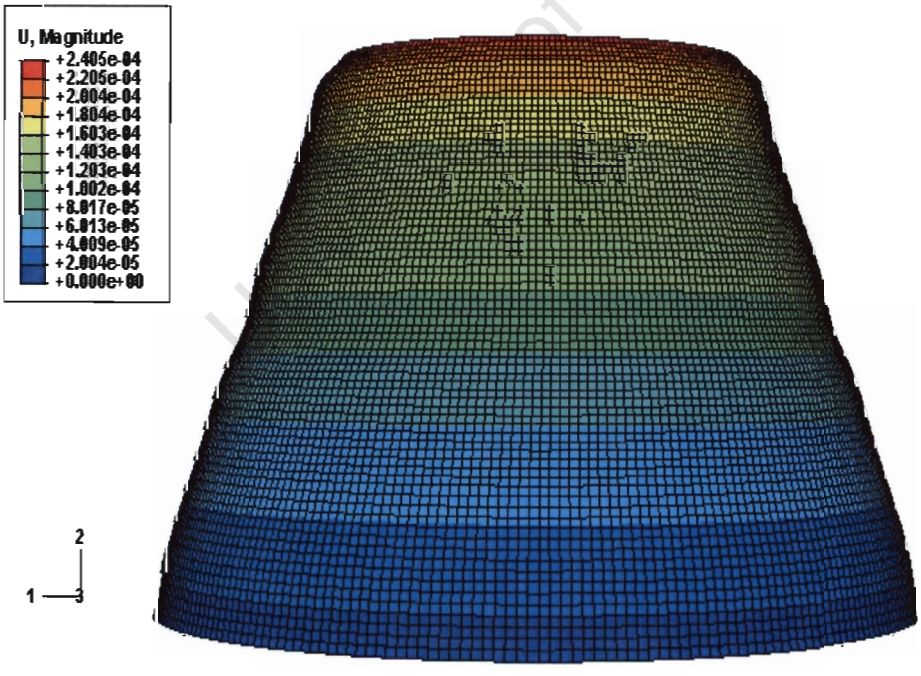

Figure 6.20: Buckling Mode Shell I1, "Fixed" Weld Shape

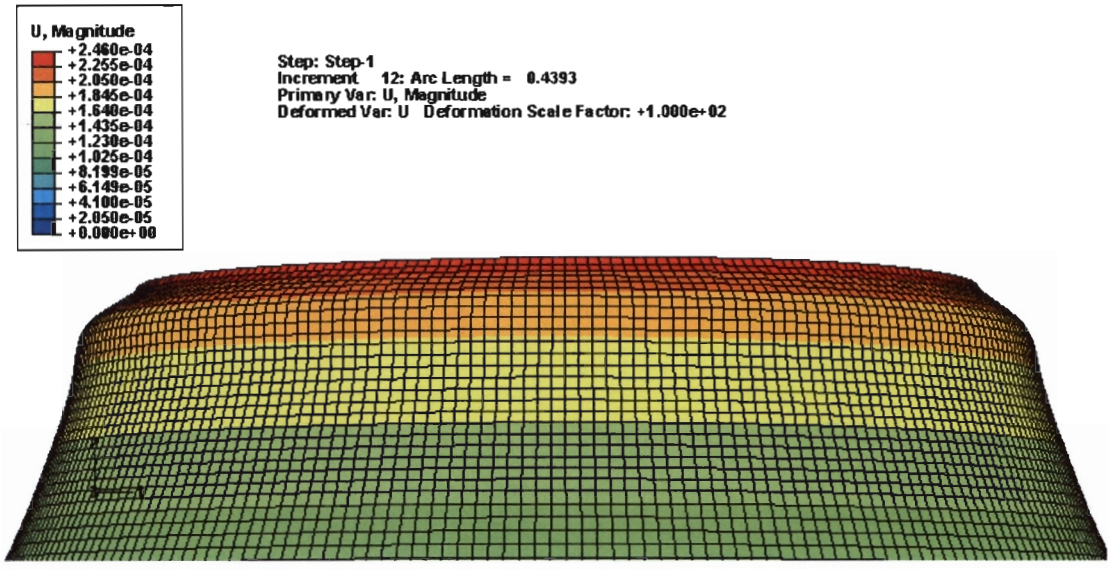

Figure 6.21: Buckling Mode Shell I2, "Fixed" Weld Imperfection

6.4 Comparison of Experimental and Finite Element Results

The respective experimental and finite element analysis for the conical shell models has been dealt with in the two previous sections. The purpose of this section is to draw conclusions based on the comparison of the respective results.

The comparison is primarily concerned with obtaining good agreement between the experimental buckling loads and the numerical buckling loads. The second comparison is to match the load deflection curves as well as the buckling modes.

In terms of the peak buckling load there is good agreement. The comparison will be drawn using the finite element models with fixed support conditions only. This is due to the actual buckling modes shown in Figure 6.10 – Figure 6.17, where there is very little displacement of the shell area at the supports which is more consistent with a fully fixed type boundary condition.

Table 6.7 shows the experimental buckling loads for the three models versus the finite element buckling loads. The table gives an indication of the percentage error between the respective buckling loads.

Table 6.7: Comparison of Actual and Numerical Buckling Loads

Model	Experimental Buckling Load P (kN)	Numerical Buckling Load P (kN)	Percentage of Experimental Buckling Load
C1	184	235	27.7%
I1	201	236	17.4%
I2	203	236	16.2%

Figures 6.22 and 6.23 give the load deflection curves for the experimental models C1 and I2 versus the finite element models.

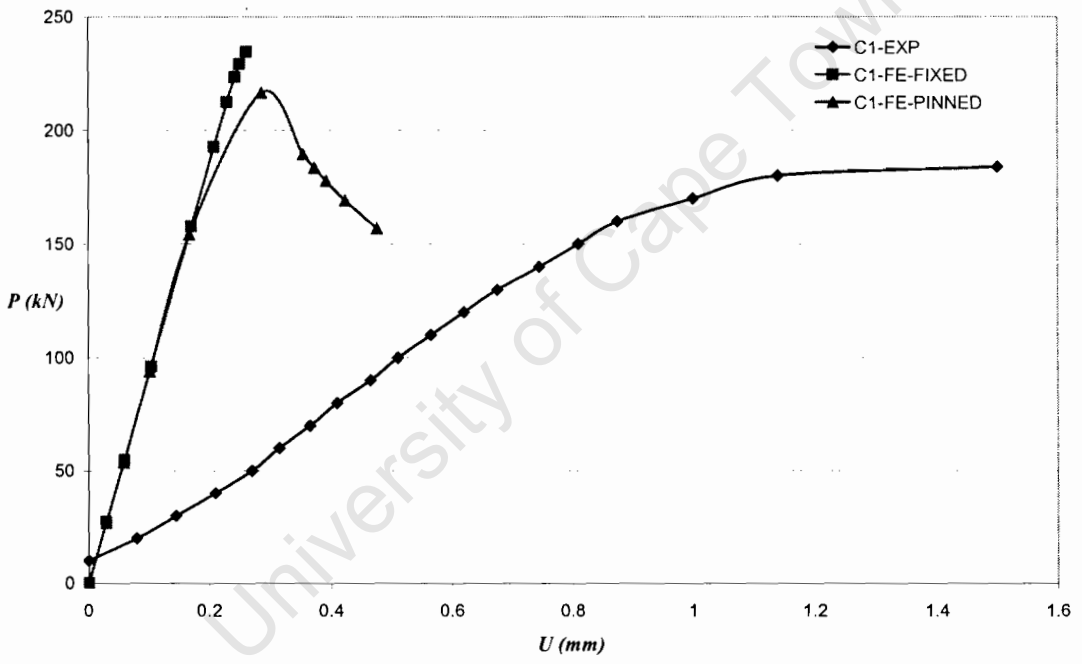

Figure 6.22: Load Deflection Curve – C1

The finite element models given in Figure 6.22 are for the case of pinned and fully fixed boundary conditions. The finite element results in Figure 6.23 are for the case of a fully fixed conical shell containing either the "Pinned" or "Fixed" geometric imperfections. It is clear that the imperfection has no effect on the buckling load, which is consistent with the observed experimental behaviour.

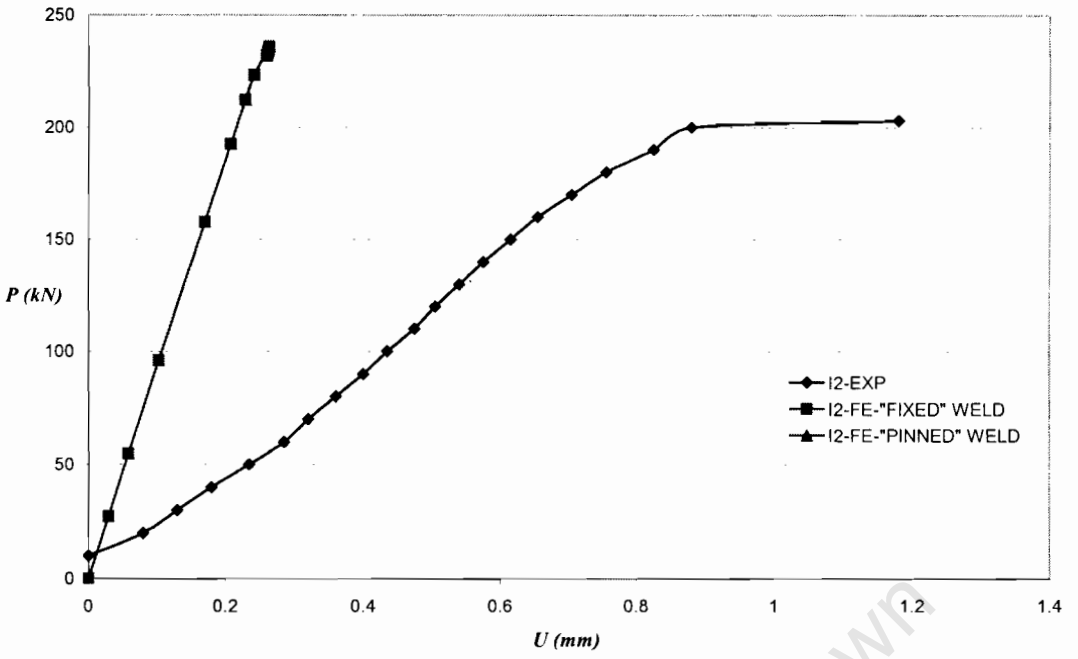

Figure 6.23: Load Deflection Curve – I2

The load deflection curves indicate that the finite element models display a higher stiffness than the actual experimental models. There is some good agreement in terms of the buckling modes, with all the numerical and experimental models showing an axisymmetric buckle in the upper portion of the conical shells.

The differences in the behaviour can be attributed to inherent imperfections with in the experimental models. The experimental buckling modes in the model C1 shows the formation of localised circumferential dimples which deviate from the axisymmetric modes. The shells I1 and I2 both have the case where the axisymmetric dimple is not on the same line of latitude as indicated in Figure 6.17. These can be results of:

- Imperfections in the circumferential radius of the conical shell. The radius is larger in the region of the seam weld.
- Imperfections due to the longitudinal weld.
- Imperfections due to the attachment of the end plates

does show the formation of dimples in the circumferential direction in Figure 6.10. The error of 22% is a conservative approach as in reality the welded end plates do not provide a fully fixed condition but some arbitrary stiffness. The difference with the numerical model having pinned supports is 14% which is relatively small in comparison to results of imperfect conical shells in the literature review. This is acceptable for the case of longitudinal imperfections due to the seam weld.

The result is that the use of a numerical model to determine the final buckling load is in relatively good agreement with the experimental results. The use of the S4 and S4R element provides reasonable approximations of the final buckling load and mode. The use of the finite element method in the classical linear buckling behaviour of spherical shells in Chapter 3 and the experimental validation indicates that the numerical modelling provides realistic and reproducible results. The experimental models did not buckle in the region of the weld-induced imperfection; this is due to the low radius to thickness ratio (much stiffer shell) which did not allow the formation of a significant imperfection in the axisymmetric direction. The numerical models also did not indicate any buckling in the vicinity of the weld-induced imperfection which is consistent. The result is greater confidence in the numerical analysis to predict the final buckling load of conical shells. This is also indicated in the literature review on the cylindrical shell studies where the experimental models obtained a good agreement between the idealised and experimental weld shapes as well as the actual and finite element methods buckling loads.

7 DISCUSSION

Chapter 5 dealt with the analysis of the spherical and conical shell containing an imperfection in the form of a circumferential weld. The analysis was conducted using the finite element method to determine the buckling capacity. The aim of this chapter is to discuss the results in terms of the findings presented in the literature review. The discussion of the spherical and conical shells will again be dealt with in two distinct sections.

7.1 Spherical Shell

The results for the imperfect spherical shell have been given in Chapter 5.1. This section will deal with a basic comparison of results recorded in the literature review.

The reduction of the buckling capacity in the spherical shell due to weld imperfections is significant. The case of a circumferential weld at a meridional angle of 20 degrees and an imperfection amplitude of 2.0t lead to a decrease of roughly 55% of the classical buckling capacity.

This can readily compared to Hutchinson's results recorded in Chapter 1.2.3. Hutchinson (1970) investigated the effect of general imperfections in the form of the lowest buckling mode. His results for a spherical shell under uniform external pressure indicate that a minimum reduction of 60% and a maximum reduction of 70% can be obtained for an imperfection amplitude of 1.0t. These results form a more critical lower bound solution in comparison to the weld imperfection. The full effect of the general imperfections can be seen in Figure 1.12.

Having drawn the conclusion that the general imperfection in the form of the lowest buckling mode results in a greater reduction of buckling capacity, it is important to review the results in terms of other findings on weld imperfections.

Grunitz work on shallow spherical caps provides a basis with which to review the buckling behaviour. In general Grunitz's results reflect the basic finding that the meridional location of the weld imperfection does influence the buckling behaviour. It is clear that the closer the circumferential weld to the apex of the spherical shell the greater the reduction of buckling strength. The comparison of results will be done using the case of a fully fixed boundary condition.

Grunitz analysis is related to a spherical shell with a radius to thickness ratio of 1667. Figure 5.9 indicates that for a corresponding radius to thickness ratio the current analysis results in a reduction of approximately 53%. Grunitz obtains a value of 55% for a weld at 20 degrees which is in fairly good agreement. It should however be noted that some fundamental differences occur between the two analyses:

- Grunitz models included the effect of residual stresses as prestressed elements were used to define the weld. As a result the actual imperfection amplitude is not given by Grunitz.
- The analysis was a conducted on a shallow spherical cap whereas the models in this dissertation were hemispherical. This does not create an inherent problem as it was found that the support location had little effect on the buckling capacity, this is given in Figure 5.12.

7.2 Conical Shell

The literature review covered previous research on imperfect conical shells by El Damatty and Chrysanthopoulos. The findings of Chapter 5.2 will be discussed in the light of their corresponding findings for imperfect conical shells.

El Damatty found that the inelastic buckling of an imperfect truncated conical shell resulted in a 30% reduction in the classical buckling load. The conical shell contained an axisymmetric imperfection given by Equation 1.55 and was analysed for the case where the apex angle was 45 degrees. The reduction of the buckling capacity in this case is not as significant as the effect of a single circumferential weld.

The findings of this thesis indicate that for a conical shell containing a circumferential weld the reduction of the classical buckling strength can be as much as 70%. By comparison Chrysanthopoulos results for an axial compressed conical shell indicate a larger loss of capacity. He drew a comparison between the ECCS knockdown factors and a conical shell containing a general axisymmetric imperfection. Chrysanthopoulos indicated that for an imperfection amplitude of $1.0t$ the ECCS knockdown factor indicates a reduction in the classical buckling load of 73.5%. His study of a conical shell containing an axisymmetric imperfection equivalent to the lowest buckling mode resulted in a equivalent reduction to the ECCS for a imperfection amplitude of $0.48t$, as given by Figure 1.15. His analysis thus indicates a reduction in the classical buckling load of approximately 78% for an axisymmetric imperfection equivalent to one wall thickness.

In both the previous cases the ECCS and Chrysanthopoulos indicate a larger reduction of the classical buckling strength for an imperfection amplitude of $1.0t$. The effect of a "Fixed" geometric weld imperfection of the same amplitude is only a 71.5% reduction. The effect of adjacent welds is more critical and can result in a 75.4% reduction, but this is still marginally higher than Chrysanthopoulos results.

The effect of the respective weld shapes is not as critical as indicated by the research into cylindrical shells. Rotter and Teng (1989) found that the difference between their analytical geometric imperfections was of the order of 5% for weld imperfection amplitude of $1.0t$. In the case of the current conical shells this difference is in the order of 2%. The buckling in the circumferential direction observed in the cylindrical shell is also only consistent with the "Fixed" weld imperfection. The "Pinned" weld resulted in a progressive failure due to the nonlinear material behaviour.

The results for a "Fixed" weld show good agreement with those obtained for the cylindrical shell by Rotter and Teng (1989). They found that the cylinder with the corresponding shape function buckled with 18 waves in the circumferential direction. The current analysis revealed the occurrence of 17 circumferential waves at the point of bifurcation.

The results on the effect of imperfections in the conical and spherical shell should provide a better understanding in the area of design. It is important to understand that the construction does introduce imperfections, in this case the weld imperfection, which reduces the classical buckling load. The aim of these results is to provide information to quantify the effect of the imperfection. It indicates the effect of the circumferential weld on the conical and spherical shell under defined loading conditions.

The final conclusions for the parametric study and the recommendations will be covered in Chapter 8.0

8 CONCLUSIONS AND RECOMENDATIONS

Chapter 7.0 focussed on the comparison of current findings with previous researchers results. It indicated that the results are within the range set out by previous researchers, and there is a good similarity between the conical and cylindrical shells. The current chapter will serve as a summary of the numerical analysis conducted in Chapter 5.0. The trends found in the parametric study will be highlighted. In order to gain a complete understanding, the aims of this thesis will be summarised along with the methodology for the investigation.

The aim of this dissertation was to investigate the effect of a weld-induced imperfection on the classical buckling loads for the conical and spherical shells. The approach was to consider the shape of the weld-induced imperfection as a deviation from the perfect shell middle surface. The effect of residual stresses was ignored as it was found in cylindrical shells that they only account for a 10% deviation of the classical buckling load. Due to the lack of measured imperfection data from the spherical and conical shells, an analytical weld-induced shape function was deduced. This method was initially adopted for the cylindrical shell and the analytical shape functions showed adequate agreement with the measured shape of the weld-induced imperfections.

8.1 Conclusions

The conclusions for the investigation will be highlighted for the spherical and conical shell in the following sections.

8.1.1 Spherical Shell

The investigation was conducted for a spherical shell under uniform external pressure, fabricated from mild steel. The conclusions for the parametric study are listed below.

- The investigation of the "Fixed" and "Pinned" weld shapes, with a varying imperfection amplitude revealed the following:
    - There is a decrease in the external classical buckling pressure load with a corresponding increase in the imperfection amplitude.
    - The "Pinned" weld shape produced a set of lower bound results and the reduction was a function of a nonlinear material response.

- The closer the weld is to the apex of the spherical shell the more the reduction in the classical buckling load.

- The effect of the radius to thickness ratio indicates that there is a reduction of the classical buckling load with an increase in the R/t ratio.

- Adjacent welds in a spherical shell were found to further reduce the buckling load from the case of a single weld-induced imperfection.

- The location of the boundary had little effect on the buckling load. This is because the weld shape accounts for the reduction in buckling capacity.

8.1.2 Conical Shell

A similar parametric study was conducted for the conical shell. The conclusions can be drawn for the case of an axially compressed mild steel conical shell.

- There is a reduction in the classical buckling load with an increase in the imperfection amplitude. The conical shell can have a reduction in the classical buckling load of 73%.

- The "Fixed" weld buckled elastically with 17 waves forming in the circumferential direction along the centre of the imperfection. The "Pinned" weld showed a progressive failure as the imperfection caused material yield at the weld centre.

- The effect of the apex angle indicates that the smaller the apex angles of a conical shell, the greater the reduction in the classical buckling axial load.

- The "Pinned" weld shape becomes more critical the lower it occurs on the conical generator. This is due to the nonlinear interaction of the boundary and the weld imperfection, the increased stresses result in yielding of the material.

- Adjacent welds further reduce the buckling capacity by approximately 75% and are more critical than a shell containing a single weld.

- Internal pressurization results in a strengthening effect as it places the circumference in tension, this needs to be overcome before buckling can occur.

8.2 Future Recommendations

Recommendations will be given for design as well as future research.

8.2.1 Design

The findings illustrated in Chapter 5.0 can be used to aid the design of mild steel conical and spherical shells. Current design regarding buckling behaviour is summarised in the ECCS, here approximate knockdown factors have been used for the design buckling load. The current results can supplement the recommendations in the ECCS by illustrating the effect of a weld-induced imperfection.

The results can give an idea of the actual buckling load as a factor of the classically derived buckling load for a given imperfection amplitude. In work on cylindrical shells it was found that the average imperfection amplitude corresponded to a single wall thickness. The following recommendations can be made for the spherical and conical shell:

- The design buckling load for a conical shell under axial compression should be 27% of the classical buckling load.

- The designer should be aware that welds can interact and further reduce the axial load capacity of the conical shell.

- The effect of internal pressure can provide extra strength which should be taken into account, however the critical case still applies when the internal pressure loading is no longer there.

- The spherical shell should be designed for an external uniform load of 50% of the classical buckling load.

- Again the effect of increased weld numbers will further reduce the buckling capacity.

8.2.2 Future Research

The current sets of results represent a small and limited scope of the problem of weld imperfections. The literature review on weld imperfections in cylindrical shells showed the extent of development that is possible in this field of study. The following steps are recommended to improve our knowledge and understanding in this area.

The analysis was all conducted using the analytically derived weld shapes. The research on cylindrical shells has indicated that numerous shape functions have been derived by different authors, many of these are obtained from actual measured data. As such there is a need to make detailed measurements of welds to determine the geometric shape and the range over which it acts. This can be achieved in two ways:

- Measurement of industrial conical and spherical shells on location. This detailed measurement of an actually built structure will provide invaluable data.

- The use of experimental models

The experimental procedure should focus on establishing realistic models. The conical shell lends itself to the testing procedure as it is easier to construct and load. In terms of experimental work attention should be paid to the radius to thickness ratios. This range should be in the region of 1000. The current experimental models had an upper radius to thickness ratio in the region of 50, as such they were stiff and did not allow the formation of the geometric weld imperfections. The buckling mode was also confined to the upper regions of the conical shell and could be the result of a flexural response rather than pure buckling.

The current analysis has been conducted for two distinct load cases. The spherical shell was subjected to external uniform pressure and the conical shell was subjected to an axial load. In reality structures have to account for different loading configurations such as internal and external uniform pressure, hydrostatic loading, point loads and line loads. Future finite element analysis can take account of different loading configurations.

The current analysis took account purely of the weld-induced shape imperfection due to shrinkage in the region of the weld. The presence of residual stresses does occur in actual structures and contrasting results have been highlighted in the literature review. The quantification of the residual stress state is a challenging problem which can be approached through future research into this topic.

The recommendations above all relate to the areas of focus for future research into this topic. The experimental measurement of actual conical and spherical shells should provide data with which to fine tune our current understanding. The better tuned and more realistic the finite element model the greater our confidence in the final designs.

9 REFERENCES

1. Amazigo J.C, Budiansky B, (1972), **Asymptotic Formulas for the Buckling Stresses of Axially Compressed Cylinders with Localised or Random Axisymmetric Imperfections**, Journal of Applied Mechanics, 39:179-184
2. Arbocz. J, Babcock, C.D, (1969), **The Effect of General Imperfections on the Buckling of Cylindrical Shells**, Journal of Applied Mechanics, 36(1):28-38
3. Arbocz J, Sechler E.E, (1974), **On the Buckling of Axially Compressed Imperfect Cylindrical Shells**, Journal of Applied Mechanics, 40(3):737-743
4. Arbocz J, (1974), **The Effect of Initial Imperfections on Shell Stability**, In Thin Shell Structures; Theory, Experimentation and Design, Edited by Fung Y.C, Sechler E.E, Prentice-Hall Inc. New Jersey
5. Balden V, (2003), **Introduction to Finite Elements II**, Course notes MEC 564Z, University of Cape Town
6. Bathe K.J, (1982), **Finite Element Procedures in Engineering Analysis**, Prentice-Hall Inc., New Jersey
7. Bornscheuer F.W, Hafner L, (1983), **The Influence of an Imperfect Circumferential Weld on the Buckling Strength of Axially loaded Circular Cylindrical Shells**, 3rd International Colloquium on the Stability of Metal Structures, Paris
8. Budiansky B, (1959), **Buckling of Clamped Shallow Spherical Shells**, IUTAM Symposium on the Theory of Thin Elastic Shells, Delft, Netherlands
9. Timoshenko, S, (1936), **Theory of Elastic Stability**, First Edition , McGraw-Hill Book Company, New York
10. Berry P.A, Rotter J.M, Bridge R.Q, (2000), **Compression Tests on Cylinders with Circumferential Weld Depressions**, Journal of Engineering Mechanics, 26(4):405-413
11. Cook R.D, (1974), **Concepts and Applications of Finite Element Analysis**, John Wiley & Sons, INC, New York
12. Brush, D.O, Almroth, B.O, (1975), **Buckling of Bars, Plates and Shells**, McGraw-Hill Book Company, New York
13. Calladine C.R, (1995), **Understanding Imperfection-Sensitivity in the Buckling of Thin-Walled Shells**, Thin-Walled Structures, 23:215-235

14. Chryssanthopoulos M.K, Poggi C, Spagnoli A, (1998), **Buckling Design of Conical Shells Based on Validated Numerical Models**, Thin-Walled Structures, 31:257-270
15. Donnell L.H (1934), **A New Theory for the Buckling of Thin Cylinders Under Axial Compression and Bending**, Transactions A.S.M.E, 56:795-806
16. Donnell L.H, Wan C.C, (1950), **Effect of Imperfections on Buckling of Thin Cylinders and Columns Under Axial Compression**, Journal of Applied Mechanics, 17:73-83
17. European Convention for Constructional Steel Research, (1988), **Buckling of Steel Shells, European Recommendations**, Fourth Edition , ECCS, Brussels
18. El Damatty A.A, El-Attar M, Korol R.M, (1998), **Inelastic Stability of Conical Tanks**, Thin-Walled Structures, 31:343-359
19. El Damatty A.A, Korol R.M, Mirza F.A, (1997), **Stability of Imperfect Steel Conical Tanks under Hydrostatic Loading**, Journal of Structural Engineering, ASCE, 123(6):703-712
20. Flügge, W, (1973), **Stresses in Shells**, (second edition), Springer-Verlag, Berlin Heidelberg New York
21. Gould P.L, (1985), **Finite Element Analysis of Shells of Revolution**, Pitman Advanced Publishing Program, Pitman Publishing LTD, London
22. Grunitz L, (2001), **The Effect of Welding on the Buckling Behaviour of Spherical Shells: A Review and Some Numerical Results**, MSc Thesis, University of Cape Town
23. Huang N, (1964), **Unsymmetrical Buckling of Thin Shallow Spherical Shells**, Journal of Applied Mechanics, 30:447-457
24. Krenzke M.A, Kiernan T.J, (1963), **Elastic stability of Near-Perfect Shallow Spherical Shells**, AIAA Journal, 1:2855-2865
25. Koiter W.T. (1945), **On the Stability of Elastic Equilibrium**, PhD Thesis, Delft University, Delft, Netherlands, English Translation NASA TT-F10.
26. Koiter W.T. (1963), **The Effect of Axisymmetric Imperfections on the Buckling of Cylindrical Shells Under Axial Compression**, Proceedings, Koninklike Nederlandische Akademie van Wetenschappen

27. Holst J.M.F.G, Rotter J.M, Calladine, C.R, (1999), **Imperfections in Cylindrical Shells Resulting From Fabrication Misfits**, Journal of Engineering Mechanics, ASCE, 125(4):410-418
28. Holst J.M.F.G, Rotter J.M, Calladine, C.R, (2000), **Imperfections and Buckling in Cylindrical Shells with Consistent Residual Stresses**, Journal of Constructional Steel Research, 54:265-282
29. Hutchinson J.W, Tennyson R.C, Muggeridge D.B, (1970), **Effect of Local Axisymmetric Imperfection on the Buckling Behaviour of a Circular Cylindrical Shell under Axial Compression**, AIAA Journal, 9(1):48-52
30. Hutchinson J.W, (1967), **Imperfection Sensitivity of Externally Pressurised Spherical Shells**, Journal of Applied Mechanics, March 1967;49-55
31. Teng J, Rotter J.M, (1992), **Buckling of Pressurized Axisymmetrically Imperfect Cylinders under Axial Loads**, Journal of Engineering Mechanics, 118(2):229-247
32. Pircher M, Bridge R.Q, (2001a), **The Influence of Circumferential Weld-Induced Imperfections on the Buckling of Silos and Tanks**, Journal of Constructional Steel Research, 57: 569-580.
33. Pircher M, Bridge R.Q, (2001b), **Buckling of Thin Walled Silos and Tanks Under Axial Load – Some New Aspects**, Journal of Structural Engineering, ASCE, 127(10):1129-1136
34. Pircher M, Berry P.A, Ding X, Bridge R.Q, (2001), **The Shape of Circumferential Weld-Induced Imperfections in Thin-Walled Steel Silos and Tanks**, Thin-Walled Structures, 39:999-1014.
35. Pircher M, Wheeler A, (2003), **The Measurement of Imperfections in Cylindrical Thin-Walled Members**, Thin-Walled Structures, 41:419-433
36. Rotter J.M, Teng J, (1989), **Elastic Stability of Cylindrical Shells with Weld Depressions, Journal of Structural Engineering**, 115(5):1244-1263.
37. Rotter J.M, (1996), **Buckling and Collapse in Internally Pressurised Axially Compressed Silo Cylinders with Measured Axisymmetric Imperfections: Imperfections, Residual Stresses and Local Collapse**, Proc. International Workshop on Imperfections in Metal Silos: Measurement, Characterisation and Strength Analysis, CA-silo, Lyon, France, pp119-140.

38. Pircher M, Bridge R.Q, (2001c), **Buckling and Post-Buckling of Cylindrical Shells with Circumferential Weld Imperfections Subjected to Axial Load**, Centre for Construction Technology Research, University of Sydney, Australia.
39. Seide P, (1956), **Axisymmetrical Buckling of Circular Conical Cones Under Axial Compression**, Journal of Applied Mechanics, ASME, 23:625-628
40. Tillman S.C, (1970), **On the Buckling Behaviour of Shallow Spherical Caps under a Uniform Pressure Load**, International Journal of Solids and Structures, 6(1):37-52
41. Tennyson R.C, Muggeridge D.B, (1969), **Buckling of Axisymmetric Imperfect Circular Cylindrical Shells under Axial Compression**, AIAA Journal, 7(11):2127-2131
42. Von Kármán T, Tsien H, (1939), **The Buckling of Spherical Shells by External Pressure**, Journal of the Aeronautical sciences, 7(2):43-50
43. Von Kármán T, Dunn L.G, Tsien H, (1940), **The Influence of Curvature on the Buckling Characteristics of Structures**, Journal of the Aeronautical Sciences, 7(7):276
44. Von Kármán T, Tsien H, (1941), **The Buckling of Thin Cylindrical Shells under Axial Compression**, Journal of the Aeronautical Sciences, 8(8):303-312
45. Zingoni, A, (1997), **Shell Structures in Civil and Mechanical Engineering**, Thomas Telford Publishing, Thomas Telford Services Ltd, London
46. Zienkiewicz O.C, (1971), **The Finite Element Method in Engineering Science**, McGraw-Hill, London
47. Zienkiewicz O.C, Taylor R.L, (2000), **The Finite Element Method: Volume 2, Solid Mechanics**, 5th Edition, Butterworth-Heinemann, London
48. ABAQUS Analysis User's Manual, Hibbitt, Karlsson & Sorensen, INC.
49. ABAQUS Theory Manual, Hibbitt, Karlsson & Sorensen, INC.